UNIVERSIDAD AUTÓNOMA DE MADRID
Programa de Doctorado en Biociencias Moleculares

Modelling the heterogeneity and complex inheritance of Left Ventricular Non-Compaction

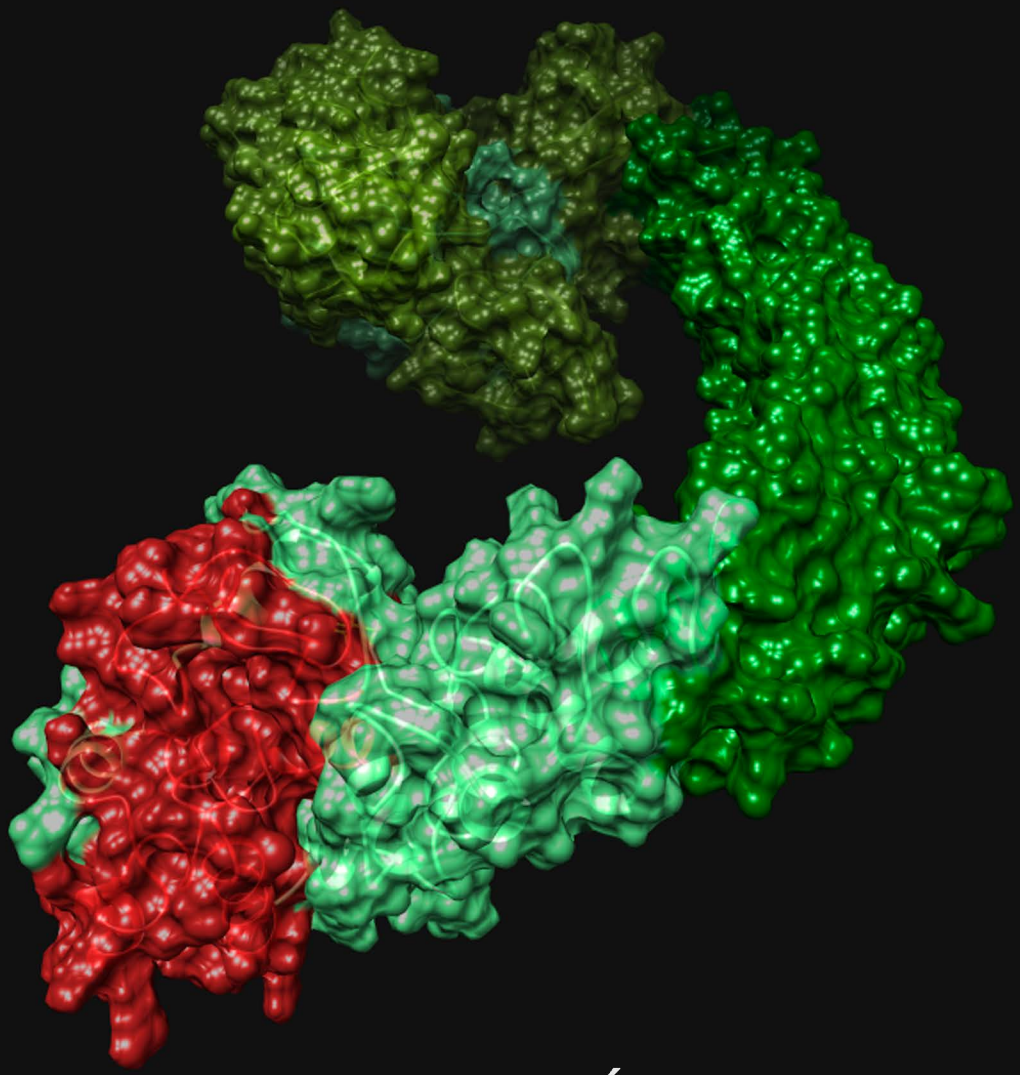

Marcos Siguero Álvarez

Madrid, 2019

DEPARTAMENTO DE BIOLOGÍA MOLECULAR

FACULTAD DE CIENCIAS

UNIVERSIDAD AUTÓNOMA DE MADRID

Modelling the heterogeneity and complex inheritance of Left Ventricular Non-Compaction

Marcos Siguero Álvarez

Licenciado en Bioquímica

Director: José Luis de la Pompa Mínguez

Madrid

CERTIFICADO DEL DIRECTOR DE TESIS

Dr. José Luis de la Pompa Mínguez, Jefe del Grupo de Señalización intercelular durante el desarrollo y la enfermedad cardiovascular,

CERTIFICO

Que Marcos Siguero Álvarez, Licenciado en Bioquímica por la Universidad Autónoma de Madrid, ha completado su Tesis Doctoral titulada "Modelado de la heterogeneidad y la herencia compleja de la Miocardiopatía No Compactada" bajo mi supervisión. Asimismo, estimo que cumple los requisitos necesarios para la obtención del título de Doctor en Biociencias Moleculares por la Universidad Autónoma de Madrid, autorizando la defensa de la mencionada memoria ante el Tribunal de Tesis designado por dicha Universidad.

Lo cual suscribo en Madrid, a 17 de octubre de 2019

José Luis de la Pompa Mínguez
Director de Tesis

Este proyecto ha sido realizado en el laboratorio de Señalización intercelular durante el desarrollo y la enfermedad cardiovascular, liderado por el Dr. José Luis de la Pompa Mínguez en el Centro Nacional de Investigaciones Cardiovasculares (CNIC) en Madrid.

Para su realización, Marcos Siguero Álvarez percibió una Ayuda para Contratos Predoctorales Severo Ochoa para la Formación de Doctores, concedida en resolución del Ministerio de Economía y Competitividad el día 9 de diciembre de 2014 y con referencia SVP-2014-068723.

La financiación del proyecto provino de diferentes entidades:

-Ministerio de Economía y Competitividad (SAF2013-45543-R, SAF2015-71863-REDT y SAF-78370-R. 2016).

-Fundación BBVA (*The NOTCH signaling pathway in Left Ventricular Non-Compaction (LVNC) cardiomyopathy: genetic studies and in vivo and in vitro modeling*, BIO14_298. 2015-2017).

-Fundació La Marató (*Investigación de los interactores genéticos y mecanísticos en cardiomiopatía familiar mediante el modelado avanzado de enfermedades*).

A Anastasia, Clemente, Esperanza y Jaro

Y a Vera

AGRADECIMIENTOS

Que si de ellas me veo libre, no se me caerá de la memoria las mercedes que en este castillo me habedes fecho, para gratificallas, servillas y recompensallas como ellas merecen.

El ingenioso hidalgo don Quijote de la Mancha, Miguel de Cervantes Saavedra

Después de todos estos años, de todo lo que se deja de lado por una Tesis y de lo que uno gana en el trayecto, en verdad es justo y necesario, es nuestro deber y salvación, dar gracias a todos los que han puesto su granito de arena, sus escalones de piedra o directamente el ascensor hasta aquí.

Empiezo agradeciendo a José Luis su compromiso con el proyecto y conmigo. Siempre disponible para escuchar los problemas técnicos o teóricos (y solucionarlos de una manera o de otra), me he podido contagiar de su pasión por la investigación. He aprendido muchísimo de cómo funciona este mundo gracias a él, tanto de lo que se cuece en la poyata como de lo que hay más allá, y también de música: ¡muchas gracias por los discos de jazz!

Gracias también a mi tutora de la UAM, Cristina Murga, por su entusiasmo contagioso y sus recomendaciones. Y a los miembros del comité del programa predoctoral del CNIC, Borja Ibañez y Alberto M. Pendás por todo lo que han aportado al proyecto. A Rui, por poner tanto interés en esta historia y plantear preguntas tan interesantes en los Notch Meetings. Millones de gracias a nuestros colaboradores en Murcia y a los pacientes y sus familias, por estar siempre tan dispuestos, y a Leticia Fernández y a los de imagen por las extracciones.

Este proyecto habría sido un infierno sin las unidades del CNIC: Genómica, Bioinformática, Histología, Microscopía, Imagen avanzada y Transgénesis. Muchas gracias a Sergio Calleja, Ana Dopazo, Jorge de la Barrera, Fátima Sánchez, Luis Miguel Criado, José María Fernández y Juande Hourcade por su enorme implicación en el proyecto.

A todo el personal de administración, limpieza, animalario, cultivos, lavados, seguridad, mantenimiento, informática, cafetería y recepción por ser siempre tan maravillosamente amables y estar tan dispuestos a ayudar. Y gracias a los jardineros del campus por mantener ese pedacito de monte en el campus que con cada lluvia me hacía sentir más cerca de Braojos.

Un agradecimiento enorme a los miembros del Comité de Empresa, pasados y presentes, por hacer de este centro algo tolerable a pesar de todo, sacrificando horas y horas y horas de vuestro tiempo de manera totalmente desinteresada. He aprendido muchísimo durante estos años gracias a vosotros.

Gracias al laboratorio de Rui, por su compañía durante las largas horas de laboratorio y por los consejos científicos y las charlas de lo divino y lo humano. Especialmente a Luis Heredia, pura devoción por la ciencia. Me alegra muchísimo ver que el mundo a veces es un poco justo y te va tan bien. Gracias,

Macarena, por seguir ahí a pesar de nuestros más y nuestro menos. 谢谢, Wen, por ser tan buen tipo y tan alegre pase lo que pase.

Thanks, Briane, for your support and your hugs, and cuddles, and for introducing Doña Carmen to me. For being always up for fun at the lab, especially. Дякую, Марія, por enseñarme a bailar bachata y por los paseos en el CNIC, que tan bien me han venido cuando estaba harto de escribir. Gracias a Cris Márquez, Cris del Carmen y Silvia por reírme las gracias y acogerme tan bien. A Sandra y Marta también, pero porque son unas macarras y me da miedo dejarlas fuera.

Mil millones de gracias, Ana, por ayudarme tantísimo durante estos últimos meses e irradiar siempre esa alegría y esa vitalidad haciendo la ciencia. Una gran parte de esto es tuya. Gracias, Luis, por tu sentido del humor tan elegante, y por volver a darnos la oportunidad de disfrutarlo. Gràcies, Vane, per les teves històries a l'hora de dinar, y per no enviar-me a fer la mà quan acumulo ¿gradetes?. Ευχαριστώ πολύ, Δημήτρης, especially for being here during this last few months. A pain like this is always better if it is shared with somebody like you. Muito obrigado, Vera, pelas conversas da ciência e sua sinceridade brutal, que é infelizmente tão escassa. Y por no haberme roto el ordenador al caérsete agua o algo así. Moltas mercès, Quim, per deixarme parlar un poc de català amb tu, i per enviar-me notícies fresquetas sempre. Moitas grazas polas leccións de galego, Piñeiro. Pola túa tolerancia á miña preferencia por Vigo e polas recomendacións de música de modernos galegos. Muchas gracias, Cachas, por no partirme la cara cada vez que digo lo gracioso que es tu acento, pero sobre todo por defender esa visión tan pura de la ciencia y poner tanta pasión en todo lo que hace. A Tamara, por esa felicidad que lleva siempre y la facilidad para sonreír que gasta. Gracias, Lucía, por entender y compartir mi gusto por El Coleta. Muchísimas gracias, Paula, por no olvidarte nunca de mi cumpleaños y por ayudarme tantísimo durante toda la Tesis con los papeles o cualquier otra cosa. ¡Hemos recorrido un camino larguísimo juntos, y lo hemos sobrevivido! Obrigado, Vítor, por sorrir com cada fado que eu compus para você e por seu compromisso com os projetos que compartilhamos. Mil gracias a Abel y Lucía por la maravilla de trabajo que hacen, por estar siempre dispuestos a ayudarme (aunque sea a destiempo) y por hacer muchísimo más fácil mi vida aquí. Thanks/merci, Donal, for your wonderful stories and for being always willing to share a drink. Gracias, Rebeca T., soportar mis bailes y cantes en la zona postdoc. Siento ser tan pesado con el trasvase. Gracias, Cris, por tu trabajo duro. Gracias a todos los que han pasado por el laboratorio y han aguantado mi pesadez y mi cabezonería. Ευχαριστώ, Τάνια, por distraer a la gente de mis moratones con tu *krav maga* (y por las cervezas que hemos compartido estos años). Gracias, Belén, por todo lo que me has enseñado durante tanto tiempo y por seguir aguantando a niñatos sin mandarnos a la mierda (mucho). También he aprendido muchísimo de Juli, Sara, Ana, Bea, Uxúe, Patri, Jesús Chamorro, Cicerones, MIRes, técnicos de prácticas… Lo mejor de esto es haber conocido a tantísima gente tan distinta.

Volviendo a la música, quiero agradecer a toda la 3N su paciencia conmigo y con mi selección musical. Me han salvado de la locura dejándome poner a Raphael o Camilo Sesto en cualquier momento del día. Gracias (y perdón) a Héctor, Cris Villa, Susana y Lin, que son las que más lo han sufrido. A Jose también, aunque diría que a él le gustan. Pero que quede claro que esto es culpa de Guille y Gaetano, que me enseñaron las normas de protocolo en este centro. O más bien el descaro absoluto. Alguna cosa más aprendí de ellos, igualmente reprobable. Gracias, Guille, por hacerme ver que no pasa nada por hacer el ridículo desde mi primer momento de Cicerone y Álvaro, por tener piedad en ese momento y tan buen humor siempre. Grazie mille, Gaetano, per l'insegnamento d'imprecazioni in italiano, e grazie, Lao e Mauro, per la vostra pazienza.

Gracias al rugby amateur. Sobre todo al XV Hortaleza R.C. A todos con los que he compartido vestuario, los que han jugado contra nosotros, los que nos han arbitrado, los que curran en la sombra, los que aportan su tiempo para que chavales como yo podamos disfrutar de algo tan intenso. A las victorias y a las derrotas, a los niños y niñas que empiezan a pelear porque esto siga siendo y a Chema y a Maca.

Gracias, Andrea, por estar siempre a unas cervezas de distancia, pase lo que pase, desde hace tantos años.

Gracias a mis abuelos, que siempre me han enseñado el valor del trabajo y del amor incondicional, aunque haya veces que parezca que no lo he aprendido muy bien. Anastasia y Clemente, os echo de menos. Jaro y Esperanza, gracias por todo lo que hacéis por vuestros nietos. Lo bueno que somos es cosa vuestra, y espero que cosas como la tesis os hagan estar un poco orgullosos de mí.

Mamá, papá, habéis conseguido juntar todas las virtudes de los abuelos en vosotros, habéis añadido más y cada día soy más consciente de la inmensísima suerte que tengo de que hayáis hecho todo lo posible para enseñármelas. Gracias por desviviros porque pueda elegir mi camino y estar ahí siempre que he necesitado consejo y ayuda. Mil gracias por todos los esfuerzos que hacéis por mí y por Josu. Os debo todo.

Gracias por tu apoyo incondicional, Josu. Por enseñarme tanto desde tan pequeño y porque, incluso cuando nos zurrábamos mientras aún eras más grande, siempre he tenido claro que estaremos en el mismo equipo. Siempre has sido una referencia para mí, aunque lo disimule. Y gracias, Helena, por sumarte a nuestra familia hace tantos años y hacerla incluso más grande con Vera.

No sé qué habría hecho sin ti, Esther. Sin tu ayuda con la tesis, sin tu compañía en los momentos chungos, en los buenos y en los medianos, siempre haciéndolos mejores. Has sufrido mi indisciplina y siento muchísimo no haberte hecho caso con tus consejos. Pero aun así me has acompañado fin de semana tras fin de semana de escritura y no sé cómo narices voy a devolverte la mitad de la mitad de lo que haces por mí, pero ten claro que lo voy a intentar. Encontraré la manera. Lo bueno es que espero tener muchísimo tiempo para hacerlo. Como una vida.

Gracias por sufrir y disfrutar esta tesis conmigo.

Pourtant ces détails, qu'on appelle à tort petits,

– Il n'y a ni petits faits dans l'humanité ni petits feuilles dans la végétation –

sont utiles.

Les misérables, Victor Hugo

Resumen
Abstract

RESUMEN

La formación durante el desarrollo cardíaco de una pared muscular suficientemente gruesa y lisa en los ventrículos es fundamental para la función cardíaca. Este proceso, llamado compactación, ocurre tardíamente durante la gestación y en la etapa perinatal, y está regulado por señales intercelulares provenientes del endocardio que controlan la maduración y la proliferación del miocardio. Las trabéculas, estructuras transitorias que han permitido el crecimiento del corazón durante las etapas anteriores del desarrollo embrionario, dan lugar durante la compactación al sistema de conducción cardíaca y quedan integradas en el miocardio compacto.

Los defectos en este proceso dan lugar a la miocardiopatía no compactada (MNC o LVNC, por sus siglas en inglés), una enfermedad congénita que puede cursar asintomáticamente o provocar arritmias o una insuficiencia cardíaca por la que los pacientes pueden llegar a requerir un trasplante cardíaco. Por otro lado, la LVNC puede presentarse como una miocardiopatía aislada o en combinación con defectos como la miocardiopatía hipertrófica o la válvula aórtica bicúspide.

Las causas genéticas más comunes de la LVNC son mutaciones en genes sarcoméricos pero, recientemente, nuestro laboratorio ha descrito mutaciones dominantes en *MIB1* (*MINDBOMB1*), un gen de la vía de señalización NOTCH, como causantes de LVNC. La importancia de Mib1 en la compactación fue confirmada con modelos condicionales de pérdida de función total en el miocardio. NOTCH es también fundamental para el desarrollo de la válvula aórtica, y, con el objeto de investigar los mecanismos subyacentes a la LVNC, generamos modelos murinos portadores de las mutaciones descritas en pacientes (*MIB1*^{R530X} y *MIB1*^{V943F}) mediante edición génica por CRISPR-Cas9. En estos modelos animales pudimos establecer que los ratones portadores de una mutación inactivadora (R530X) mostraban fenotipo de LVNC cuando este alelo se combinaba con el alelo nulo condicional (flox), mientras que los ratones portadores del alelo de cambio de sentido (V943F) no mostraban LVNC pero sí fenotipos de alteración en el desarrollo valvular cuando este alelo se combinaba con mutaciones inactivadoras de la vía NOTCH. En base a estos resultados y teniendo en cuenta la heterogeneidad genética y fenotípica de la LVNC, nos planteamos la hipótesis de que podría haber mutaciones adicionales ocultas por el patrón autosómico dominante, e identificamos mutaciones candidatas mediante secuenciación de exoma de las familias portadoras. Estas mutaciones afectan a genes no descritos en LVNC: *APCDD1* y *ASXL3*, para una de las familias; *CEP192*, *TMX3* y *BCL7A*, para la otra.

La generación de ratones portadores de dichas mutaciones nos ha permitido identificar nuevos genes implicados en la LVNC (ratones *Mib1*$^{R530X/+}$ *Apcdd1*$^{V150I/+}$ *Asxl3*$^{M1416V/+}$) y en la válvula aórtica bicúspide (ratones *Mib1*$^{V943F/+}$ *Cep192*$^{T1522M/+}$ *Tmx3-204*$^{F191X/+}$). El análisis de estas líneas, y de la combinación de la última con la mutación de *Bcl7a*, podrá arrojar luz sobre mecanismos comunes y divergentes en la patogénesis de la LVNC y otras enfermedades cardíacas congénitas, así como la variabilidad fenotípica dentro de la LVNC.

ABSTRACT

The compaction or formation of a thick and smooth cardiac ventricular wall is a fundamental process for cardiac function. This process takes place during late gestation and early postnatal period, and it is regulated by intercellular signalling from endocardium that controls myocardial proliferation and maturation. During compaction, the transient trabeculae that allowed cardiac growth in early development give rise to the cardiac conduction system, and are integrated in the thick compact wall. Defects in this process of compaction give rise to left ventricular non-compaction or LVNC. This cardiomyopathy can range from asymptomatic to causing arrhythmia or heart failure, even requiring heart transplantation. In addition, LVNC has been described isolated or combined with other congenital heart diseases (CHD), such as hypertrophic cardiomyopathy (HCM) or bicuspid aortic valve (BAV).

The most common genetic causes underlying this disease are mutations in sarcomeric genes, but mutations affecting *MIB1* (*MIB1*^{R530X} and *MIB1*^{V943F}), a member of the NOTCH signalling pathway, were recently identified by our lab as causative of LVNC in two different families. LVNC was observed in mice lacking *Mib1* expression in the myocardium, confirming its importance in chamber development.

As defects in NOTCH signalling pathway have also been described as causing BAV, we aimed at generating mouse models with the point mutations found in *MIB1* by CRISPR-Cas9 to investigate the mechanisms underlying LVNC. These mouse lines allowed us to confirm that the inactivating mutation (*Mib1*^{R530X}) showed LVNC when combined with the conditional heterozygous null allele in the myocardium, while the missense mutation (*Mib1*^{V943F}) did not cause LVNC, but affected valve development when combined with heterozygous NOTCH inactivating mutations.

These findings and the genetic and phenotypic heterogeneity of LVNC led us to hypothesise that there were other candidate mutations masked behind the autosomal dominant inheritance pattern. We performed exome sequencing in the families carrying the mentioned *MIB1* variants, and could identify polymorphisms affecting novel candidates as *APCDD1* and *ASXL3* in one family, and *CEP192*, *TMX3* and *BCL7A* in the other.

The generation of mouse lines harbouring each set of mutations allowed us to identify new genes implicated in LVNC (*Mib1*$^{R530X/+}$ *Apcdd1*$^{V150I/+}$ *Asxl3*$^{M1416V/+}$ mice) or in BAV (*Mib1*$^{V943F/+}$ *Cep192*$^{T1522M/+}$ *Tmx3-204*$^{F191X/+}$ mice). Further analysis of these lines and the combination of the last one with the *Bcl7a* mutant, could help elucidating the distinct molecular mechanisms behind the variability of the severity or the ones that cause combined with CHD or isolated LVNC.

Index

Index of tables

Index of figures

ABBREVIATIONS

Abbreviation	Meaning
AF	Alexa Fluor
ANOVA	Analysis of variance
AVC	Atrioventricular canal
BAV	Bicuspid aortic valve
CCS	Cardiac conduction system
cDNA	Complementary DNA
CHD	Congenital heart disease
CNIC	Centro Nacional de Investigaciones Cardiovasculares
crRNA	CRISPR RNA
ECM	Extracellular matrix
EMT	Endothelial to mesenchymal transition
EPDCs	Epicardial derived cells
FHF	First heart field
GATK	Genome analysis toolkit
GERP	Genomic evolutionary rate profiling
H&E	Haematoxylin and eosin
HCM	Hypertrophic cardiomyopathy
IB4	Isolectin B4
IF	Immunofluorescence
ISH	*In situ* hybridisation
KO	Knock-out
LCA	Left coronary artery
LoF	Loss-of-function
LVNC	Left ventricular Non-compaction
ns	Not significant
NC	Neural crest
NMD	Nonsense mediated decay
OFT	Outflow tract
PAM	Protospacer adjacent motif
PFA	Paraformaldehyde
qPCR	Quantitative PCR
RFLP	Restriction fragment length polymorphism
sgRNA	Single guide RNA
SHF	Second heart field
SNP	Single nucleotide polymorphism
ssODN	Single-stranded donor oligonucleotides
tracrRNA	Transactivating CRISPR RNA
VSD	Ventricular septal defects

INTRODUCTION

HEART DEVELOPMENT

Despite morphological differences, hearts are present in all groups of bilateral animals, with a likely common ancestor having cardiomyocyte-like cells lining a peristaltic tubular heart (Olson, 2006). Through divergent and convergent evolution, changes in metabolic and environmental selective pressures drove the diversification and specialisation of this structure to generate organs as diverse as those of *Malacostraca* or *Gastropoda* (Chen et al., 2015; Wirkner, 2009), and the four-chambered heart of endotherm amniotes (Jensen et al., 2013). A summary of the main developmental processes that form the adult mammalian heart from a subset of mesodermal cells is outlined in the following pages and depicted in Figure 1.

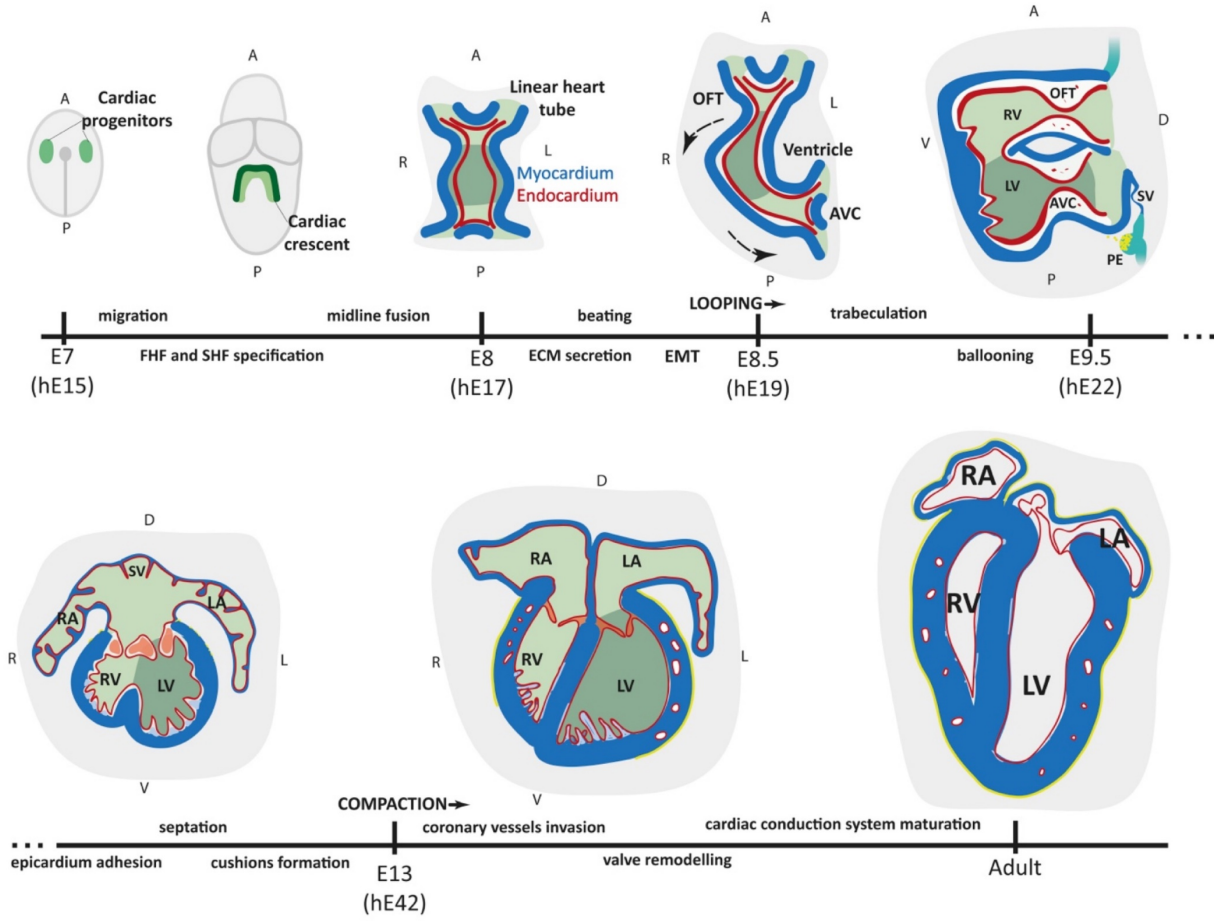

Figure 1: ***Cardiac development in mammals.*** *Chronological summary of the main events during heart development, with the fundamental processes for chamber formation and maturation in capital letters. Myocardium is shown in blue shades, with the trabecular myocardium and its derivative, the cardiac conduction system, light blue, and the compact myocardium in dark blue. Endocardium is drawn red, proepicardium and epicardium yellow, and cardiac jelly white or orange, when populated with mesenchymal cells. Structures derived from the first heart field or the second heart field are shaded in dark green and light green, respectively. Approximate developmental stages in mouse are shown under the time axis, with corresponding human stages in parentheses. A, anterior; P, posterior; R, right; L, left; V, ventral; D, dorsal; OFT, outflow tract; AVC, atrioventricular canal; RV, right ventricle; LV, left ventricle; RA, right atrium; LA, left atrium; SV, sinus venosus; PE, proepicardium.*

Cardiac progenitors and linear heart tube

The first events in heart development are common in all bilaterians, with cardiac progenitor cells arising from the lateral mesoderm (an evolutionary innovation of metazoans) regulated by transcription factors as NK homeodomain homologs, (*tinman* in Drosophila, *NKX2-5* in vertebrates) or GATA genes (*pannier* and *GATA4*) and following conserved signals from BMP (*dpp* and *Bmp2, 4* and *7*), WNT (*wingless* and *WNT11, 5A*) and NOTCH (*delta, serrate* and *DELTA-LIKE* and *JAGGED*) pathways (reviewed in Olson, 2006; Zaffran and Frasch, 2002).

In vertebrates, these cardiac progenitor cells differentiate from lateral mesodermal regions (Rawles, 1936) that are MESP1/2^{+} (Bondue et al., 2008; Kitajima et al., 2000), migrating to the anterolateral region under the head folds, and start to express cardiac regulators as NK-homologs, following mesodermal cues from the WNT pathway. These progenitors form the cardiac crescent, containing the first heart field (FHF) and the second heart field (SHF). FHF is characterised by the early induction of *Nkx2-5* and *GATA4*, while the SHF expresses *Isl1* and *Foxh1* (reviewed in Buckingham et al., 2005).

These cardiac progenitors are already differentiated into myocardium or endocardium, with early endocardial progenitors already showing NOTCH pathway activity at E7.5 in mouse (de la Pompa and Epstein, 2012; Olson, 2006; Pucéat, 2013).

The next crucial step is the midline fusion of the FHF, forming a beating linear heart tube composed of an inner endocardium separated from surrounding myocardium by a layer of extracellular matrix (ECM). This layer of ECM, termed cardiac jelly, is produced first by endocardial and myocardial progenitors and incorporates ECM synthesised by lateral mesodermal cells (Aleksandrova et al., 2012; Suzuki et al., 1995). This linear heart tube continues to grow by addition of SHF cells anteriorly and posteriorly (Buckingham et al., 2005) and by proliferation of cells already in the tube (de Boer et al., 2012a).

In mouse, at E8.5, as these additional cells are added, the tube starts to loop rightwards (Patten, 1922), in a process regulated by Nodal and other symmetry genes. This process is dependent on physical forces exerted by the growth of the tube while anchored to the splanchnic mesoderm through the prospective outflow tract (OFT, anterior) and atrioventricular canal (AVC, posterior), without increasing the distance between both ends (Le Garrec et al., 2017).

During this process of looping, the heart starts to undergo a regionalisation, with atria and ventricles beginning to differentiate from OFT and AVC. *Tbx2* and *Tbx3* are expressed in non-chamber myocardium that will give rise to OFT and AVC, while expression of *Anf* is specific of the chamber territories (reviewed in Ivanovitch et al., 2017). Left and right ventricles already differ in the transcriptional program (*i.e.* bHLH transcription factor *Hand2* is expressed in the right ventricle and *Hand1*, in the left ventricle in mouse embryos (Srivastava et al., 1997)). Proliferation rate in the outer curvature of the chambers is higher than in the inner curvature (de Boer et al., 2012a, 2012b),

increasing the size in a process called ballooning, creating a lumen and completing the cardiac looping by E9.5 in mouse development (Ivanovitch et al., 2017).

Valvulogenesis

As detailed in Figure 2, at around E9, the myocardium of the non-chamber region of the looping heart tube, determined by *Tbx2*/*3* signals, begins the process of valve specification. Through the intervening cardiac jelly, myocardial *Bmp2* (Ma et al., 2005; Rivera-Feliciano and Tabin, 2006) and *Tgfβ2* (and *Tgfβ3* in chicken) signals, in interaction with Notch1 regulate the expression of cell-to-cell adhesion molecules in the endocardium (Luna-Zurita et al., 2010; Niessen et al., 2008; Papoutsi et al., 2018; Timmerman et al., 2004), eliciting endothelial to mesenchymal transition (EMT). This EMT, in addition to the migration of neural crest (NC) derived cells to the OFT (de Lange et al., 2004), populates the cardiac jelly with mesenchymal cells, forming the cardiac cushions in the AVC and the OFT (Markwald et al., 1977).

Epicardium and coronary vessels formation

When looping is about to complete (around E9.5 in mouse, hE29 in human), another layer adds to the complexity of the heart. Coming from the proepicardial protrusion, a mass of mesoderm-derived cells formed in the *septum transversum* region, an epithelial-like layer of epicardial cells starts to cover the heart of vertebrates. The main signals regulating the formation of proepicardium are, as in valve endocardium, NOTCH and BMP2, with an important role of Tcf21. The mechanism used by proepicardial cells to reach the outer layer of myocardium varies in different organisms (Männer, 1992; Peralta et al., 2013; Viragh and Challice, 1981), but, in all cases, the attachment requires BMP2 expression (reviewed in Perez-Pomares and De La Pompa, 2011). Once attached, epicardial cells form a monolayered epithelial structure that ends up covering the whole heart at around E12.5 in mouse. In humans, however, this process ends up around hE40, with a monolayer covering the atria and a multi-layered epicardium surrounding the ventricles (Risebro et al., 2015).

The dramatic proliferative expansion of the myocardium, especially of the compact layer, needs to be sustained by an additional input of blood that, in turn, allows the heart to increase its size appropriately to the growing embryo. When the compact myocardium is not being properly supplemented with O_2 by diffusion from the lumen, it starts to produce hypoxia signals as VEGF-A (Tomanek et al., 1999a, 1999b) that reach the epicardium and stimulate the formation of epicardial derived cells (EPDCs) that take part in the formation of coronary vessels (Perez-Pomares et al., 2002). An EMT-like process also drives the formation of endocardial derived vessels, mainly in the interventricular septum, while most free wall coronary vessels originate at the *sinus venosus,* (Wu et al., 2012; Zhang et al., 2016), elicited by VEGF-C signals (Chen et al., 2014a, 2014b). The *sinus venosus* is a chamber formed in the confluence of systemic veins in vertebrate, upstream of the atrium in fish and of the right atrium in *tetrapoda*, which, besides taking part in the formation of the coronary system, it assists with the filling of the

atrium in ectotherms and gives rise to the sinoatrial node, the main pacemaker of the heart (Faber et al., 2019). A graphical summary of epicardial and coronary vessels contribution to cardiac wall formation, can be found in Figure 3.

Trabeculation and chamber septation

Simultaneously to epicardial formation, the primitive myocardium is differentiated in two cameral subpopulations: trabecular (inner) and compact (outer). The trabecular myocardium extends into the lumen creating a mesh of sheet-like protrusions, somehow thicker in the right than in the left ventricle (reviewed in Sedmera et al., 2000). The process or processes governing the formation of this trabeculae is not fully understood. It has been proposed that the mechanical effect of looping itself "squeezes" cardiomyocytes producing trabecular ridges from the compact myocardium (Sedmera et al., 2000), that cardiomyocytes protrude by themselves into the luminal surface (Staudt et al., 2014) or that they migrate and divide into the lumen in an orientation orthogonal to compact myocardium (Li et al., 2016). What is known is that this process of trabeculation is regulated by signals between myocardium and endocardium, as Nrg1-Erbb2 (Gassmann et al., 1995; Lee et al., 1995; Meyer and Birchmeier, 1995) or EphrinB2-EphB4 (Gerety et al., 1999), that are governed and coordinated by Notch1 activity in the endocardial cells (Grego-Bessa et al., 2007). In response to the mechanism or combination of mechanisms that give rise to those trabeculae, compact and trabecular cardiomyocytes start expressing different transcriptional programs, with the most prominent markers being *Anf* and *Bmp10* in the trabeculae, and *Hey2* in the compact myocardium (Tian et al., 2017). These trabeculae increase the interchange surface of endocardium and myocardium with the blood in the developing heart (Sedmera et al., 2000). They also allow an increase in volume driven by proliferation of both compact and trabecular myocardium, regulated by the overlying ECM and endocardium (del Monte-Nieto et al., 2018), and will be fundamental for the conduction system.

After looping and regionalisation of the heart, the next step in avian and mammalian four chambered hearts is the septation. Several signals regulating septum formation (both atrial and ventricular) are part of the family of *T-box* genes, involved in chamber specification and different morphological processes in the developing heart. One of them is *Tbx5* (Bruneau et al., 2001). In mammals and chicken, expression of this gene is completely absent in the right ventricle and delimits sharply the side of the septum derived from the left ventricle, while this differential expression is not as clear in incompletely septated hearts from turtles or in the common ventricle of amphibians or fish, where *Tbx5* is homogenously transcribed. Mouse experiments revealed that this abrupt patterning of *Tbx5* is necessary for the formation of the interventricular septum (Koshiba-Takeuchi et al., 2009). Another T-box gene involved in cardiac septation, in this case relating semilunar valve septation and formation of the ventricular septum, is *Tbx1*, which exerts its function through *Fgf10*, a growth factor with an opposite expression to *Tbx5*, clearly restricted to the right ventricle and the arterial pole of the heart

(Kelly et al., 2001; Xu, 2004). Atrial septation, in turn, is linked to pulmonary development, with *Hedgehog* produced in lung mesoderm activating Gli1, expressed in the *Tbx5*$^{+}$ posterior SHF of the atria, to initiate the septation (Hoffmann et al., 2009; Xie et al., 2012).

Cardiac conduction system

The main function of the heart, pumping blood by contraction of cardiomyocytes, needs to be coordinated once chambers are defined, as the slow impulse transmission of the peristaltic pump is not the most efficient way to deliver blood through the four chambers. This is achieved by the differentiation of a fast cardiac conduction system (CCS) transmitting impulse from several slow conducting pacemakers. The first of these pacemakers is the sinoatrial node described above. It transmits the electrical impulse rapidly through the atria, which contract simultaneously and are isolated from the ventricles by the *annulus fibrosus*, a non-myocardial region derived from the junction of AVC cushions and epicardial *sulcus* tissue (Wessels et al., 1996). In the atrial side of the *annulus fibrosus*, repression of fast conduction genes as *Gja5* and *Gja1* by *Tbx3* creates another pacemaker, the atrioventricular node, connected to the ventricular region through the ridge of the interventricular septum. At the early steps of development of CCS, rapid electric impulse is transmitted through the *Gja5*$^{+}$ trabeculae but, as development proceeds, only cardiomyocytes at the tips of the trabeculae express that high conductance gap junction protein, forming the prospective Purkinje fibres that transmit depolarisation first to the apex and then to the free walls (reviewed in Miquerol et al., 2011; van Weerd and Christoffels, 2016).

Valve remodelling and maturation

Cardiac cushions, as described above, are cellularized in a process driven by eNOS (Fernández et al., 2009; Lee et al., 2000), increasing their size and fusing, forming the membranous interventricular septum and the primordial atrial septum (Los and Eijndthoven, 1973). This increase in size obliterates the lumen of the AVC and the OFT, and makes it necessary for the valves to remodel in a process parallel to the formation of the epicardial envelope and the development of the coronary vessels. In addition to this, OFT has to be septated to separate the semilunar valves: the aortic, which prevents systemic circulation backflow in the heart; and the pulmonary valve, that mediates blood flow to the lungs. Valve remodelling and septation processes require a tight coordination between myocardium, mesenchyme and endocardium, with NFATc1 and Notch1 endocardial activity as fundamental regulators (MacGrogan et al., 2016; de Pompa et al., 1998; Ranger et al., 1998). Activation of these pathways drives the decrease of deposited ECM, and NOTCH activity allows the correct migration of cardiac NC derived cells to the OFT valves that elicit an increase in apoptosis and the formation of the OFT septum, separating also the leaflets of the semilunar valves (Fernández et al., 2009). NOTCH activation also induces the expression of *Hbegf* in the endocardium which will, in turn, inhibit BMP dependent proliferation in

valve mesenchymal cells (reviewed in MacGrogan et al., 2018). Those processes of cell migration, apoptosis and ECM degradation lead to the sculpting and maturation of the valves (Figure 2, Jain et al., 2011; Kirby et al., 1983).

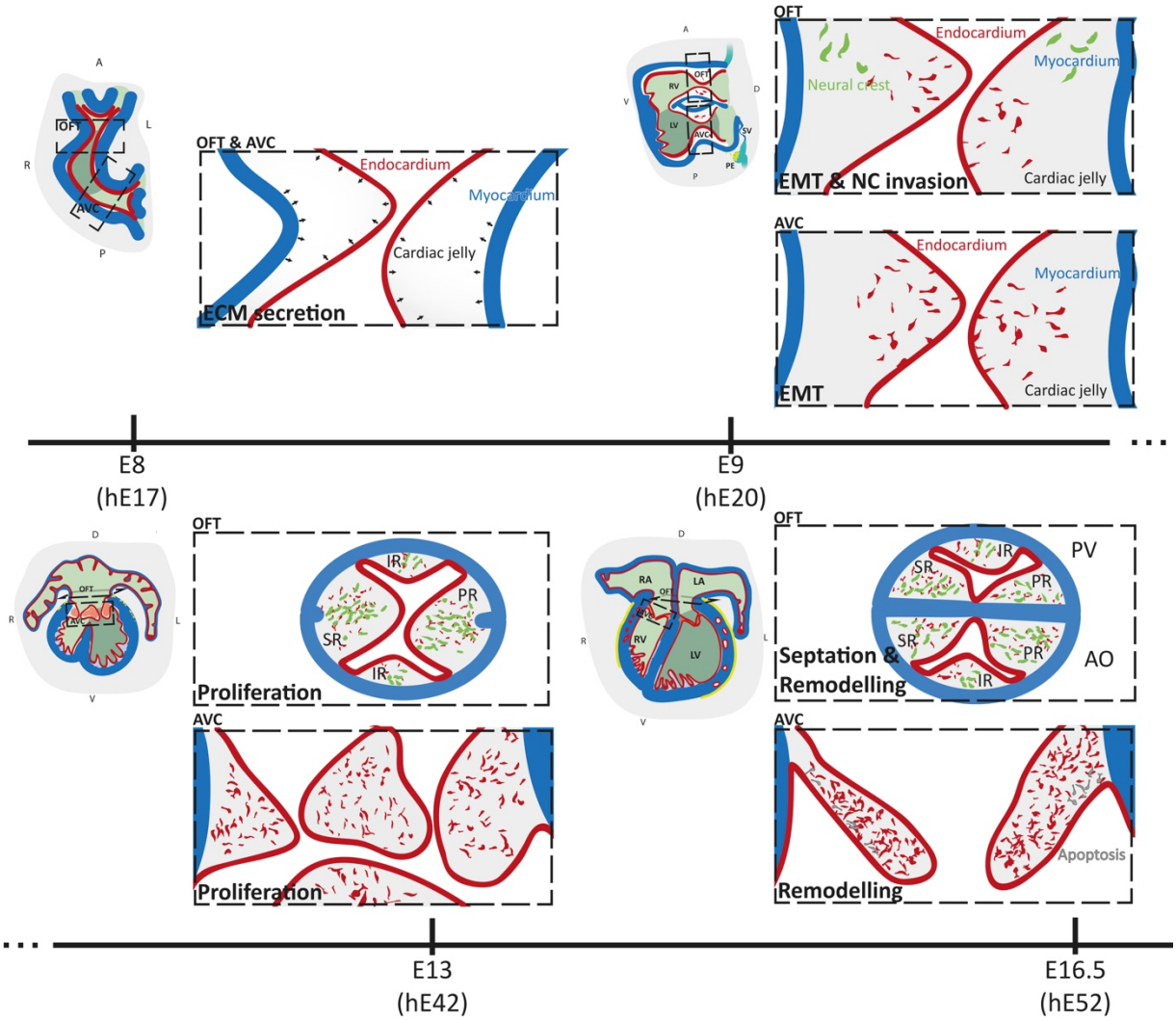

Figure 2: ***Scheme of main events in valve development.*** *After ECM secretion and formation of the cardiac jelly, it is populated by endocardial-derived cells through EMT (AVC) and by endocardial- and NC-derived cells by EMT and migration (OFT). These cells then proliferate to generate endocardial cushions that fuse and are then septated by myocardial tissue in a process regulated by NC-derived cells (OFT) and sculpted by apoptosis. Septation splits both the septal (SR) and the parietal ridges (PR), separating the aortic (AO) and pulmonary valves (PV), each formed by a leaflet derived from the SR, one derived from the PR, and one from the corresponding intercalated ridges (IR).*

Myocardial compaction

The aforementioned growing coronary vessels, depicted in Figure 3, are able to supply enough nutrients and oxygen for the compact layer of the myocardium to increase its size after around E13.5. In utero, compaction is produced mainly by an increase in proliferation in the compact myocardium regulated by genes as 14-3-3ε (Kosaka et al., 2012) and controlled by Hippo and WNT pathways (Heallen et al., 2011). The resulting adult chamber has a smooth luminal surface, without trabeculae, which gave

rise to the conduction system, with the only roughness being the papillary muscles that support the AVC valves. Compaction is an intricate process tightly dependent in coronary vessels development, and the exact mechanism by which this lack of trabeculae is achieved is a subject of debate. It is not fully clear if trabecular myocardium is integrated in the compact region by engulfment by the proliferating compact myocardium, if trabeculae collapse against each other and fuse, with both strategies generating endocardial sinuses that transform into coronary vessels (Wu et al., 2012 and reviewed in D'Amato et al., 2016), or if these trabeculae just become insignificant in size compared to the compact region (Jensen et al., 2016, 2017). Molecularly, after P7, when compaction is well advanced and myocardial proliferation has ceased, the only cardiomyocytes expressing embryonic trabecular markers are those in the conduction system, while studies in mutant embryos and lineage tracing shows that although most of the working myocardium comes from compact myocardium cells, there is an intermediate zone, or hybrid myocardium, formed by a mixture of trabecular and compact layer derived cardiomyocytes (D'Amato et al., 2016b; Tian et al., 2017).

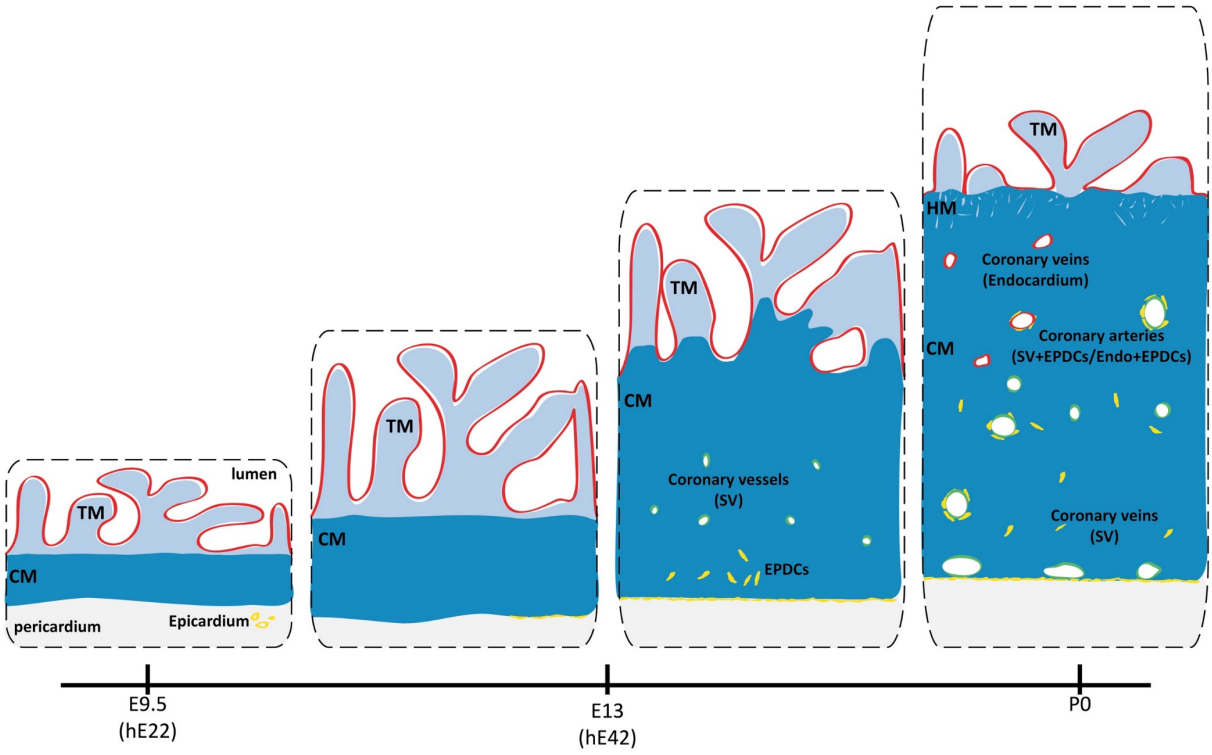

Figure 3: ***Cardiac wall maturation.*** *Two different myocardial layers are formed after looping: trabecular, luminal (TM, light blue), and compact myocardium, to the pericardial side (CM, dark blue). TM is composed of thin protrusions of myocardium covered by endocardium (red). Both myocardial layers and endocardium are highly proliferative at early stages. Epicardial cells (yellow) detached from the proepicardium cover the pericardial side of the compact myocardium, and around E13 undergo EMT to invade the compact layer, giving rise to epicardial-derived cells (EPDCs). At this stage TM has lost its high proliferative capacity, while CM maintains its growth, increasingly sustained by the formation of coronary vessels composed of endothelial cells derived from the* sinus venosus *(SV, green). These vessels are then specialized to arteries, with smooth muscle cells coming from EPDCs, or veins. Some of these coronaries are also derived from the endocardial layer, which, in turn, covers the decreasing TM that will form the CCS. In addition to this TM, the postnatal myocardial wall is composed by a thick CM, a hybrid myocardium (HM) formed by cardiomyocytes derived from both the TM and the CM.*

CONGENITAL HEART DISEASE

Defects in any of the aforementioned steps in heart development can lead to congenital heart disease (CHD), the leading type of defect in newborn children with an incidence of 7.53‰ in Europe (EUROCAT Access Prevalence Tables, 2017 data) and 9.5‰ in the United States of America (Hoffman and Kaplan, 2002) These figures exclude BAV, which shows a prevalence of 13.56‰ births on its own. Advances in diagnosis (Pérez-Lescure Picarzo et al., 2018), termination of pregnancy for foetal anomaly, surgical procedures and postoperatory treatments have decreased perinatal death rate (Dolk et al., 2011) and improved CHD patient's life expectancy in the European Union (Brida and Gatzoulis, 2019), with earlier detection and correction of the defects. The rate of survival has rocketed from 15% in the 1950s to more than 90% nowadays (Brida and Gatzoulis, 2019). However, patients of CHD still face the same risk of early mortality after operation, and 15% of them have to undergo repeated surgery before 15 years of age (Raissadati et al., 2015). The incidence of CHD is stable, reflecting an increase in mild forms, which are better diagnosed, a slight decrease of very severe cases and a conserved incidence of severe forms (Pérez-Lescure Picarzo et al., 2018). The CHDs of interest for this project are:

Ventricular septal defect

Correct development of the septum is fundamental for the isolation of the high-oxygen and low-oxygen circulations. Defects in the ventricular septation are, excluding bicuspid aortic valve (BAV), the most common of the CHDs at birth, with a prevalence of 33.99‰ in the European Union (EUROCAT Access Prevalence Tables, 2017 data). The management of this CHD is highly dependent on the size of the interventricular communication, with most ventricular septal defects (VSD) affecting the muscular part of the septum (dorsal) closing spontaneously during the first year of life by the hypertrophy of the surrounding muscular wall, while many membranous or perimembranous (ventral) VSDs have to be intervened by transcatheter surgical closure (reviewed in Morray, 2019 and Zhang et al., 2015). Genetic causes underlying VSD are mainly related to *Tbx5* directly (Basson et al., 1997; Bruneau et al., 2001; Yi Li et al., 1997) or indirectly (Garg et al., 2003), although mouse models of NFATc1 loss-of-function (LoF) and mutants of the NOTCH pathway affecting valve development also show VSD (MacGrogan et al., 2016; de Pompa et al., 1998).

Bicuspid aortic valve

Bicuspid aortic valve is the most prevalent CHD, with 13,556 cases every million births in the United States of America (Hoffman and Kaplan, 2002). It consists on the defective development of the normal three leaflets. This can be caused either by failure of the cushions to form properly due to EMT defects, typically giving rise to a fusion of the right coronary and the noncoronary cusps (the most common type), or by defects in septation that provoke the merge of the right and the left coronary cusps (less common), with or without raphe (a bulge formed due to the late fusion of the cushions), because of

aberrant migration of the NC cells (Fernández et al., 2009). This malformation can lead to turbulent blood flow in the aortic arch, increasing the shear stress in the aorta and causing aortic dilation. BAV can also cause aortic coarctation and regurgitation, leading to fatigue, palpitations, or even aortic aneurysm (reviewed in Abdulkareem et al., 2013). In addition, BAV causes early calcification, due primarily to turbulent blood flow that leads to aortic sclerosis and progressive ossification of the leaflets and stenosis, which may eventually require replacement (Otto, 2002). Genetic causes behind BAV are mainly related to OFT development *via* EMT or NC migration disruption, with genes such as *eNOS* (Lee et al., 2000) and GATA (Alonso-Montes et al., 2018) involved in the pathogenesis of BAV and calcification. NOTCH pathway mutations have also been linked to this disease in mouse and human (Garg et al., 2005; MacGrogan et al., 2016; McKellar et al., 2007; Theis et al., 2015). This could help to explain why BAV appears in combination with other CHDs linked to this and other pathways, as hypoplastic left heart syndrome (Liu et al., 2017; McBride et al., 2008; Theis et al., 2015), tetralogy of Fallot (Page et al., 2019) or LVNC (Agarwal et al., 2013).

Left ventricular non-compaction

Left ventricular non-compaction (LVNC) is a cardiomyopathy with a variably reported prevalence, as clinically used diagnostic criteria are not homogeneous, and some patients identified by imaging techniques do not show any functional symptom. It has been described as affecting from 5 in each 10000 births in the general population (Ritter et al., 1997) to 1.3% (Weir-McCall et al., 2016), probably also due to the imaging technique used. In general, diagnosis of this condition has increased in parallel to the rise in the use of cardiac magnetic resonance (CMR) and the awareness of LVNC (Towbin et al., 2015). Main diagnostic criteria are those taking into account the thickness or the mass of the trabecular *vs.* the compact region (using echocardiography: Chin et al., 1990; Jenni et al., 2001; Stöllberger et al., 2002 or CMR: Jacquier et al., 2010; Petersen et al., 2005; with the reported prevalence of each reviewed in Ross et al., 2019), although a criterion taking into account the complexity of trabeculae, the fractal dimension, has been published recently (Captur et al., 2013, 2016). Given all the variability present in the epidemiology of this condition, it has been proposed that LVNC would be the most severe form of a *continuum* comprising subclinical hypertrabeculation (Weir-McCall et al., 2016). Patients fulfilling diagnostic criteria can range from asymptomatic to suffering heart failure and needing transplantation, with increased risk of arrhythmias or thromboembolism (Luxán et al., 2013; reviewed in Sedaghat-Hamedani et al., 2017). LVNC is caused by defects during compaction, generating a thinner compact myocardium and prominent trabeculae with deep recesses into the ventricular wall. The excessive trabeculae present in the adult non-compacted hearts do not conserve the foetal identity, which is lost during *in utero* development, and are more similar to the compact myocardium than to embryonic trabeculae (D'Amato et al., 2016b; Jensen et al., 2017; Luxán et al., 2013). An important aspect of LVNC is also the insufficient thickness of the compact myocardium, caused in some mouse models by defects

in compact cardiomyocyte proliferation (Kosaka et al., 2012), but also described as derived from altered patterning of the cardiomyocytes cytoskeleton (Li et al., 2011), correlating with the main genes carrying identified mutations in human patients, that are sarcomeric or structural myocardial genes. (Sedaghat-Hamedani et al., 2017; Towbin et al., 2015). However, mutations affecting genes involved in signalling pathways are gaining attention as causative of the disease (Campbell et al., 2015; Chang et al., 2013; Luxán et al., 2013), and the presence of LVNC associated to other CHDs as VSD or BAV (Towbin and Jefferies, 2017) points to signalling pathways playing a more general role in cardiac development. The different severity of the condition and the combination with other pathologies suggest that more complex genetic interactions may cause this disease, as has been recently described (Gifford et al., 2019).

NOTCH PATHWAY

One of the most important pathways in heart development (and many other morphogenetic processes, reviewed in Kopan and Ilagan, 2009) is the NOTCH signalling pathway. It regulates several critical steps, as valvulogenesis, trabeculation, NC cells migration and OFT septation, coronary vessels development, valve remodelling and compaction (reviewed in MacGrogan et al., 2018).

In the canonical signalling pathway in mammals (summarised in Figure 4), the different membrane-bound Notch receptors (Notch1-4) are *trans* activated by membrane-bound ligands from two different families: Delta-like (Dll1, 3 or 4) or Jagged (Jag1 or 2). Both the receptors and the ligands are rich in EGF-like domains, through which they interact with each other. This interaction is modulated by glycosyl transferases from the Fringe family (Manic, Radical or Lunatic Fringe), that favour the Dll-Notch activation in detriment of the Jag-Notch signalling by adding N-acetyl-glycoseamines to specific EGF-like domains of the receptor in the Golgi apparatus. It is in the Golgi apparatus where the receptor is cleaved by Furin in two domains (NICD, intracellular; NECD, extracellular) that are trafficked to the plasma membrane non-covalently bound. Other important glycosyl transferases necessary for the maturation of the receptor are Rumi or POFUT, which also modify the EGF-like domains in the endoplasmic reticulum (reviewed in Kovall et al., 2017). Once the ligand-receptor interaction has occurred, the receptor is cleaved in its S2 (extracellular, by ADAM metalloproteases) and S3 (intracellular, by γ-secretases) sites to release the active intracellular domain. This NICD is translocated to the nucleus and can be modified integrating different signalling inputs as hypoxia or WNT (reviewed in Borggrefe et al., 2016). Once in the nucleus, it releases RBPjκ from its corepressors and recruits coactivators as Mastermind-like (MAML), eliciting the transcription of target genes that regulate differentiation and proliferative status. The exposure of the S2 cleavage site is mediated by the pulling force exerted by the endocytosis of the ligand-receptor complex by the signalling cell (the one expressing the ligand). This endocytosis is elicited by the ubiquitination of the intracellular domain of

the ligand by E3 ubiquitin transferases as Epsin (EPN1-3), Neuralized (Neur1 or 2) or Mindbomb (Mib1 or 2), depending on the cell identity and status (reviewed in Hori et al., 2013).

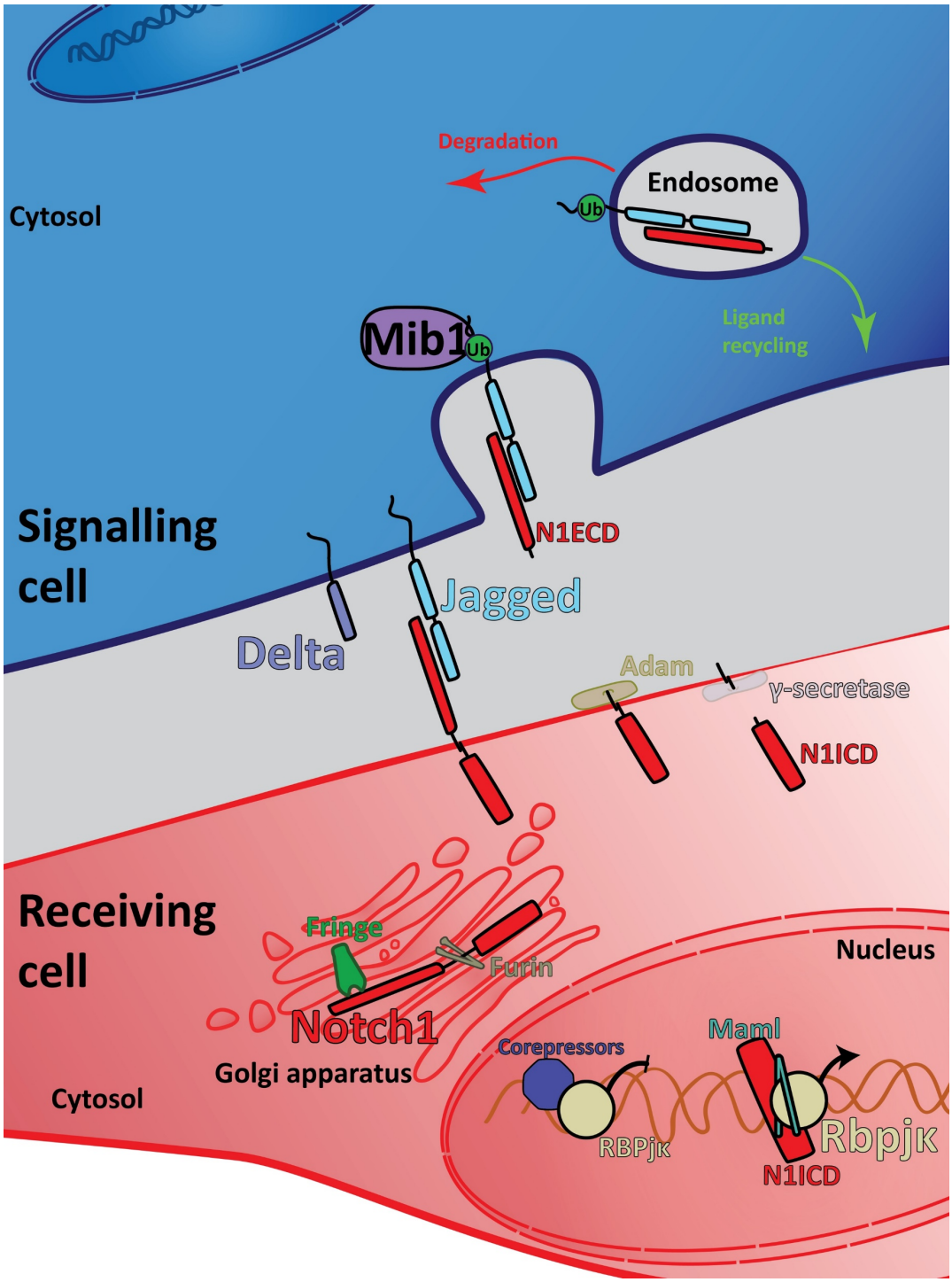

Figure 4: ***NOTCH pathway.*** *The receiving cell (red) expresses receptors from the Notch family that are modified in the Golgi apparatus by Furin or glycosyl transferases as Fringe homologs. Once in the membrane this receptor binds ligands from the Delta and Jagged families expressed by the signalling cell (blue). After this interaction, Mib1 ubiquitinates the intracellular domain of the ligand, eliciting the endocytosis of the ligand-receptor complex and exposing the S2 cleavage site in the receptor recognised by Adam metalloproteinases. This induces the effect of γ-secretases that release the intracellular domain (N1ICD). N1ICD is translocated to the nucleus, where it binds to Rbpjκ releasing its corepressors and activating its transcriptional program by recruiting coactivators as Maml. Mib1-driven endocytosis of the ligands can lead them to degradation or recycling and exposure in the membrane.*

Mib1

One of the key members of the NOTCH pathway is Mindbomb1 (Mib1), an E3 Ubiquitin ligase for Jagged and Dll proteins (Pitsouli and Delidakis, 2005). There is a homologous protein in mammals, Mib2, with redundant functions but an expression pattern almost restricted to adult tissues, and whose deletion does not cause any phenotype during embryonic or foetal development (Koo et al., 2005a, 2007). Other E3 ubiquitin ligases for NOTCH ligands, Neur1 or 2 are also dispensable during mouse development (Koo et al., 2007), while deletion of *Mib1* results in embryonic lethality at E10.5 caused by defects in NOTCH signalling, namely impaired somitogenesis, defective yolk sac angiogenesis and nervous system development and absence of heart tube looping (Barsi et al., 2005; Koo et al., 2005b). Mib1 also regulates NOTCH signalling pathway during chamber and valve maturation (D'Amato et al., 2016b; Luxán et al., 2013; MacGrogan et al., 2016).

The substrate binding region of Mib1 is composed, from the N- to the C-terminus, of two Herc2 domains separated by a ZZ zinc finger domain (MZM) and two Mib1 repeats domains (Mib1-REP). The MZM region recognises the so-called N-box of the intracellular domain of both Jag1 and delta ligands, while the Mib1-REP domains bind to the C-box from Jag1 (absent in delta and Delta-like ligands), suggesting functional differences in the ubiquitination of both ligands (McMillan et al., 2015). Separating this substrate-binding region from the C-terminal domains, there are 9 ankyrin-type repeats. The C-terminal part of the protein is composed by three RING domains (in contrast to the two present in Mib2) which bind to E2 ubiquitin ligases and transfer the ubiquitin to the substrates. It is worth noting that the third RING domain is necessary for the efficient ubiquitination of RYK, WNT pathway receptor (Berndt et al., 2011). Besides the interaction with ligands from the NOTCH pathway and the RYK receptor, Mib1 has been found to ubiquitinate PCM1, a pericentriolar protein, regulating the ubiquitination of Cep131, and, thus, inhibiting the formation of cilia in an unstressed cellular context (Villumsen et al., 2013; Wang et al., 2016). The evidence supporting the role of Mib1 in the regulation of centrosome, ciliogenesis and oriented cell division is increasing rapidly (Čajánek et al., 2015; Dho et al., 2019).

In the cardiac development context, two different mutations in *MIB1* have been related to LVNC with an autosomal dominant inheritance pattern and full penetrance. One of the mutations (rs201850378, c.1588C>T) found is a nonsense variant in amino acid Arg530 that induces nonsense mediated decay (NMD) of the transcript. The other one (rs200035428, c.2827G>T) is a missense mutation that substitutes Val943 for a phenylalanine and has a dominant negative effect on the protein. Conditional deletion of *Mib1* in mouse myocardium mimicked the disease (Luxán et al., 2013).

OBJECTIVES

The initial objective of this project was the generation of two murine models of left ventricular non-compaction harbouring previously reported point mutations in MIB1. The following specific objectives derived from the main one:

1. Characterization of the structural and molecular phenotype of *Mib1*^{R530X} and *Mib1*^{V943F} mouse lines.

2. Identification of novel genes potentially involved in the heterogeneity of LVNC.

3. Generation and characterization of mouse models carrying mutations in identified genes.

4. Identification of the different mechanisms underlying isolated and CHD-associated LVNC.

5. Development of novel genetic diagnosis tools that would allow LVNC patients stratification.

MATERIALS AND METHODS

MOUSE LINES GENERATION

All animal procedures and handling were carried out following institutional, regional and European guidelines by capable staff.

Knock-in mouse lines harbouring the mutations found in the patients were generated using CRISPR-Cas9 technology. Specific sequences for single guide RNAs (sgRNAs) or CRISPR RNAs (crRNAs) were designed using CNB's Breaking-Cas (http://bioinfogp.cnb.csic.es/tools/breakingcas/), Sanger Institute's HTGT WGE (https://www.sanger.ac.uk/htgt/wge/) and CRISPOR-TEFOR (http://crispor.tefor.net/crispor.py) online tools. sgRNA and crRNA sequences with less off-targets and higher efficiency scores as close to the nucleotide of the intended mutation as possible were selected. Single stranded oligodeoxynucleotides (ssODNs) were designed to insert the intended mutation and silent variants disrupting either the protospacer adjacent motif (PAM) sequence or the specific motif recognised by the crRNA, and allowing PCR genotyping. Sequences can be found in Table 1.

For the generation of *Mib1*^{V943F} and *Mib1*^{R530X} alleles, Cas9 mRNA was *in vitro* transcribed using mMESSAGE mMACHINE SP6 Transcription Kit (AM1340, Invitrogen). A PCR fragment with the SP6 promoter sequence and comprising the Cas9 CDS and a polyA sequence was used as template. Specific sgRNAs templates were obtained after PCR amplification of a fragment with T7 promoter sequence, specific protospacer and non-specific sgRNA from pX330 plasmid (Plasmid #42230**,** Addgene). Amplicons were transcribed using Megashortscript T7 transcription kit (AM1354, Invitrogen). All RNA species were purified using NucAway Spin Columns (AM10070, Ambion).

For the rest of the mutations inserted in the mouse genome, synthetic crRNA and transactivating CRISPR RNA (tracrRNA) were used (AltR CRISPR-Cas9 system, IDT) in combination with AltR *S. p*. Cas9 Nuclease (1081058, IDT).

Microinjections were performed by the Transgenics Unit at CNIC in one of the *pronuclei* in C57Bl/6(Crl) fertilised embryos in Potassium supplemented simplex optimised medium (KSOM). Concentrations of the reagents were as follow: Cas9 mRNA, 30 ng/µL; Cas9 protein, 30 ng/µL in all microinjections; *Mib1*^{R530X} and *Mib1*^{V943F} sgRNAs, 30ng/µL; crRNA, 0.61 pmol/µL if one crRNA was used or 0.3 pmol/µL each if two different crRNAs were injected; tracrRNA, 0.61 pmol/µL; ssODN, 10 ng/µL (excepting *Mib1*^{R530X} ssODN: 30 ng/µL). Survival was assessed at two-cell stage and alive embryos were transferred into CD1 pseudopregnant mothers (~25 embryos per female).

Animals alive at weaning were genotyped and the alleles of interest were sequenced either directly after PCR amplification (*Mib1*^{R530X}) or after TA cloning in pGEM-T Easy vector (A137A, Promega) to isolate each allele. Sequencing was performed by Sanger-style BigDye terminator chemistry on an ABI730xl sequencer by CNIO's DNA Sequencing Service for the *Mib1*^{R530X} and *Mib1*^{V943F} experiments and by Eurofins' LightRun Sequencing Service for the rest of the experiments.

Experiment	Specific sgRNA/crRNA	ssODN
Mib1^{R530X}	TACGCTTATTACGAGCATTC	TGCTGTCATAGAAGTCCTACACCGAGGCAGTGCTGATCTGAATGCTCGTAATAAGCGTTGACAGACGCCTCTTCATATTGCTGTC AATAAAGGTCATCTTCAAGTTGTGA
Mib1^{V943F}	CTGCACATCTGCGTTAACAT	TATTCTAGCAAGTGGGAATATCCCAGTGCTGCAGAAGGACAAAGACAACACAAATTTTAACGCAGATGTGCAGAAACTGCAGC AGCAGCTTCAGGACATTAAGGAGCAGG
Apcdd1	CCTCTGTGTGGCAGATGACT	CCCTCATCATCCGAGGCAAGATCCGGCTTCGCCAGGCGTCCTGGATCATCCGTGGGGGCACCGAAGCTGACTACCAGCTTCACG GCATTCAAGTCATCTGCCACACAGAGGCAGTCGCTGAACAGCT
Asxl3	TCGCCCATCGCAATGTTTGC	TCTGTTTAGAGGCCCTGAATTGTTGTCCAAGTTCTCCCCACTTAATTTGGGAGGACAGTTGTAAGAGTTTGCAGTGAGCATGTTT CCTGCGAAGACGGCGATGGGCGAGCGTGGAACCAGTGAATCA
Bcl7a	TGGGGGCTCTGACTGTTTGA	AGTCAGACAATCATCCAAGAGTTCGTGTGTGCGTGCATGCCTCTGTGTGTGTGCGCACACTGGGGAGCGGCATAAATATCTAAT TCTATCAAACAGTCAGAGCCCCCAAGCCTTGGCAGGTTGTCTC
Cep192	GGAAAACGTGAAACAGCGCC	TAAATTATACTGCTGAGAGCCTGGTCACACCTGTACTGCTCTGCCTTTGCTGAACTGACTTTGTGTCCTGAACAGAATGCCGTAG CTTGGAGATGTTTCATGTTTTCCAAAGAGCCCATCCATGTGT
Tmx3	CTCAGAAGATGTGGTTCCTG	ACAACATTATGAATAAATCTGACATGTAAAATCAAATCATAATTCTTATGAATAAATTATTATCATTAAATCAAATATTATATTAC TTCAGGAACCACATCTTCTGAGGCAGAAAAAAAGTATGTAT

Table 1: ***sgRNAs, crRNAs and ssODNs used in the microinjection experiments.*** *Nucleotides modified to introduce the desired mutations are highlighted in yellow, while ancillary synonymous variants preventing further Cas9-induced cleavage are shown in pink.*

MOUSE SAMPLES COLLECTION

Pregnant females at different gestational stages were euthanized according to laboratory animal welfare guidelines by cervical dislocation. Uterus was then dissected and transferred to RT PBS. Yolk sac was removed from embryos up to E13.5 for genotyping. Mice older than E13.5 were immediately beheaded in PBS. Then, abdomen was removed, and a piece of limb was used for genotyping. For histological procedures, whole embryos and torsos were fixed in 4% paraformaldehyde (PFA) in PBS for 2h at room temperature (RT) or overnight at 4°C. For procedures involving protein or RNA extraction, whole hearts or ventricles were dissected in cold PBS and placed in -80°C tubes for later processing.
Adult mice were euthanized by cervical dislocation and, after resection of the descending aorta, heart was perfused through the right ventricle with 1 mL of PBS at RT and 1 mL of PFA 4%. Then, heart was weighed and incubated for 2 days in 4% PFA at RT. For tibial length measurements, tibia was dislocated, and remaining muscle was removed after 1 hour in distilled water at 94°C.

PROCESSING OF TISSUE FOR HISTOLOGICAL PROCEDURES

Fixed embryos and torsos were washed two times in PBS for 1 hour in PBS at RT and transferred to 70% ethanol overnight.
Haematoxylin and eosin (H&E) and Masson's trichrome stainings were performed according to standard protocols by the Histopathology Unit at CNIC.

GENOTYPING

DNA samples were obtained from biopsies of the tail of adult mice and genomic DNA extraction was performed incubating the samples with 500 µL of 50 mM NaOH at 95˚C for 10 minutes and equilibrating with 50 µL of 1M Tris-HCl pH8. Yolk sac or a piece of limb was used for the genotyping of embryonic and foetal samples, after overnight digestion at 700 revolutions per minute (rpm) of the tissue with Proteinase K (03115801001, Roche) in 200 µL of 50mM KCl, 10mM Tris pH8.3, 2mM $MgCl_2$, 0.45% Igepal-CA630 (I3021, Sigma), 0.45% Tween 20 (P9416, Sigma) and 0.01% Gelatine (G2500, Sigma). When possible, specific PCRs were designed to amplify either the WT or the mutant alleles. Primers and reaction conditions can be found in Table 2. PCR reactions were performed using 200 nM of each primer, 1 µL of extracted DNA and DreamTaq Green PCR Master Mix (K1081, Thermo Scientific) or, specifically for *Bcl7a* genotyping, AccuStart II PCR SuperMix (95137, QuantaBio) in a total reaction volume of 21 µL.
For the *Mib1*^{R530X} line, the PCR product was digested with 0.75 U of AccI (R0161S, NEB) in a total volume of 30 µL of a solution containing 3 µL of CutSmart buffer (B7204, NEB) at 37°C for 45 minutes. Then, the whole digestion was loaded in a 3% agarose gel for band separation.

QUANTITATIVE PCR

Pools of embryonic whole hearts at E10.5 and foetal ventricles at E12.5, E14.5 and E16.5 (6 samples/pool, at least) were obtained. RNA was extracted after homogenization with steel beads for 5 minutes at 50 Hz in a TissueLyser LT (85600, Qiagen) in Trizol Reagent (15596026, Invitrogen) and purified using RNeasy Mini Kit (74014, Qiagen).

Complementary DNA (cDNA) was obtained using High Capacity cDNA Reverse Transcription Kit (4368814, Applied Biosystems), with 1 µg of total RNA as template and Random Hexamers as primers, using the protocol supplied by the company. It was then diluted 10 times in MilliQ water.

Quantitative PCR (qPCR) reactions were performed using Power SYBR Green PCR Mastermix (4367659, Applied Biosystems) in 7900HT Fast Real-Time PCR system (4329001, Applied BioSystems) for embryonic whole hearts' RNA and CFX384 Touch Real-Time PCR detections system (185-5484, BioRad) for foetal samples.

qPCR primers can be found in Table 2.

Data analysis was performed using $2^{-\Delta\Delta Ct}$ method using Microsoft Excel software.

Gen	Forward primer	Reverse primer	T_a (°C)	Fragment (bp)
Apcdd1 WT	CGCTGTTGGCTTTATCTAGCTC	GTGTGGCAGATGACTTGGAC	59.3	271
Apcdd1 V150I	ACTACCAGCTTCACGGCATT	ACTACTCCTCAGAACACGAAC	61.0	576
Asxl3 WT	GCTCGCCCATCGCAATGTTT	TGTCCATTCTAAAGCCCTTGTCT	59.2	822
Asxl3 M1416V	GCTCGCCCATCGCCGTCTTC	AGTACTTGAGTTTCGTGCTT	58.6	539
Cep192 WT	AGCAGTAGCCACTTTGCCTTAT	AAACGTGAAACAGCGCCAGG	56.3	559
Cep192 T1522M	AGAATGCCGTAGCTTGGAGA	CATGCCATCTTCCCCATTTTCC	56.2	477
Bcl7a WT	CTGACTGTTTGATGGAATTAA	GAGGACTTCCCCAAGAGCAA	58.8	577
Bcl7a AG,GA	CTGACTGTTTGATAGAATTAG	CGTGCATGTCCATCATCCCA	55.6	223
Tmx3 WT	TGGTTCCTGAGGTAATATTT	ACTATTTTCTACTCACACAT	50.5	422
Tmx3-204 F191X	ATGTGGTTCCTGAAGTAATATA	GTGTTGTTTCTCAAATATGTAAGGTA	52.1	561
qPCR *Mib1*	CCAGAGTGGTGCGAGGAGTG	CATGCCCTCAAAGCCAACCC	60.0	173
qPCR *Apcdd1*	ATCCAGACAGCAGATCGCAC	TTGTCATGAACTCCGGACCC	60.0	192
qPCR *Asxl3*	ACGGGCAAAAATCTCCCACT	AAATGCTGAGGGAAGGAGGC	60.0	190
qPCR *Cep192*	ACGACTCAGCTTTCAGGGTG	GCAGCGTTAGCTTGCTTCTC	60.0	117
qPCR *Bcl7a*	CCGATGGAAAAGAGCACCCT	GGCACTCCTTCCAAATCCTGA	60.0	169
RT-PCR *Tmx3* Long	GACTTGGCATATAATTACCG	AATCTGACATGTAAAATCAAA	51.9	322
RT-PCR *Tmx3* Short	GACTTGGCATATAATTACCG	TATCATTAAATCAAATATTA	49.1	277

Table 2: ***PCR, qPCR and RT-PCR primers.***

IN SITU HYBRIDISATION

ISH was performed according to (Jostarndt et al., 1994), using riboprobes labelled with digoxigenin synthesised with Dig RNA labelling mix (11277073910, Roche) and purified with Illustra AutoSeq G-50 columns (27534001, GE Life Sciences).

IMMUNOFLUORESCENCE

The basic protocol was the one published in Del Monte et al., 2007, with the antibodies and dilutions specified in Table 3. Samples were incubated for 5' with tyramide signal amplification (TSA) Plus Fluorescein System (NEL701A001KT, Perkin Elmer) to amplify Mib1 signal in combination with the anti-mouse IgG secondary antibody coupled with horseradish peroxidase (HRP). cTnT signal was detected directly with an AF-488 coupled antibody, as was performed to detect endomucin, using an AF-647 coupled anti-rat IgG antibody. Isolectin B4 (IB4) was incubated overnight.

Antibody	Dilution IF	Reference	Species
α Cleaved Notch1 (Val1744) (D3B8)	1:100	4147S, Cell Signaling Technology	Rabbit monoclonal
α cTnT	1:50	CT3, DSHB	Mouse monoclonal
α Endomucin (V.5C7)	1:100	sc-53941, Santa Cruz Biotechnology	Rat monoclonal
Isolectin GS- (IB4), Alexa 647 conjugate	1:100	I32450, Invitrogen	*G. simplicifolia*
Biotin-SP Fragment anti rabbit IgG	1:100	111-066-003, Jackson Immuno Research	Goat, polyclonal
Anti-rat IgG, AF647	1:100	A21247, Thermo Fisher Scientific	Goat, polyclonal
Anti-mouse IgG, AF488	1:100	A11029, Thermo Fisher Scientific	Goat, polyclonal

Table 3: ***Antibodies used in Immunofluorescence (IF).***

IMAGING

Whole mount images were acquired using a Leica MZFL III binocular scope coupled to an Olympus DP71 CCD and Olympus cellSense software.

Bright field (H&E and ISH) imaging was performed using an Olympus BX51 Microscope and Olympus cellSense software.

Confocal imaging was carried out using Leica SP5 or Leica SP8 Navigator systems and LAS X software.

HUMAN DNA SAMPLES EXTRACTION

All human samples were extracted after subjects were fully informed by our collaborators in Hospital Virgen de la Arrixaca, Murcia, and written consent was signed. Genomic DNA was obtained from 1 mL of blood samples extracted in EDTA using DNAEasy Blood & Tissue Kit (69506, Qiagen).

EXOME SEQUENCING AND DATA ANALYSIS

Extracted DNA was sequenced using Illumina HiSeq2500 o Illumina HiSeq3000 by CNIC Genomics Unit. Bioinformatics processing of the sequences was performed by Bioinformatics Unit at CNIC as follows: Variant discovery from next generation sequencing (NGS) data was addressed based on Genome Analysis Toolkit (GATK) Best practices for germline short variants using GATK version 3.7 (DePristo et al., 2011). GATK bundle reference files for genome version b37/GRCh37 was used. The workflow includes:

Pre-processing sequence data:

Quality trimming and adapter removal was done using Trimmomatic 0.38 (Bolger et al., 2014) in paired mode (ILLUMINACLIP:TruSeq3-PE.fa:2:30:10). Low quality bases from the beginning and the end of the read pair were deleted if score was below 3 (LEADING:3 TRAILING:3) and if average quality was below 15 using a sliding window of size 4 for the whole read (SLIDINGWINDOW:4:15). The read pair is discarded if resulting length after trimming was smaller than 36 bp (MINLEN:36)

Mapping reads:

Reads were mapped to GRCh37/b37 human genome using BWA mem version 0.7.10-r789 setting shorter split hits as secondary (-*M*) (Li and Durbin, 2009).

Identification of PCR duplicates:

Reads originated from the same DNA fragment (duplicates) during library construction were identified using Picard v1.97 (MarkDuplicates).

For reads obtained from HiSeq 2500 runs (unpatterned flowcell) the maximum offset between two duplicated clusters parameter (*OPTICAL_DUPLICATE_PIXEL_DISTANCE*) was set to 100 while it was set to 2500 for reads obtained from HiSeq3000 (patterned flowcell).

Base Quality Score Recalibration:

Quality score of bases was recalibrated to better account for systematic errors using BaseRecalibrator tool from GATK 3.7. Set known polymorphic sites databases (-knownSites) were:

- 1000G_phase1.snps.high_confidence.b37.vcf.gz
- Mills_and_1000G_gold_standard.indels.b37.vcf.gz
- dbsnp_137.b37.vcf.gz

HaplotypeCaller:

Intermediate gVCF files with single nucleotide polymorphisms (SNPs) and Indels calls were created for each sample independently using GATK HaplotypeCaller, restricting calling regions to the enrichment targeted regions (-L). “SureSelect Human All Exon V6” target intervals were downloaded from Agilent (https://www.agilent.com).

GenotypeGVCFs:

Joint genotyping from gVCF files was performed using GATK GenotypeGVCFs tool from GATK 3.7.

Variant Effect Predictor:

Variants were annotated using VEP (Variant Effect Predictor) of ensembl-tools version 84 with plugin modules LoFtool and CADD (version 1.3) using offline cache version 90 (McLaren et al., 2016).

Variant Quality Score Recalibration:

For each putative variant a VQSLOD score (variant quality score log-odds) was calculated using VariantRecalibrator and ApplyRecalibration tools of GATK 3.7. SNPs and Indels were treated separately. For SNPs (-mode SNP); QualByDepth (QD), RMSMappingQuality (MQ), MappingQualityRankSumTest (MQRankSum), ReadPosRankSumTest (ReadPosRankSum), FisherStrand (FS), StrandOddsRatio (SOR) covariates were annotated. Additionally hapmap_3.3.b37.vcf.gz was set both as truth and training set (prior 15.0). 1000G_omni2.5.b37.vcf.gz and 1000G_phase1.snps.high_confidence.b37.vcf.gz were set as training set (prior 12.0 and 10.0 respectively). dbsnp_137.b37.vcf.gz was set as known set (prior 2.0). For Indels (-mode INDEL); max number of Gaussians for the positive model (-maxGaussians) was set to 4. QualByDepth (QD), FisherStrand (FS), StrandOddsRatio (SOR) MappingQualityRankSumTest (MQRankSum), ReadPosRankSumTest (ReadPosRankSum) covariates were annotated. Besides, Mills_and_1000G_gold_standard.indels.b37.vcf.gz was set both as truth and training set (prior 12) and dbsnp_137.b37.vcf.gz was set as known set (prior 2.0).

In both cases, truth sensitivity level was set to 75 (--ts_filter_level) in order to achieve a Ti/Tv ratio close to the expected value for Whole Exome Sequence (2.8). Finally, it was decided not to use VQSLOD for filtering (just as guidance of accuracy) to avoid the lack of sensitivity and due to the possibility that offers family data (pedigree) to discard mendelian inconsistencies as presumable false positives.

VENTRICULAR MORPHOLOGICAL PARAMETERS QUANTIFICATION

At least three H&E or endomucin or IB4 and cTnT IFs sections per animal (at least three) were used blindly to determine the trabecular and compact territories. Images were turned to 8 bit, black and white, and thresholded to convert into binary images. Areas of each region were measured. Edges of the endocardium were found and fractal dimension was determined using the box counting method. The compact region was straightened using the epicardium as a reference and thickness was measured in one third of the lines perpendicular to the epicardium. The script used for these measurements can be found in the Annexes.

QUANTIFICATION OF ENDOCARDIAL N1ICD^{+} NUCLEI

At least three different sections form three different animals from each group (mutant or WT) were analysed. Images obtained by confocal imaging of IF with DAPI, myocardial (cTnT) and endocardial (endomucin or IB4) markers and N1ICD labelling were used. Images were automatically thresholded for the endocardial marker and endocardium was manually selected. A mask was generated and applied

to the DAPI channel, which was then processed to detect and count the nuclei ($DAPI^+$). The same processing was applied to the N1ICD channel. The script used can be found in the Annexes.

STATISTICAL ANALYSIS

Data was analysed using Microsoft Excel and Graphpad Prism 6 software. Hypothesis testing was performed with at least three samples per group, and, when multiple groups were tested, we performed Analysis of Variance test (ANOVA), with multiple t-test comparing each average with Tukey correction. In the case of compact vs. trabecular area ratio, in which the H_0 was that mutant proportion was not smaller, we used one-tailed t-tests. For the rest of comparisons of two groups we used two-tailed t-test. In the analysis of linkage, frequencies were compared to expected ratios using a binomial test.

RESULTS

GENERATION OF MICE HARBOURING HUMAN *MIB1* MUTATIONS USING CRIPSR-CAS9

In order to obtain new genetic models of LVNC of biomedical interest we aimed to introduce the mutations identified in LVNC patients by Luxán et al., 2013 in mouse *Mib1*. Human p.Arg530Ter (rs201850378) is caused by c.1588C>T transition, which implied the generation of c.1588A>T in the mouse gene. p.Val943Phe (rs200035428) is encoded in c.2827G>T transversion in human, which is the same mutation we had to edit into the murine gene. For that purpose, we designed specific sgRNAs that were predicted as the most effective and with their PAMs as near as possible to the intended point mutations. sgRNAs with potential off-targets in Chr. 18, where *Mib1* is located, were avoided to facilitate the isolation of the edited variants by outbreeding with C57Bl/6 mice. Symmetrical ssODNs were used as template for the homologous recombination process, and they carried additional silent mutations to disrupt the PAM sequence, preventing further cleavage of the already edited DNA.

Cas9 mRNA and sgRNA were *in vitro* transcribed using PCR amplicons as templates. Their purity and integrity were assessed with the Bioanalyzer system (Figure 5a). ssODNs were chemically synthesised, and microinjected together with *Cas9* mRNA and the specific sgRNA in C57Bl/6 embryos in the pronuclear stage. The surviving embryos at two-cell stage were transferred to CD1 pseudopregnant females. (Figure 5b). After weaning, we confirmed the generation of the mouse lines carrying each of the mutations by restriction fragment length polymorphism (RFLP) after PCR amplification (Figure 5c) and by Sanger sequencing (Figure 5d). We generated 2 (6.67% of weaned pups) founders for the $Mib1^{R530X}$ line and 4 (17.4%) for the $Mib1^{V943F}$ line. Details on concentrations, number of experiments and mice obtained are summarised in Table 4.

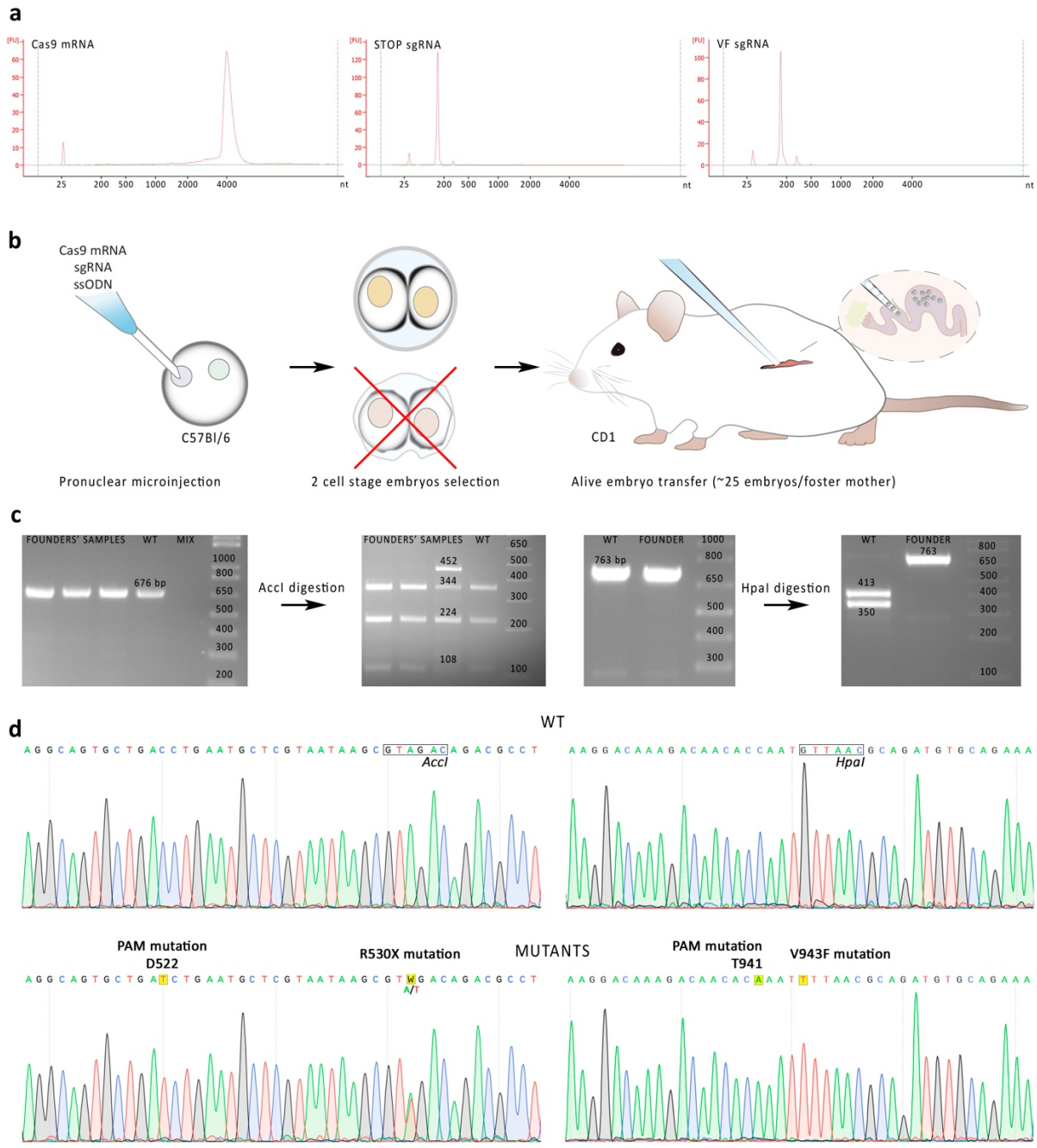

Figure 5: ***Generation of the gene edited lines harbouring mutations identified in LVNC patients****. a.-Bioanalyzer profile of the RNAs in vitro transcribed. b.- RNAs and ssODNs were microinjected in pronuclear stage, and alive embryos were selected at 2 cell stage and transferred to CD1 pseudopregnant mothers. c.- Born pups were analysed by RFLP, as mutant amplicons lose a restriction enzyme target site, producing an additional 452 bp fragment for the R530X mutation and an undigested 763 bp band for the V943F mice. d.- Sequencing results for WT and mutant pups, indicating the enzyme restriction sites and the point mutations introduced (including the synonymous variants that disrupt the PAM sequences).*

Microinjection	Embryos	[Cas9 mRNA] (ng/µL)	[sgRNA] (ng/µL)	[ssODN] (ng/µL)	Born	Weaned	Mutant (NHEJ+HDR)	Founders (HDR only)
Mib1^{R530X}	120	30	30	30	11	9	0	0
Mib1^{R530X}	118	30	30	10	11	8	1 (12.5%)	1 (12.5%)
Mib1^{R530X}	154	10	10	10	30	22	1 (4.5%)	1 (4.5%)
Mib1^{V943F}	130	30	30	30	6	6	5 (83.3%)	2 (33.3%)
Mib1^{V943F}	137	10	10	10	17	17	16 (94.1%)	2 (11.8%)

Table 4: ***Cas9 mRNA, sgRNA and ssODN microinjection efficiently generated the desired point mutations****. Percentages represent the number of mutant pups in the total of weaned animals.*

MIB1$^{R530X/R530X}$ MICE EXHIBIT A CLASSICAL NOTCH LOSS-OF-FUNCTION PHENOTYPE

To validate the mouse models generated, we first analysed the phenotype of homozygous *Mib1*^{R5390X} mice. At E10.5, embryos homozygous for the nonsense *Mib1* mutation show defects in yolk sac angiogenesis (Figure 6a, black arrowheads), problems in the development of the nervous system and in somitogenesis (Figure 6a, middle panel, white arrowheads and black arrows, respectively), and impairment of heart looping (Figure 6a, magnifications), resembling previously described phenotypes of NOTCH pathway mutants (Grego-Bessa et al., 2007; Koo et al., 2005b; Oka et al., 1995). Histological analysis of the cardiac phenotype revealed absence of cardiac cushions and increased ECM between endocardium and myocardium, as well as thinned myocardium in the chambers (Figure 6b). As expected, these mice show a diminished Notch1 activity (Figure 6c, quantitated in d) that is easily explained due to the significant decrease of *Mib1* RNA in homozygous mutants, most likely through NMD (Figure 6e). This phenotype leads to embryonic death at E10.5 (Table 5).

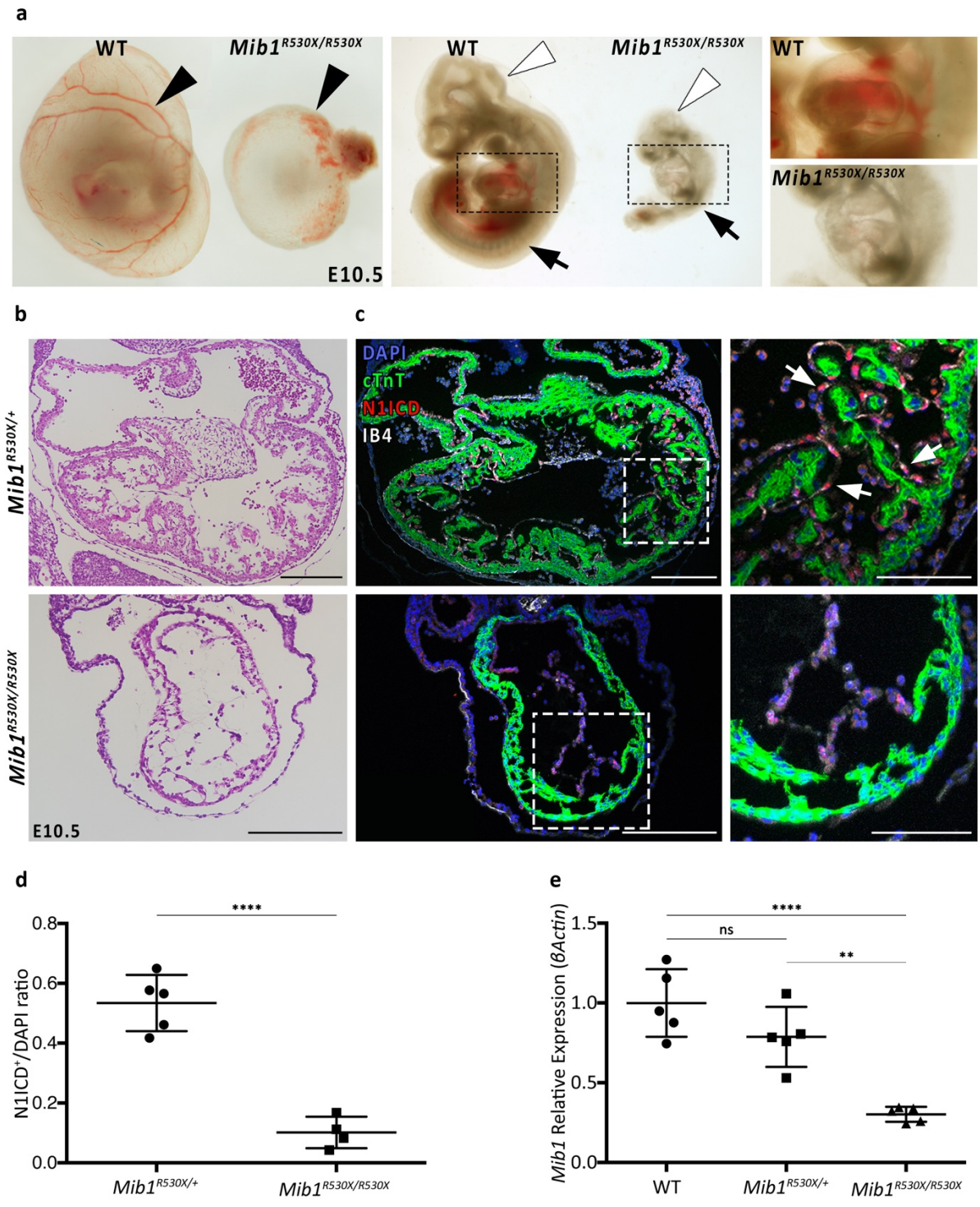

Figure 6: ***The phenotype of Mib1$^{R530X/R530X}$ mice resembles classical NOTCH loss-of-function (LoF) defects****. a.- Imaging of whole WT and homozygous mutant embryos at E10.5. Black arrowheads indicate impaired angiogenesis in the yolk sac; white arrowheads, problems in central nervous system development, and black arrows, irregular somitogenesis. Magnifications show lack of heart looping and ballooning. b.- H&E staining of the heart at the same stage reveals a clearly thinned compact myocardium, reduced trabeculae and increased ECM. c.- Immunostaining of E10.5 hearts for the active form of Notch1 (N1ICD) and markers of myocardium and endocardium shows a decrease in the activity of NOTCH pathway in homozygous mutants. d.- Quantification of the proportion of N1ICD positive nuclei. Activity of NOTCH pathway is significantly decreased in homozygous hearts compared to heterozygotes. e.- Mib1 relative to* βActin *expression analysed by qPCR of E10.5 hearts. Transcription is significantly reduced in homozygous mutant hearts compared to WT and heterozygotes. Scale bars represent 200 µm in b and c (left panels) and 100 µm in magnifications in c. ** p-value<0.01, **** p-value<0.0001, ns, non-significant.*

	Mib1$^{+/+}$	*Mib1*$^{R530X/+}$	*Mib*$^{R530X/R530X}$	Resorptions	# of litters
E9.5	1	1	5	0	**1**
TOTAL: 7	14.29%	14.29%	71.43%		
E10.5	14	26	13	10	**8**
TOTAL: 53	26.42%	49.06%	24.53%		
E11.5	4	10	4*	6	**3**
TOTAL: 18	22.22%	55.56%	22.22%		
E16.5	10	43	0	31	**10**
TOTAL: 53	18.87%	81.13%	0.00%		
P21[§]	452	413	-	-	**157**
TOTAL: 865	52.25%	47.75%	-		

Table 5: **Mib1$^{R530X/R530X}$** ***mice die at E10.5.*** *Lethality table of the mouse line carrying the identified nonsense mutation in MIB1. *Dead embryos of which DNA could be recovered. [§]Weaned mice come from* Mib1$^{R530X/+}$ *x C57Bl/6 outcrosses.*

Histological abnormalities found in these mice correspond to disruption of the patterning of molecular markers in the prospective ventricles. *Hey2*, a transcript normally restricted to compact myocardium, is expanded into the morphologically trabecular myocardium in mutant hearts (Figure 7a). *Hey2* is also expressed in the endocardium of the AVC in WT hearts, but this expression is lost in *Mib1*$^{R530X/R530X}$ mice (Figure 7a, black arrowheads), consistently with the loss of Notch1 activity in the endocardium. Moreover, *Anf*, which typically labels trabeculae, is absent in mutant ventricles (Figure 7b), although its expression is maintained in the atrial region (Figure 7b, white arrowheads).

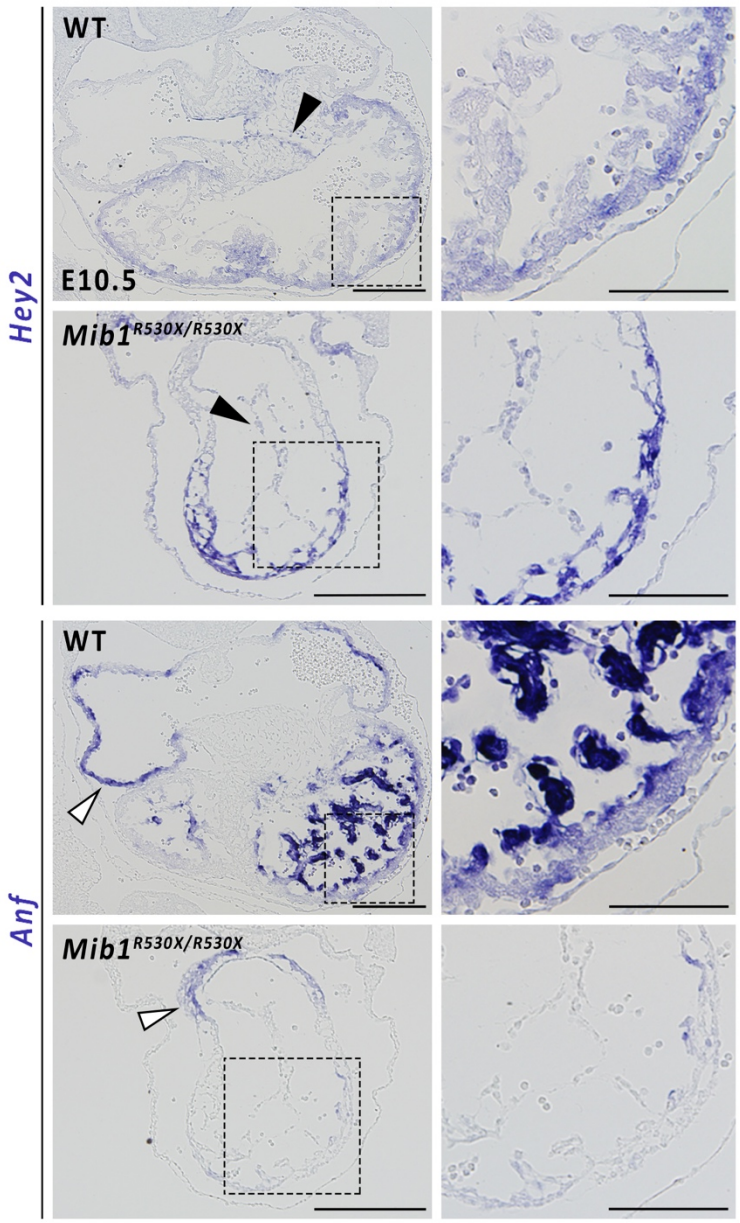

Figure 7: ***Trabecular and compact myocardium identities are altered in*** **Mib1$^{R530X/R530X}$** ***E10.5 hearts.*** Hey2, *a typical marker of compact myocardium is strongly expressed in mutant compact myocardium (upper panels, magnifications) and expanded to morphological trabeculae, while its transcription is lost in AVC endocardium (black arrowheads). On the other hand,* Anf, *expressed in trabeculae in WT hearts, is lost even in morphological trabeculae the mutant primitive ventricle, although its transcription is maintained in the prospective atrium (white arrowheads). Scale bars: 200 µm, left panels; 100 µm, magnifications.*

Mib1$^{R530X/+}$, *Mib1$^{V943F/+}$* AND *Mib1$^{V943F/V943F}$* MICE SHOW NO CARDIAC PHENOTYPE

Mib1^{R530X} and Mib1^{V943F} mutations were identified in patients of LVNC heterozygous for the variants. Thus, to better mimic the human situation, we first analysed E16.5 hearts from both *Mib1$^{R530X/+}$* and *Mib1$^{V943F/+}$* foetuses, as compaction is well advanced at this developmental stage. After careful examination of these hearts, we found no phenotype either in chambers (Figure 8, left panels, magnifications in middle panels) or in valves (Figure 8, AVC valves in left panels; OFT valves in right panels). Then, to determine if the missense mutation in homozygosity caused any phenotype, we examined *Mib1$^{V943F/V943F}$* hearts, which do not show any cardiac morphological defect (Figure 8).

We also bred *Mib1$^{R530X/+}$* animals with C57Bl/6 mice to obtain adults and to determine if they reach weaning at the expected ratio of 50%. *Mib1$^{R530X/+}$* mice survived normally, with 47.75% of the weaned animals with this genotype (Table 5). *Mib1$^{V943F/+}$* and *Mib1$^{V943F/V943F}$* adult mice were obtained through

inbreeding of heterozygotes, and were obtained at the predicted percentages (45.00% and 23.57%, compared to the expected 50% and 25%, respectively) (Table 6).

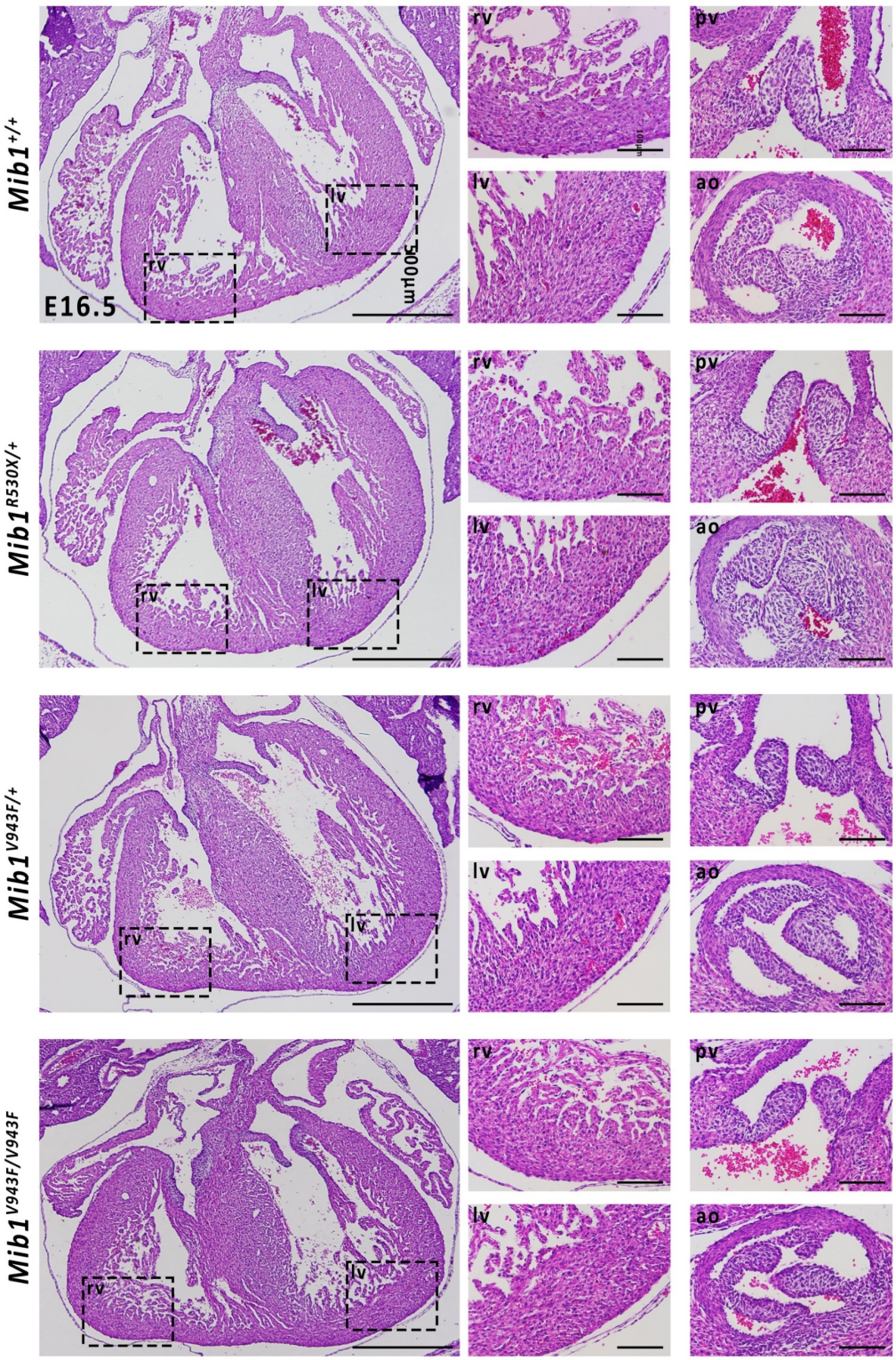

Figure 8: **Mib1$^{R530X/+}$, Mib1$^{V943F/+}$ *and* Mib1$^{V943F/V943F}$ *mice show no cardiac phenotype.*** *H&E staining of E16.5 hearts reveals that there is no gross cardiac abnormality (left panels) and compact and trabecular myocardium are not affected (magnifications, middle panels). Valves are also normal. Scale bars: 500 µm, left panels; 100 µm, middle and right panels. pv, pulmonary valve; ao, aortic valve.*

	Mib1$^{+/+}$	*Mib1*$^{V943F/+}$	*Mib*$^{V943F/V943F}$	Resorptions	# of litters
E16.5	23	50	24	9	**10**
TOTAL: 97	23.71%	51.55%	24.74%		
P21	44	63	33	-	**20**
TOTAL: 140	31.43%	45.00%	23.57%		

Table 6: **Mib1^{V943F}** ***mice reach weaning at the expected proportions.*** *Animals coming from the inbreeding of the mouse line carrying the identified missense mutation in MIB1.*

MIB1$^{R530X/FLOX}$; TNNT2-CRE MICE SHOW STRUCTURAL FEATURES OF LVNC

As homozygous *Mib1*$^{R530X/R530X}$ mice die at E10.5 (Figure 6d), in order to further study the phenotype of the *Mib1*^{R530X} mice, we bred this line with *Mib1*$^{flox/+}$*; Tnnt2-Cre/+* animals. This conditional line lacks the expression of one *Mib1* allele in all myocardial cells, so *Mib1*$^{R530X/flox}$*; Tnnt2-Cre/+* mice would be deficient for both *Mib1* alleles in the myocardium and haploinsufficient in the endocardium (and all other *Tnnt2* negative tissues). These mice show dilated hearts with prominent trabeculae in both ventricles and thinner compact myocardium at E16.5 (Figure 9a, quantified in b). This morphological phenotype is indicative of LVNC, with a decreased compact to trabecular myocardium area ratio (Figure 9b). All these cardiac development defects led to lethality *in utero* (Table 7).

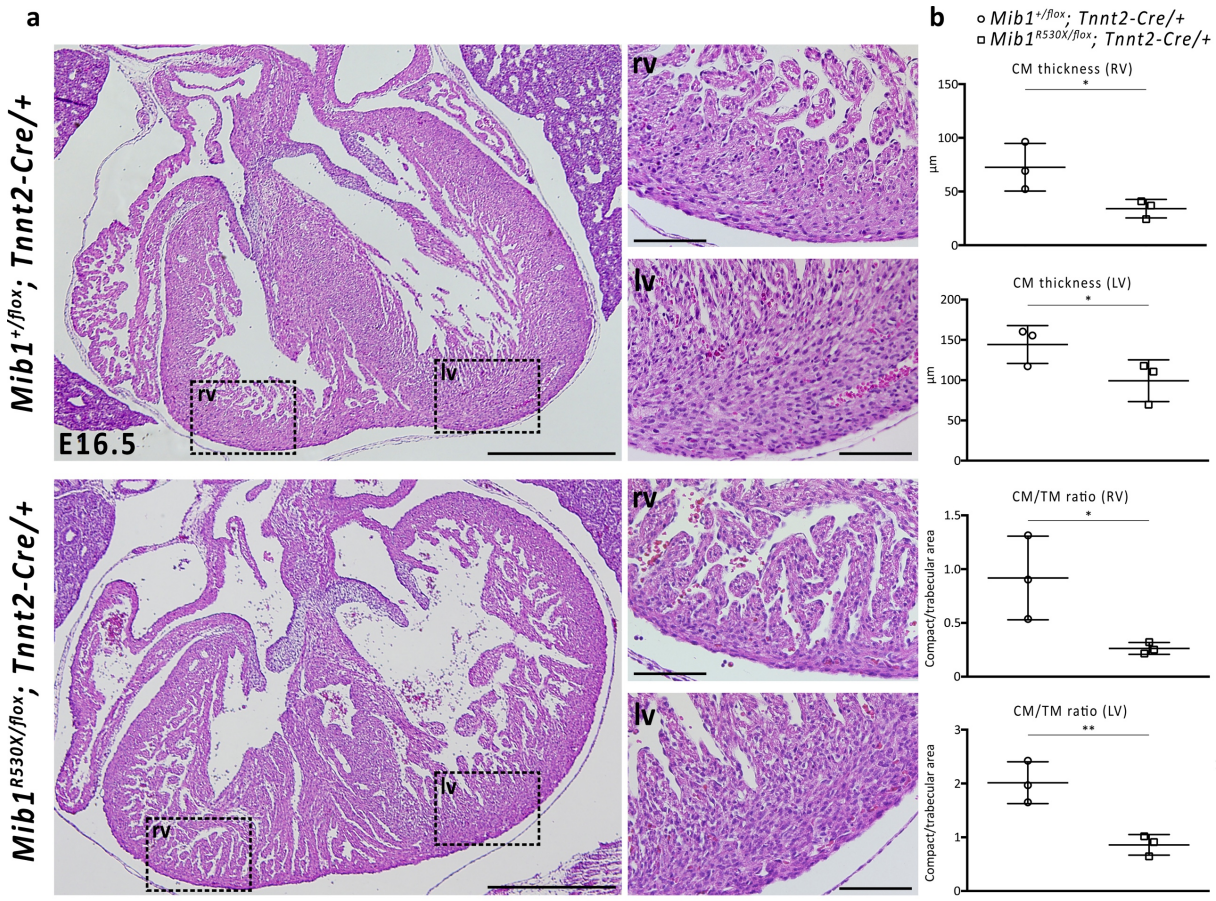

Figure 9: **Mib1$^{R530X/flox}$; Tnnt2-Cre *mice show LVNC.*** *a.- Mutant mice show cardiac morphological defects at E16.5: compact myocardium (CM) is thinner, and trabeculae are persistent and larger than in control hearts (left panels and magnifications). b.- Quantifications demonstrate the thinning of the CM and the decreased ratio of CM versus trabecular myocardium (TM) in both ventricles. Scale bars: 500 µm, left panels; 100 µm, right panels. *, p-value< 0.05; **, p-value<0.01.*

Paradoxically, we did not find a significant reduction in Notch pathway activity in E15.5 embryos, as measured with an antibody against the active form of the receptor (N1ICD) (Figure 10a, b). In contrast, the expression of trabecular (*Anf*) and compact myocardium (*Hey2)* molecular markers was disrupted in *Mib1$^{R530X/flox}$; Tnnt2-Cre/+* mice (Figure 10c, d).

The expression of molecular markers typical of trabecular and compact myocardium is disrupted, with morphological trabeculae expressing *Hey2* and devoid of *Anf* expression. This phenotype is likely not caused by Notch1 lack of activity alone, as the active form of the receptor (N1ICD) is only slightly decreased (without reaching significance) at E15.5.

	Mib1$^{+/+}$; +/+	***Mib1$^{R530X/flox}$; Tnnt2-Cre/+***	***Mib1$^{+/flox}$; +/+***	***Mib1$^{+/flox}$; Tnnt2-Cre/+***
E12.5	1	5	1	4
TOTAL: 22	4,55%	22,73%	4,55%	18,18%
E13.5	3	2	2	2
TOTAL: 18	16,67%	11,11%	11,11%	11,11%
E15.5	47	30	33	25
TOTAL: 276	17,03%	10,87%	11,96%	9,06%
E16.5	13	15	14	19
TOTAL: 132	9,85%	11,36%	10,61%	14,39%
P0	2	0	1	4
TOTAL: 16	12,50%	0,00%	6,25%	25,00%

	Mib1$^{R530X/flox}$; +/+	***Mib1$^{R530X/+}$; Tnnt2-Cre/+***	***Mib1$^{R530X/+}$; +/+***	***Mib1$^{+/+}$; Tnnt2-Cre/+***
E12.5	2	3	2	4
TOTAL: 22	9,09%	13,64%	9,09%	18,18%
E13.5	2	3	2	2
TOTAL: 18	11,11%	16,67%	11,11%	11,11%
E15.5	30	34	37	40
TOTAL: 276	10,87%	12,32%	13,41%	14,49%
E16.5	14	23	17	17
TOTAL: 132	10,61%	17,42%	12,88%	12,88%
P0	1	4	4	0
TOTAL: 16	6,25%	25,00%	25,00%	0,00%

Table 7: ***Lethality table of mice coming from the intercross between*** **Mib1$^{R530X/+}$** ***females with*** **Mib1$^{flox/+}$; Tnnt2-Cre/+** ***males.*** *Mutant mice are not born, although they are alive in the expected ratio at E16.5. The specified totals refer to the sum of all genotypes at each stage.*

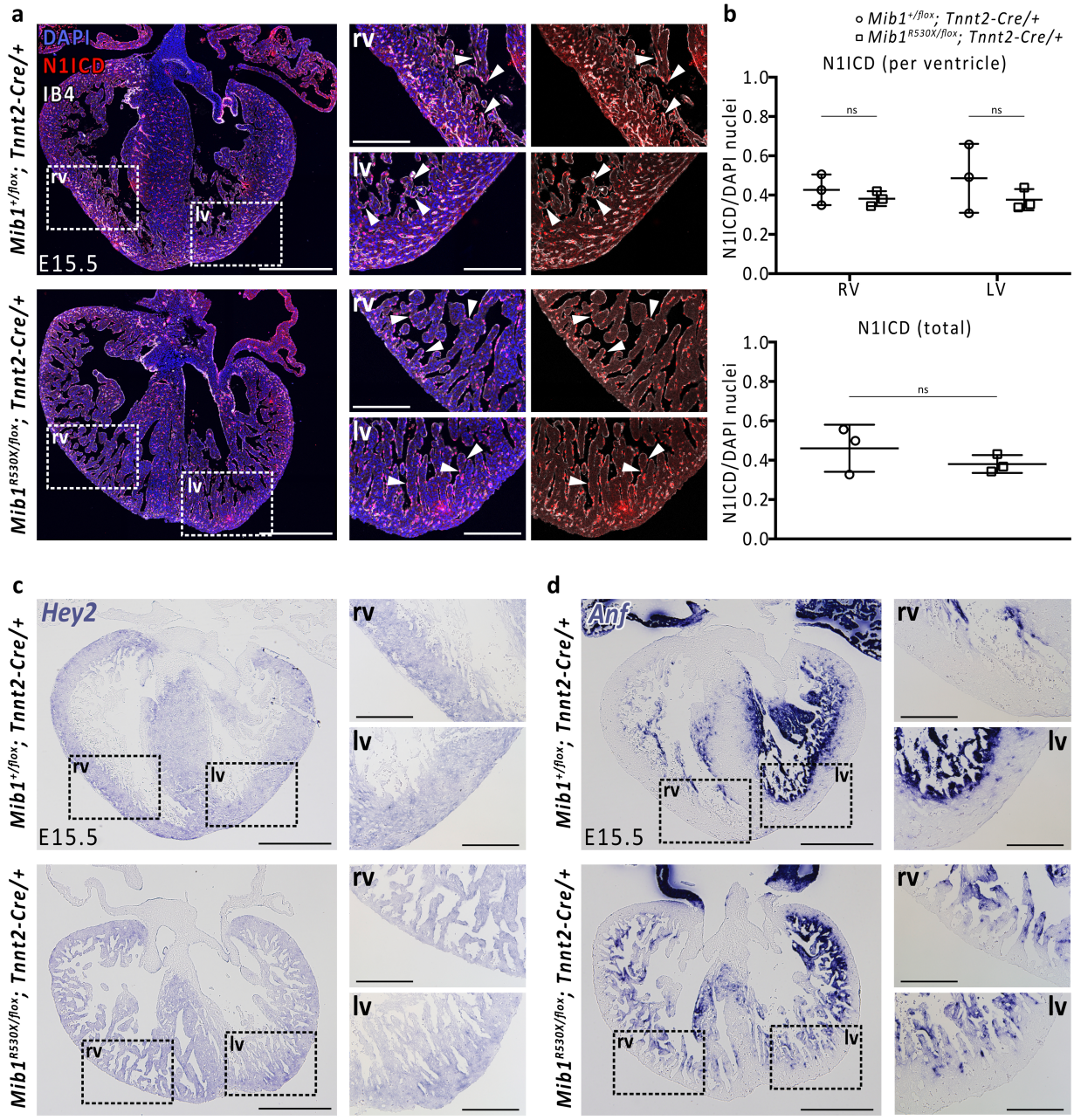

Figure 10: **Mib1$^{R530X/flox}$; Tnnt2-Cre** ***hearts show no statistically significant decrease of N1ICD in the E15.5 endocardium, but myocardial patterning is disrupted.*** *a.- Activity of the NOTCH pathway, detected as nuclear N1ICD staining (white arrowheads), is not altered in mutant endocardium. b.- Quantification of nuclear N1ICD ratio in the endocardium of each ventricle (upper panel) or both (lower panel). Data were not statistically significant in any comparison. c.-* Hey2 in situ *hybridisation (ISH) shows that morphological trabeculae express this compact myocardial marker. d.-* Anf *shows a decrease in its transcription, especially in the apex of the left ventricle. Scale bars: leftmost panels (a, c and d), 500 µm; magnifications, 200 µm.*

NOTCH PATHWAY SENSITISATION EXPERIMENTS DEMONSTRATE AN EFFECT OF *MIB1* MUTATIONS IN VALVE DEVELOPMENT

Due to the lack of phenotype in Mib1^{V943F} mice, we decided to genetically sensitise these mice introducing the *Notch1^{KO}* mutation in heterozygosity, thus lowering the overall amount of Notch1 receptor. We bred our *Mib1^{R530X}* and *Mib1^{V943F}* lines (both in a C57Bl/6 background) with *Notch1$^{KO/+}$* mice (in a CD1 background) and dissected hearts at E16.5. H&E staining showed increased prevalence of valve defects in double heterozygous mice compared to *Notch1$^{KO/+}$* (Table 8). Although no chamber phenotype was present in double mutants (Figure 11a), we observed a higher frequency of enlargement of left coronary artery (LCA) roots, BAV, and thickening of the pulmonary valves (PV) (Table 8, Figure 11b). This increased penetrance indicated that both the nonsense and the missense mutations affect Mib1 function, synergizing with Notch1 haploinsufficiency. It also suggests that, in the mouse, valve development is more sensitive to NOTCH pathway insufficiency than the ventricles.

	Mib1^{V943F}	***Mib1$^{R530X/+}$***	***Mib1$^{V943F/R530X}$***	***Mib1$^{V943F/+}$; N1$^{KO/+}$***	***Mib1$^{V943F/V943F}$; N1$^{KO/+}$***	***Mib1$^{R530X/+}$; N1$^{KO/+}$***	***N1$^{KO/+}$***
Normal	12	11	11	5	9	7	8
BAV	-	-	-	1	1	2	-
Wide LCA root	-	-	-	2	-	-	-
Thickened PV	-	-	-	3	2	5	2
TGA	-	-	-	-	-	1	1
PV misalignment	-	-	-	1	-	-	-
MV&TV defects	-	-	-	1	-	1	-
VSD	-	-	-	1	1	1	1
TOTAL	12	11	11	10	12	13	11
% with phenotype	**0%**	**0%**	**0%**	**50%**	**25%**	**46%**	**27%**

*Table 8: **Mib1 mutations increase the prevalence of valve defects in a Notch1 sensitised background.** Mib1$^{V943F/+}$ or Mib1$^{V943F/V943F}$ (both under Mib1^{V943F} category), and Mib1$^{R530X/+}$ mice do not show any valve phenotype. Penetrance of BAV increases when these mutations are present in Notch1$^{KO/+}$ background, and, overall, the penetrance of valve defects is increased in double heterozygotes (50% and 46% for Mib1$^{V943F/+}$ and Mib1$^{R530X/+}$, respectively, and 27% for N1$^{KO/+}$mice).*

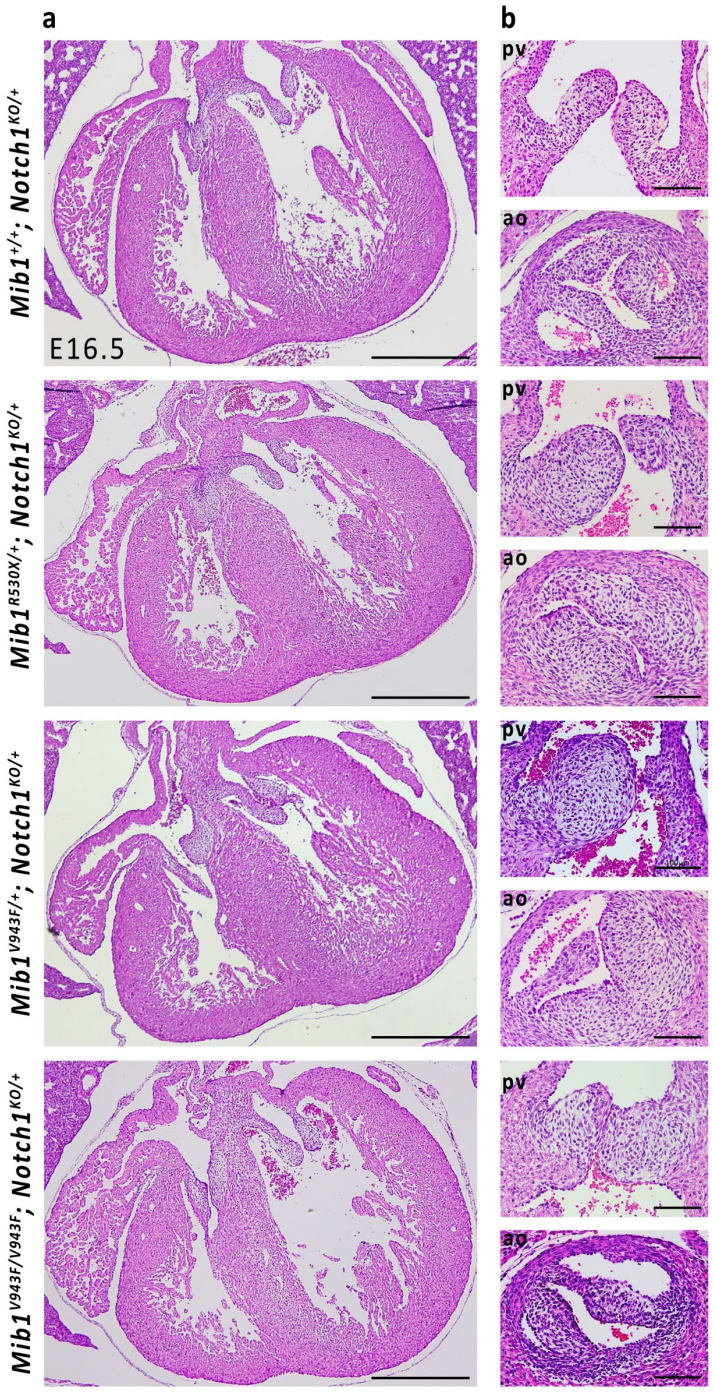

Figure 11: ***Mib1 point mutations combined with Notch1$^{KO/+}$ mutation increase the prevalence of thickened pulmonary valves and BAV.*** *a.- Mutant mice do not show any morphological defect in chamber development. b.- Double mutants show increased proportion of pulmonary valve thickening and BAV. Scale bars: a, 500 µm; b, 100 µm. pv, pulmonary valve; ao, aortic valve.*

IDENTIFICATION OF VARIANTS COSEGREGATING WITH *MIB1* MUTATIONS USING EXOME SEQUENCING

Our results suggest that, despite affecting Mib1 function, mutations identified in LVNC patients may not be the only cause of the disease, suggesting that LVNC could have an oligogenic nature. To identify possible additional variants that could be cosegregating with the disease and with *MIB1* mutations, our collaborators recruited more members from the two initial families, thus expanding the initial pedigrees (Figure 15 andFigure 16). We performed exome sequencing in 8 LVNC patients and 6 healthy relatives from the R530X family, and in 7 individuals with LVNC, 1 hypertrophic cardiomyopathy (HCM) patient, 1 member with a hypertrabeculated heart (but not fulfilling diagnostic criteria) and 4 of the healthy kin from the V943F family. We sequenced DNA obtained from blood samples and used the strategy summarised in Figure 12 to identify potential cosegregating variants.

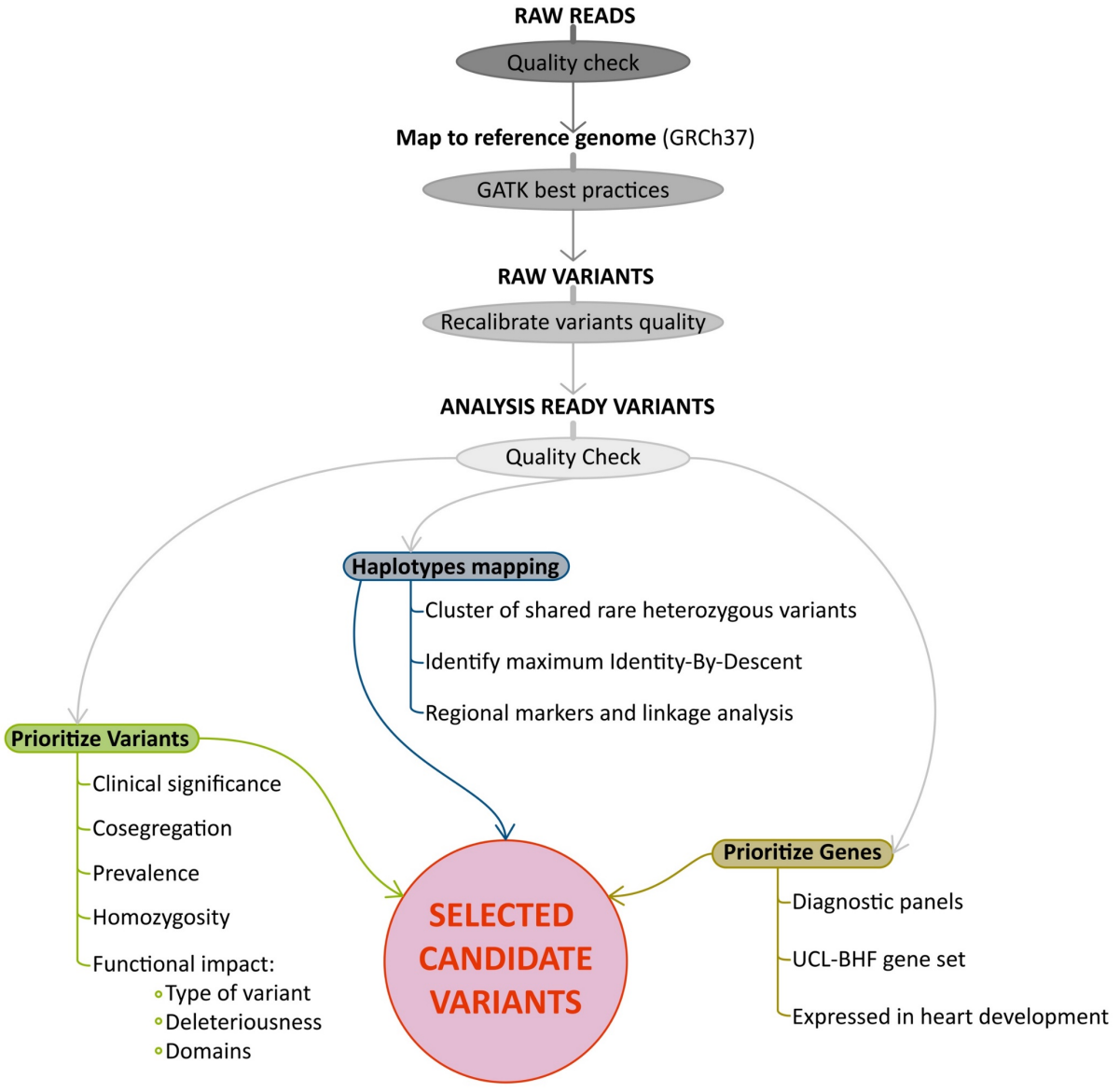

Figure 12: ***Diagram of the strategy followed to identify candidate variants causing LVNC after exome sequencing.***

As a summary, after obtaining the raw reads and filtering out the sequences with low quality, we mapped them to the last reference human genome (GRCh37). These mapped reads were subjected to GATK best practices (McKenna et al., 2010), including labelling duplicates, local realignment, reassessment of base quality scores and using HaplotypeCaller, that can better identify indels. The quality of the raw variants called through this procedure was recalibrated to obtain variants ready for the analysis. Then, we used three different approaches to select candidate variants:

1.- Filtering based on variants: We used databases as ClinVar to consult if the found variants were already described in CHD or related syndromes. We also checked the prevalence of the polymorphisms and their presence in homozygous condition in gnomAD (Karczewski et al., 2019). Another criterion was their predicted functional effect, based on the type of mutation (nonsense, missense, synonymous…), how deleterious they can be (using CADD, PolyPhen, SIFT and LoFtool, from the Variant Effect Prediction of ensembl) or the domain that they can affect (based on PFAM, PROSITE, etc.) (McLaren et al., 2016).

2.- Haplotypes mapping: Looking for rare variants inherited together in affected relatives, using variants themselves (Rare Heterozygous Rule Out) or markers of regions (Identity-By-Descent or Collapsed Haplotype Patterning described in (Wang et al., 2014).

3.- Gene-centred strategy: We searched several gene databases for information regarding their linkage to CHD (e.g. HealthInCode's), their annotation in Cardiovascular Gene Ontology (University College of London and British Heart Foundation) and their expression in heart development (National Center for Biotechnology Information (NCBI), published RNA Sequencing experiments).

Using this combination of filters, and given that our cohorts were big enough, we could identify two candidate variants in the R530X family: rs3748415, Val150Ile mutation in APCDD1, and rs181303838, Met1415Val in ASXL3. These variants were found in heterozygosity in all affected members of the family and in none of the healthy relatives (Figure 13).

APCDD1 is an inhibitor of WNT signalling pathway (Shimomura et al., 2010), which is fundamental in heart development (Marvin, 2001; Schneider and Mercola, 2001) and interacts with NOTCH pathway (Berndt et al., 2011; Li et al., 2012). ASXL3 is a member of *Additional Sex Comb-like* family, containing a Plant Homeodomain and thus presumably regulating the expression of homeotic genes (Fisher et al., 2006; Katoh and Katoh, 2003). It has also been shown to repress target genes of LXRα, playing a role in lipid homeostasis (Shin et al., 2014) and nonsense mutations in this gene have been linked to the human Bainbridge-Ropers syndrome (Bainbridge et al., 2013).

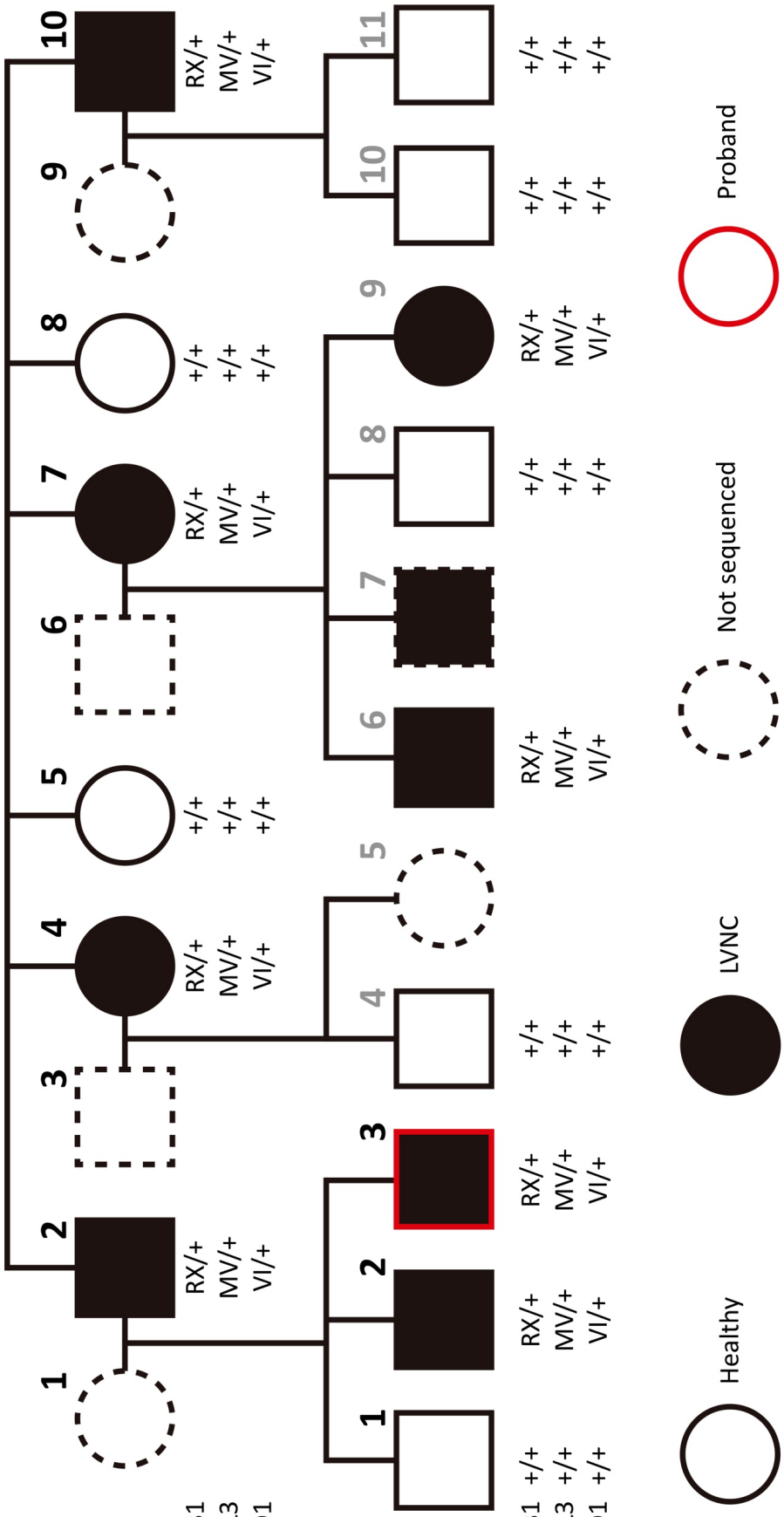

Figure 13: ***Variants found in R530X family.*** *All sequenced LVNC patients (filled shapes) carry the identified mutations (ASXL3^{M1415V} and APCDD1^{V150I}) in addition to the previous MIB1^{R530X} variant, while healthy relatives (blank shapes) do not carry any of them. Grey numbers indicate newly recruited family members.*

In the family carrying *MIB1* missense mutation, the situation was more complex. As our hypothesis was that LVNC inheritance pattern is oligogenic, and given that this disease has a wide range of severity and is frequently associated with other cardiomyopathies, we looked for different combinations of variants in these family members. We found that all the sequenced LVNC patients carry four mutations in heterozygosity in combination with $MIB1^{V943F}$: rs141331552, Thr1522Met in CEP192; rs143627864, Phe191STOP in TMX3 isoform 3; and rs884785 and rs884786, two intronic variants (c.175-56A>G and c.175-27G>A, respectively) in intron 2 of *BCL7A*. The relative with the hypertrabeculated heart only carries $MIB1^{V943F}$ and $CEP192^{T1522M}$ heterozygous mutations. The HCM patient carries both *BCL7A* mutations in homozygosity. The other relatives do not carry any of these mutations (Figure 14).

CEP192 is a centrosomal protein (Andersen et al., 2003) fundamental for the formation of the mitotic spindle (Gomez-Ferreria et al., 2007) and for the recruitment of Polo-like kinase 4 (Plk4), essential for the duplication of centrioles (Sonnen et al., 2013). TMX3 is a thioredoxin-related protein that catalyses the isomerization of protein disulphide bonds (Haugstetter et al., 2005). Mutations in this gene have been linked to microphtalmia (Chao et al., 2010) and it is located to the locus deleted in the *no turning* mutant, that showed a cardiac phenotype similar to NOTCH LoF, with incomplete heart looping and dilated pericardial cavity (Melloy et al., 1998). BCL7A was first described in a Burkitt lymphoma linked translocation (Zani et al., 1996). It is a context specific part of the SWI/SNF complex (Wischhof et al., 2017) that has significant homology to the domain that mediates actin binding in Caldesmon and to the α-helical repeat found in the smooth-muscle cell isoform of that actin-myosin binding interaction regulator (Zani et al., 1996). *Bcl7a* deletion in the whole embryo caused late foetal or perinatal lethality, while deletion in nervous system caused motor neuron coordination defects in adult mice (Wischhof et al., 2017).

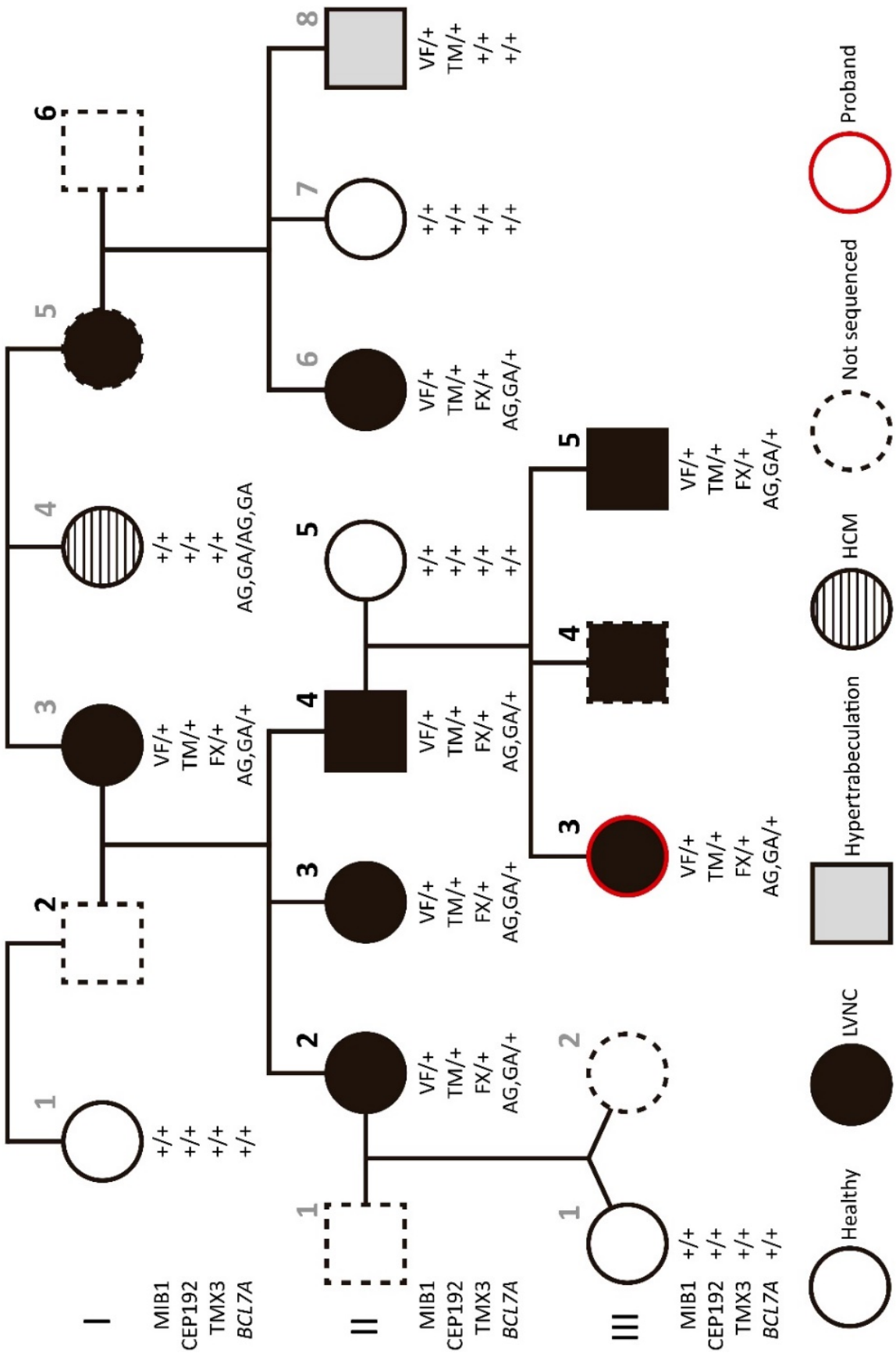
I
II
III
MIB1
CEP192
TMX3
BCL7A
+/+
VF/+
TM/+
FX/+
AG,GA/+
AG,GA/AG,GA
Healthy
LVNC
Hypertrabeculation
HCM
Not sequenced
Proband

Figure 14: ***Variants found in V943F family.*** *All sequenced LVNC patients (black filled shapes) carry the identified mutations (MIB1$^{V943F/+}$ CEP192^{T1547M} TMX3^{F191X} and* BCL7A^{AG,GA} *in heterozygosity). HCM patient (striped circle) only carries* BCL7A^{AG,GA}*, but in homozygosity. The relative with hypertrabeculation (grey shaded square) has MIB1^{V943F} and CEP192^{T1547M} mutations, also in heterozygosity. The other healthy members (blank shapes) do not carry any of them. Numbers in grey indicate newly recruited family members.* *(Previous page)*

R530X family

Importantly, the additional genes mutated in R530X family are all located in chromosome 18, where *MIB1* maps. Both are physically very close to *MIB1*, increasing the chances of cosegregation. In mouse chromosome 18 *Apcdd1* is in the long arm, contrary to human, where it is in the short arm, closer to *MIB1* than *ASXL3* (Figure 15a).

The mutation found in *APCDD1* alters Val150, conserved from human to zebrafish (Figure 15b, left panel). *ASXL3*, however, has no direct orthologue in *Danio rerio*. Met1415 is conserved in all eutherians examined (Human and mouse (Met1416) shown as examples), and its hydrophobicity is maintained in *Xenopus laevis*' Leu1368. (Figure 15b, right panel). Deleteriousness predictions and prevalence data were not clear for any of the variants. While APCDD1^{V150i} mutation was predicted as more deleterious than ASXL3^{M1415V} (higher intolerance of the gene to LoF variants (LoFTool, 0.555 and 0.222, respectively), and more evolutionarily conserved (CADD Phred (18.23 and 11.29) and Genomic Evolutionary Rate Profiling (GERP, 2.36 and -1.32)), its prevalence was far higher. Despite this high presence in human populations (0.116), we did not discard this mutation, as its combination with MIB1^{R530X} would still fit in the frequency of LVNC (Figure 15c). The final filter used to select these variants was to confirm the expression of these genes during mouse heart development, especially in the period where compaction starts (E12.5-E14.5). We performed qPCR of whole hearts from C57Bl/6 animals at stages ranging from E10.5 to E16.5 and demonstrated that *Apcdd1* and *Asxl3* are regulated differentially during this time frame (ANOVA p-value less than 0.0001 in both cases). *Apcdd1* peaks at E12.5 and then its expression declines progressively, as is the case for *Asxl3* (although this gene does not increase its transcription from E12.5 to E14.5) (Figure 15d).

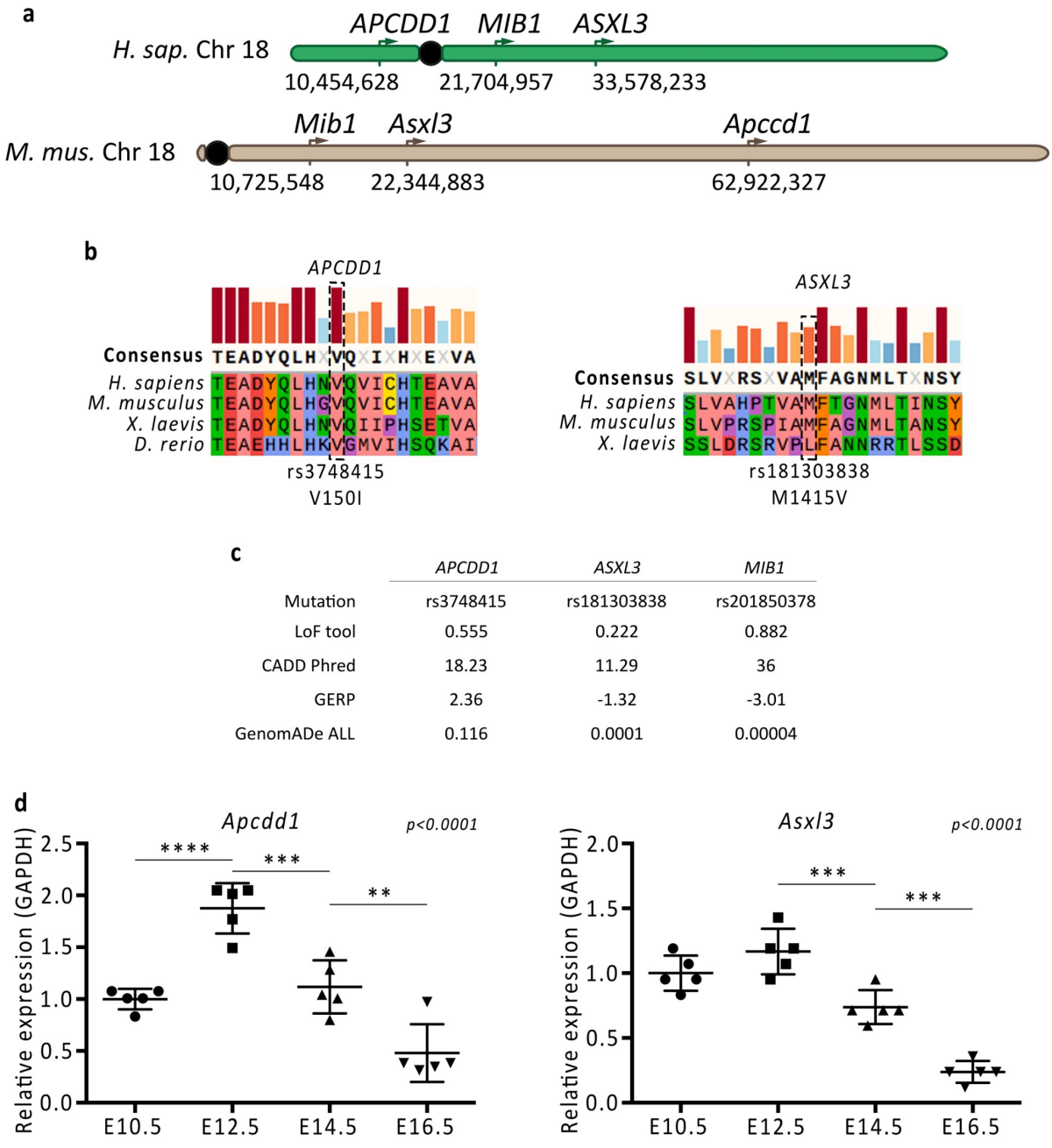

Figure 15: ***Characterization of candidate variants and genes selected in R530X family.*** *a.- Chromosomal locations of the candidate genes identified in human and murine chromosome 18. b.- Conservation of the affected aminoacids found altered in LVNC patients. c.- Predicted scores of deleteriousness and functional effect of the variants, and prevalence in genomADe database. d.- qPCR results of the candidate genes in murine hearts at several stages of development, relative to* GAPDH *levels. Both genes peak around the time when myocardial compaction starts, and their transcription is regulated through this time period (ANOVA p-values indicated, and symbols depicting multiple t-test comparisons). **, p-value<0.01; ***, p-value<0.001; ****, p-value<0.0001.*

V943F family

CEP192 and *TMX3*, two of the candidate genes identified in V943F family are physically linked to *MIB1*, but BCL7A is not. In the case of humans, *CEP192* locates in the short arm, very close to *MIB1*. In mice, however, this gene is further away in a translocated region of the long arm. In both species, *TMX3* is localised at the end of the long arm, almost 50 Mb away from *MIB1* in humans and 80 Mb away from *Mib1* in mice. *BCL7A* is located in chromosome 12, suggesting that its cosegregation with *MIB1* was less likely, making it an interesting candidate gene (although sample size was not big enough to determine its statistical significance). This gene is located in the long arm of murine chromosome 5 (Figure 16a). CEP192 Thr1547 (Thr1522 in mouse) is located in a highly conserved region of the amino acidic sequence in zebrafish and all *tetrapoda*, although the substitution for a Methionine found is present in *Xenopus laevis*, changing that position from nucleophilic to hydrophobic (Figure 16b, left panel). In the case of *BCL7A*, both intronic mutations are conserved from *Danio rerio* to *Homo sapiens*, although there are small differences in the distance between them depending on the species (Figure 16b, right panel). *CEP192* is quite tolerant to missense mutations, but not so much to LoF (LoFtool=0.85). CADD value, which takes conservation and effect on the protein into account, is high for CEP192^{T1547M} (20.8), although under the threshold usually considered as deleterious. As expected, this predictor for *BCL7A* intronic variants shows low numbers (5.562 and 1.843), as does GERP (-2.73 and -5.73). GERP score for CEP192^{T1547M} (0.90) was also not very promising. But the prevalence of this mutation is low enough (0.00003) to take it into account. *BCL7A* mutations are quite prevalent (rs884785, 0.11; rs884786, 0.032), but, in combination with *MIB1* mutation or in homozygosity, they are under LVNC or HCM prevalence (Figure 16c). As qPCR results showed, these genes are expressed from E10.5 to E14.5, with a significant decline in their transcription after this stage, showing a time-dependent expression (ANOVA p-value is 0.029 for *Cep192* and 0.0002 for *Bcl7a*) (Figure 16d).

The study of the *TMX3* mutation turned out to be more complex due to the existence of several protein coding isoforms. The mutation identified (c.637+16_637+17del) affects intron 9 of the main isoform (*TMX3-201*). But it is also a nonsense mutation in Phe191 (TTT) of isoform *TMX3-202*, located in its exon 8 (exon 9 of the main isoform with part of intron 9, as alternative splicing discards exon 6), that creates a stop codon when the last two Ts from the codon are deleted moving ahead the first two As from Asp192 (AAC). The remaining protein coding isoform, *TMX3-204*, is composed of the first 8 exons of the main isoform, with an alternative 3'end fragment including part of intron 8 of *TMX3-201*. This third isoform encodes VIFKI sequence in this fragment of intron 8, with a Phe191 (TTT) in this isoform too, followed by Lys192 (AAA). The deletion c.579+8_c.579+9_del, analogous to that generating TMX3-202^{F191X}, would thus cause the same nonsense mutation, but in TMX3-204 (Figure 17a).

Although the DNA sequence is conserved at that amino acid position, in mouse there is a previous stop codon (Q189X). In the case of humans, the TMX3-202^{F191X} mutation generates a 6 amino acids shorter

protein. Surprisingly, similarity is higher between *H. sapiens* and *D. rerio,* where the shortening of the protein sequence would be far larger, than with *X. laevis* (Figure 17b, left panel).

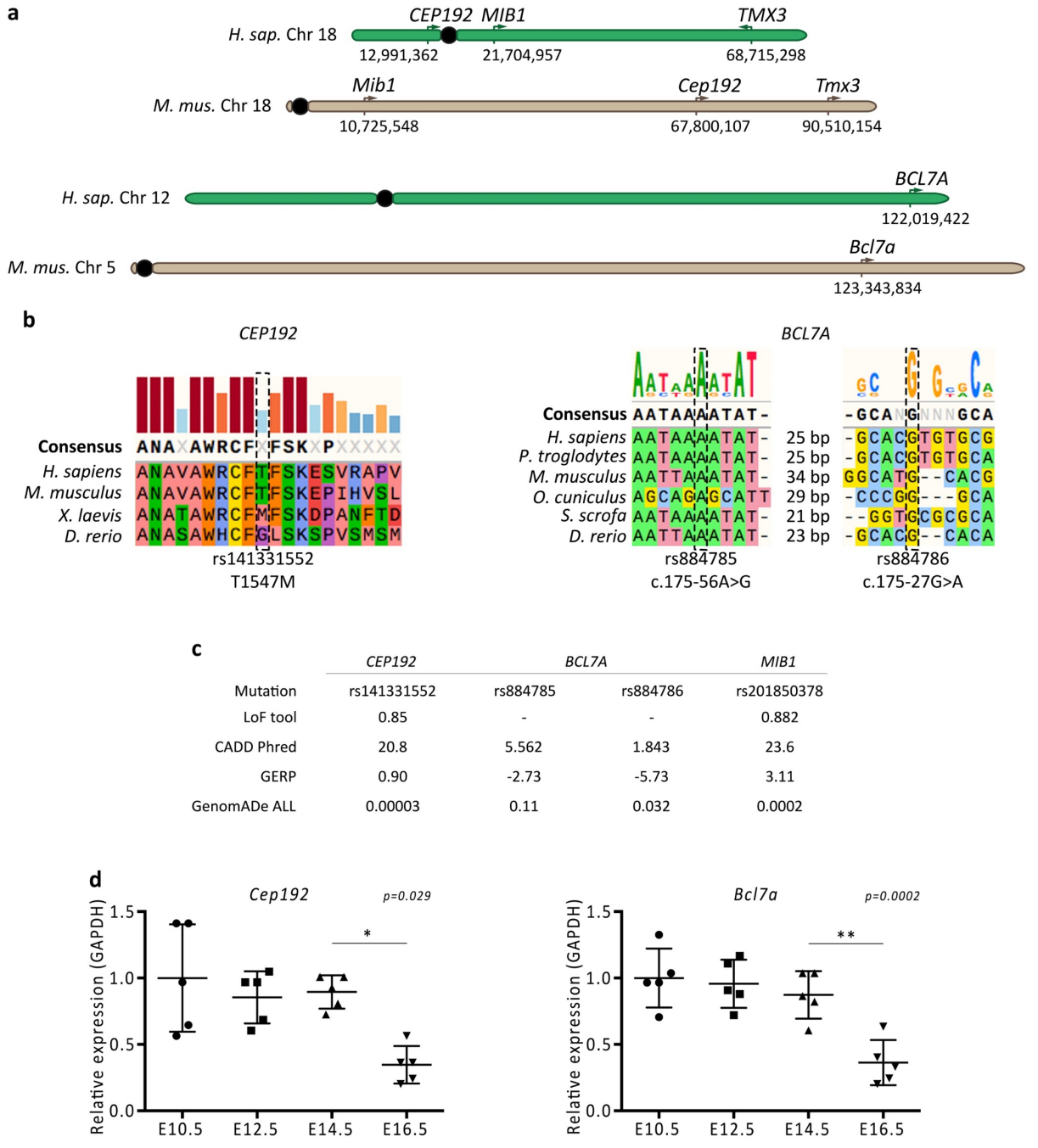

Figure 16: ***Characterization of candidate variants and genes selected in V943F family.*** *a.- Chromosomal locations of the genes in which variants were found in human and mouse. b.- Conservation of the amino acidic and DNA sequences in the regions affected by the variants. c.- Main predictors and prevalence data of the identified variants. d.- Expression of the genes during mouse heart development, evaluated by qPCR as relative to* GAPDH *levels. ANOVA test was performed, and both genes shoed a dynamic expression through the period examined. *, p-value<0.05; **, p-value<0.01.*

TMX3-204^{F191} is conserved in human, mouse and zebrafish, and in African clawed frog this position is occupied by a Tyr, maintaining most physicochemical properties. The nonsense mutation of this residue would lead to a two aminoacids shorter protein in both human and mouse, a 12 aminoacids long loss in *X. laevis*, and a protein lacking 61 aminoacids in zebrafish (Figure 17b, right panel). The mutation found in *TMX3*, the one affecting *TMX3-202*, modifies a not very sensitive to LoF mutations gene (LoFTool score: 0.19), but in a residue that is somehow subject to selective pressure (GERP score: 0.90) and with a substitution with a frequency that could fit in LVNC prevalence in combination with any of the other suspect mutations found in V943F family (Figure 17c).

The homolog isoforms to *TMX3-202* and *TMX3-204* are not annotated in mouse. To determine if there is a *Tmx3-204* isoform expressed in mouse heart, we designed two different pairs of primers for RT-PCR. One forward (long) primer binds to exon 6, the other (short) is homologous to a sequence in exon 7. The common reverse primer binds to the putative 3'UTR, located in the intron 8 of the main isoform, and allows us to amplify *Tmx3-204* alone. When we performed the RT-PCR with RNA extracted from whole E14.5 hearts we could detect this undescribed isoform in mouse (Figure 17d).

GENERATION OF MICE CARRYING MUTATIONS IDENTIFIED BY EXOME SEQUENCING

After the identification of the candidate variants, we decided to generate the triple (*Mib1*$^{R530X/+}$ *Apcdd1*$^{V150I/+}$ *Asxl3*$^{M1416V/+}$) and quadruple (*Mib1*$^{V943F/+}$ *Cep192*$^{T1522M/+}$ *Tmx3-204*$^{F191X/+}$; *Bcl7a*$^{AG,GA/+}$) mutants using CRISPR-Cas9. This approach was intended to mimic the autosomal dominant pattern of inheritance of the disease found in the patients, generating a more similar genetic model for LVNC. In order to make the maintenance of the lines easier, we decided to try to generate the *cis*-heterozygote lines so, if the genes are linked, we would obtain a higher frequency of multiple heterozygotes. For us, this was feasible considering the results obtained in the previous microinjections (Table 4), and having the *Mib1*$^{R530X/+}$ and *Mib*$^{V943X0+}$ lines already established.

We performed the microinjections in zygotes coming from crosses between *Mib1* mutant males (*Mib*$^{V943F/V943F}$ or *Mib*$^{R530X/+}$) and C57Bl/6Crl females, as depicted in Figure 18, left illustrations, with synthetic crRNA and tracrRNA incubated beforehand with Cas9 protein and with ssODN at the concentrations indicated in Table 9. Founders were identified by PCR (Figure 18, middle panels) and confirmed by Sanger sequencing (Figure 18, right panel). We were able to obtain single and multiple mutants in all microinjections but the second Cep192 + Tmx3 experiment, as no pup was born. In the other experiment with these reagents, we obtained 1 triple heterozygote founder (*Mib1*$^{V943F/+}$ *Cep192*$^{T1522M/+}$ *Tmx3-204*$^{F191X/+}$) out of 4 survivors (25%). In the Bcl7a microinjection, with only one crRNA and one ssODN carrying the intronic variants, we obtained 13 founders out of 21 pups (61.9%) with both intronic mutations. For the polymorphisms found in R530X family, we got 2 triple heterozygotes (*Mib1*$^{R530X/+}$ *Apcdd1*$^{V150I/+}$ *Asxl3*$^{M1416V/+}$) out of 16 (12.5%) (Table 9).

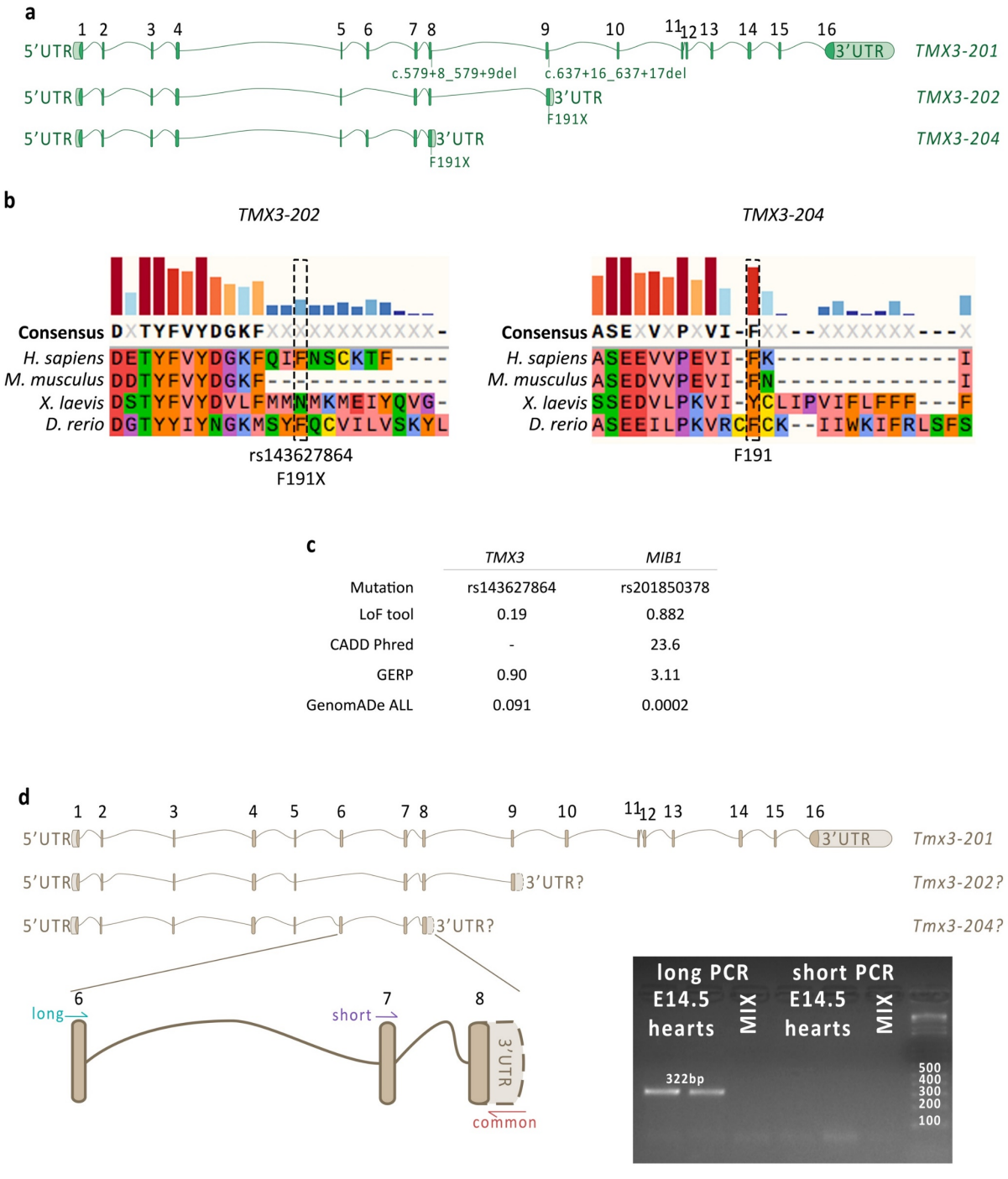

Figure 17: ***Different protein coding isoforms of*** **TMX3** ***and characteristics of the mutation identified in V943F family and the one introduced in mouse.*** *a.- Structure of the gene in human. Exons are numbered and represented by boxes, introns as lines. Each isoform is labelled at the right, with* TMX3-201 *being the main isoform. The effect of the mutations is shown in the affected isoform, and in the main isoform as intronic. The identified variant is a deletion of two base pairs in intron 9 that creates a nonsense mutation in exon 8 of the* TMX3-202 *isoform. The mutation we introduced in mouse is a similar deletion in the previous intron that generates a premature STOP codon in exon 8 of the other isoform. b.- The terminal part of the protein encoded by isoform 202 is not conserved (left panel), but the one introduced in mouse genome affects a conserved Phe (right panel). c.- Main characteristics found regarding the variant found in human compared to those of MIB1^{V943F}. d.- Genetic structure of* Tmx3 *in mouse. The mouse homologous isoform to human main isoform shares its structure, but other protein encoding transcript are not described. Testing if the putative homologous isoform to human* TMX3-204 *was expressed in E14.5 hearts by RT-PCR was successful, using primers hybridising at exon 6 and predicted 3'UTR of the isoform (bottom panels).*

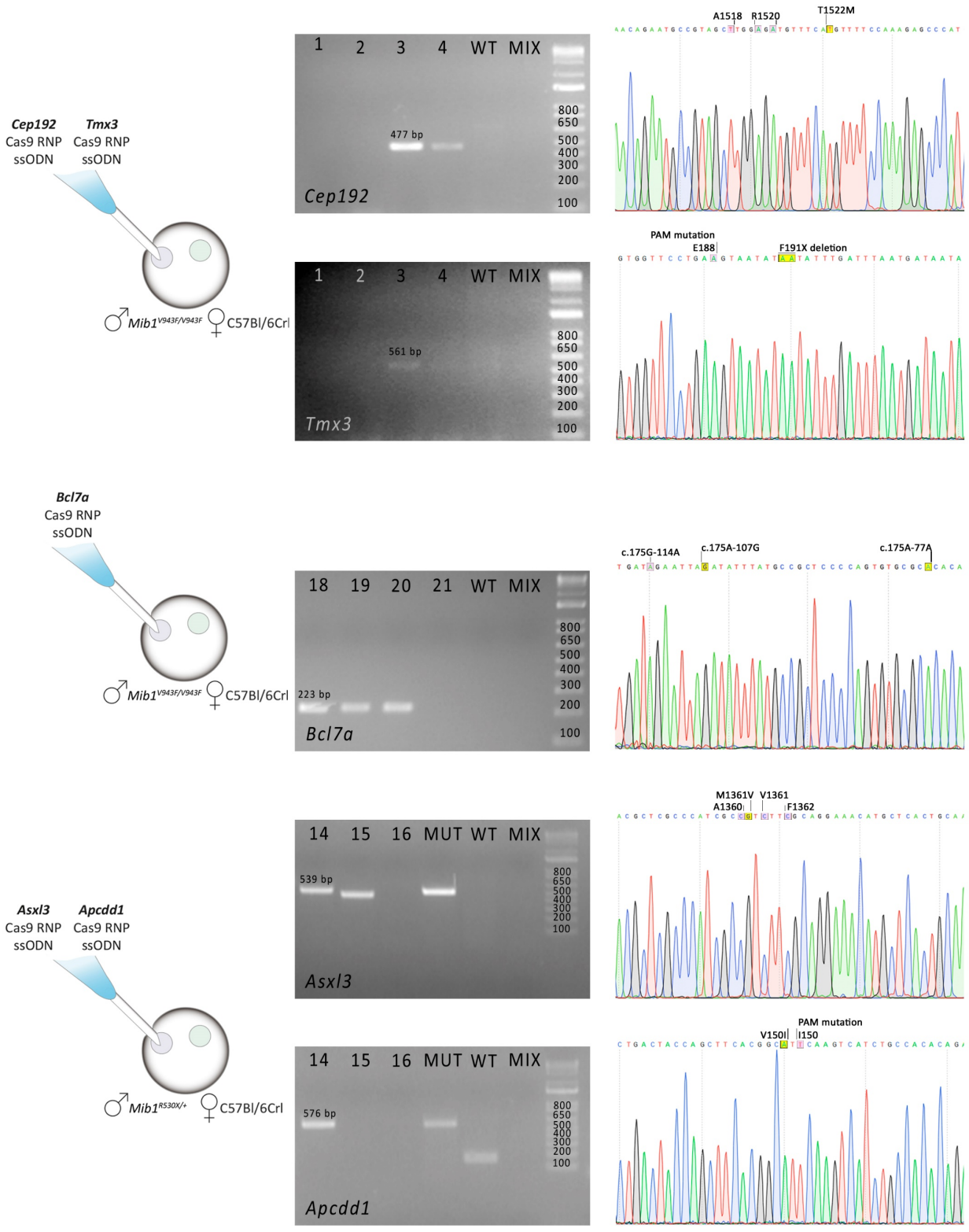

Figure 18: ***Microinjection and screening strategy to obtain double and triple heterozygotes.*** *Reagents used in each microinjection are shown in left panels, together with the genotypes of the parents of the microinjected oocytes. When born pups were weaned, we subjected tail biopsies to specific PCRs for the detection of the inserted mutations (middle panels), and the fragment surrounding the mutations was amplified, subcloned and sequenced by Sanger (rightmost panels), demonstrating the successful obtaining of gene-edited animals with both mutations in the cases of* Tmx3 *and* Cep192 *(animal 3) and* Asxl3 *and* Apcdd1 *(Animal 14) and mutants of* Bcl7a *carrying both intronic mutations.*

Microinjection	Embryos	[Cas9] (ng/µL)	[crRNAs] (µM)	[tracrRNA] (ng/µL)	[ssODN] (ng/µL)	Born	Weaned	Mutant (1)	Mutant (2)	Founders (1∩2)
Cep192 (1) + Tmx3 (2)	68	30	0.305 + 0.305	0.61	5 + 5	8	4	1	1	1 (25.0%)
Cep192 (1) + Tmx3 (2)	102	20	0.244 + 0.244	0.488	5 + 5	0	0	0	0	0
Bcl7a	75	30	0.305	0.61	10	21	21			13 (61.9%)
Asxl3 (1) + Apcdd1 (2)	61	30	0.305 + 0.305	0.61	5 + 5	16	13	2	2	1 (7.7%)
Asxl3 (1) + Apcdd1 (2)	95	20	0.305 + 0.305	0.61	5 + 5	3	3	1	1	1 (33.3%)

Table 9: ***Generation of double mutants in the background of previously generated Mib1 knock-in lines.*** *Results of each experiment to generate the triple mutant lines of Chr. 18 and the Bcl7a double mutant line.*

The founders generated were then bred with C57Bl/6 mice to dilute as much as possible the effect of any possible off-target of CRISPR-Cas9 gene edition. These crosses also allowed us to examine if the mutations were introduced in *cis* heterozygosity or in *trans* and to begin analysing the phenotype of the mice. The results of this cross (Table 10) show that obtaining single mutants was very rare, while most of the animals were either triple heterozygotes or completely WT, indicative of *cis* heterozygosity. We compared the proportions of the double mutant combination with the complementary segregation, and found that mice carrying *Asxl3*$^{M1415V/+}$*Apcdd1*$^{V150I/+}$ were obtained in a significantly decreased ratio than their counterpart (31.03% *vs.* 41.38% of the total, 42.86% and 57.14% of mice in which both genes cosegregated). In addition to that, we could ascertain that we had generated the *cis* triple heterozygote comparing the number of mice with cosegregating alleles *versus* the number with mixed markers. We found all the pairs of genes to be linked (Table 11).

	Mib1$^{R530X/+}$ ***Asxl3***$^{M1416V/+}$ ***Apcdd1***$^{V150I/+}$	***Mib1***$^{R530X/+}$ ***Asxl3***$^{+/+}$ ***Apcdd1***$^{V150I/+}$	***Mib1***$^{R530X/+}$ ***Asxl3***$^{M1416V/+}$ ***Apcdd1***$^{+/+}$	***Mib1***$^{+/+}$ ***Asxl3***$^{M1416V/+}$ ***Apcdd1***$^{V150I/+}$
E12.5	8	2	3	1
TOTAL: 20	40.00%	10.00%	15.00%	5.00%
E14.5	11	0	3	0
TOTAL: 26	42.31%	0.00%	11.54%	0.00%
E16.5	18	5	11	0
TOTAL: 79	22.78%	6.33%	13.92%	0.00%
P21	50	8	8	2
TOTAL: 165	30.30%	4.85%	4.85%	1.21%

	Mib1$^{R530X/+}$ ***Asxl3***$^{+/+}$ ***Apcdd1***$^{+/+}$	***Mib1***$^{+/+}$ ***Asxl3***$^{+/+}$ ***Apcdd1***$^{V150I/+}$	***Mib1***$^{+/+}$ ***Asxl3***$^{M1416V/+}$ ***Apcdd1***$^{+/+}$	***Mib1***$^{+/+}$ ***Asxl3***$^{+/+}$ ***Apcdd1***$^{+/+}$
E12.5	0	2	0	4
TOTAL: 20	0.00%	10.00%	0.00%	20.00%
E14.5	1	2	0	9
TOTAL: 26	3.85%	7.69%	0.00%	34.62%
E16.5	3	12	0	30
TOTAL: 79	3.80%	15.19%	0.00%	37.97%
P21	16	23	1	57
TOTAL: 165	9.70%	13.94%	0.61%	34.55%

Table 10: ***Results of breeding triple mutant mice carrying mutations identified in the R530X family with C57Bl/6 mice.*** *The specified totals refer to the sum of all genotypes at each stage.*

	Mib1$^{R530X/+}$ Asxl3$^{M1416V/+}$	***Mib1$^{R530X/+}$ Apcdd1$^{V150I/+}$***	***Asxl3$^{M1416V/+}$ Apcdd1$^{V150I/+}$***
TOTAL: 264	112 38.62%	102 35.17%	90* 31.03%
	Mib1$^{+/+}$ Asxl3$^{+/+}$	***Mib1$^{+/+}$ Apcdd1$^{+/+}$***	***Asxl3$^{+/+}$ Apcdd1$^{+/+}$***
TOTAL: 264	139 47.93%	101 34.83%	120 41.38%
	Mib1-Asxl31	***Mib1-Apcdd1***	***Asxl3-Apcdd1***
TOTAL: 264	251 86.55%****	203 70.00%****	210 72.41%****

Table 11: ***Mutations identified in R530X family were introduced in the mouse genome in* cis.** *First and second rows indicate the number of mice carrying each combination and their relative frequencies. Third row shows the sum of the data above. All combinations show higher frequencies than expected in non-linked alleles, and double* Asxl3 Apcdd1 *mutants are underrepresented. Numbers come from the total number of mice analysed in the lethality table. The specified total refers to the sum of all genotypes at all stages. * p-value=0.0451; ****p-value<0.0001.*

In the other set of mutations, we obtained similar results although cosegregation seems to be less complete than in *Mib1$^{R530X/+}$ Apcdd1$^{V150I/+}$ Asxl3$^{M1416V/+}$* mice (Table 12). When comparing the pairs of genes, we did not find any significant difference between mutant and WT alleles but we did find that, despite the distance between *Tmx3* and *Mib1* (almost 80 Mb), the three genes were linked to each other (Table 13).

	Mib1$^{V943F/+}$ Cep192$^{T1522M/+}$ Tmx3$^{F191X/+}$	***Mib1$^{V943F/+}$ Cep192$^{T1522M/+}$ Tmx3$^{+/+}$***	***Mib1$^{V943F/+}$ Cep192$^{+/+}$ Tmx3$^{F191X/+}$***	***Mib1$^{+/+}$ Cep192$^{T1522M/+}$ Tmx3$^{F191X/+}$***
E16.5	20	2	0	13
TOTAL: 85	23.53%	2.35%	0.00%	15.29%
P21	26	6	0	7
TOTAL: 72	36.11%	8.33%	0.00%	9.72%
	Mib1$^{V943F/+}$ Cep192$^{+/+}$ Tmx3$^{+/+}$	***Mib1$^{+/+}$ Cep192$^{T1522M/+}$ Tmx3$^{+/+}$***	***Mib1$^{+/+}$ Cep192$^{+/+}$ Tmx3$^{F191X/+}$***	***Mib1$^{+/+}$ Cep192$^{+/+}$ Tmx3$^{+/+}$***
E16.5	5	0	12	33
TOTAL: 85	5.88%	0.00%	14.12%	38.82%
P21	11	1	2	19
TOTAL: 72	15.28%	1.39%	2.78%	26.39%

Table 12: ***Results of breeding triple mutant mice carrying mutations identified in the V943F family with C57Bl/6 mice.*** *The specified totals refer to the sum of all genotypes at each stage.*

	Mib1$^{V943F/+}$ Cep192$^{T1522M/+}$	***Mib1$^{V943F/+}$ Tmx3$^{F191X/+}$***	***Cep192$^{T1522M/+}$ Tmx3$^{F191X/+}$***
TOTAL: 157	54 34.39%	46 29.30%	66 42.04%
	Mib1$^{+/+}$ Cep192$^{+/+}$	***Mib1$^{+/+}$ Tmx3$^{+/+}$***	***Cep192$^{+/+}$ Tmx3$^{+/+}$***
TOTAL: 157	66 42.04%	53 33.76%	68 43.31%
	Mib1-Cep192	***Mib1-Tmx3***	***Cep192-Tmx3***
TOTAL: 157	110 76.43%****	99 63.06%**	134 85.35%****

Table 13: ***Mutations identified in V943F family were introduced in the mouse genome in* cis.** *First and second rows indicate the number of mice carrying each combination and their relative frequencies. Third row shows the sum of the data above. All combinations show higher frequencies than expected in non-linked alleles. Numbers come from the total number of mice analysed in the lethality table. The specified total refers to the sum of all genotypes at all stages. ** p-value=0.0013, ****p-value<0.0001.*

Mib1$^{R530X/+}$ Apcdd1$^{V150I/+}$ Asxl3$^{M1416V/+}$ COMBINATION AFFECTS CHAMBER DEVELOPMENT

Triple heterozygous animals reach adulthood and are fertile, but their hearts show signs of developmental defects, especially in, but not restricted to, the right ventricle. These animals develop a thinner right ventricular compact myocardium at E16.5 (Figure 19a) that leads to a decreased compact/trabecular area ratio. This ratio is affected by the different combinations of mutations, and *Apcdd1$^{V150I/+}$* seems to decrease it more than *Asxl3$^{M1416V/+}$* (Figure 19b, left graph). This ratio in left ventricle is not significantly decreased, although genotype plays a role in its determination (ANOVA p-value=0.0310) (Figure 19b, right panel).

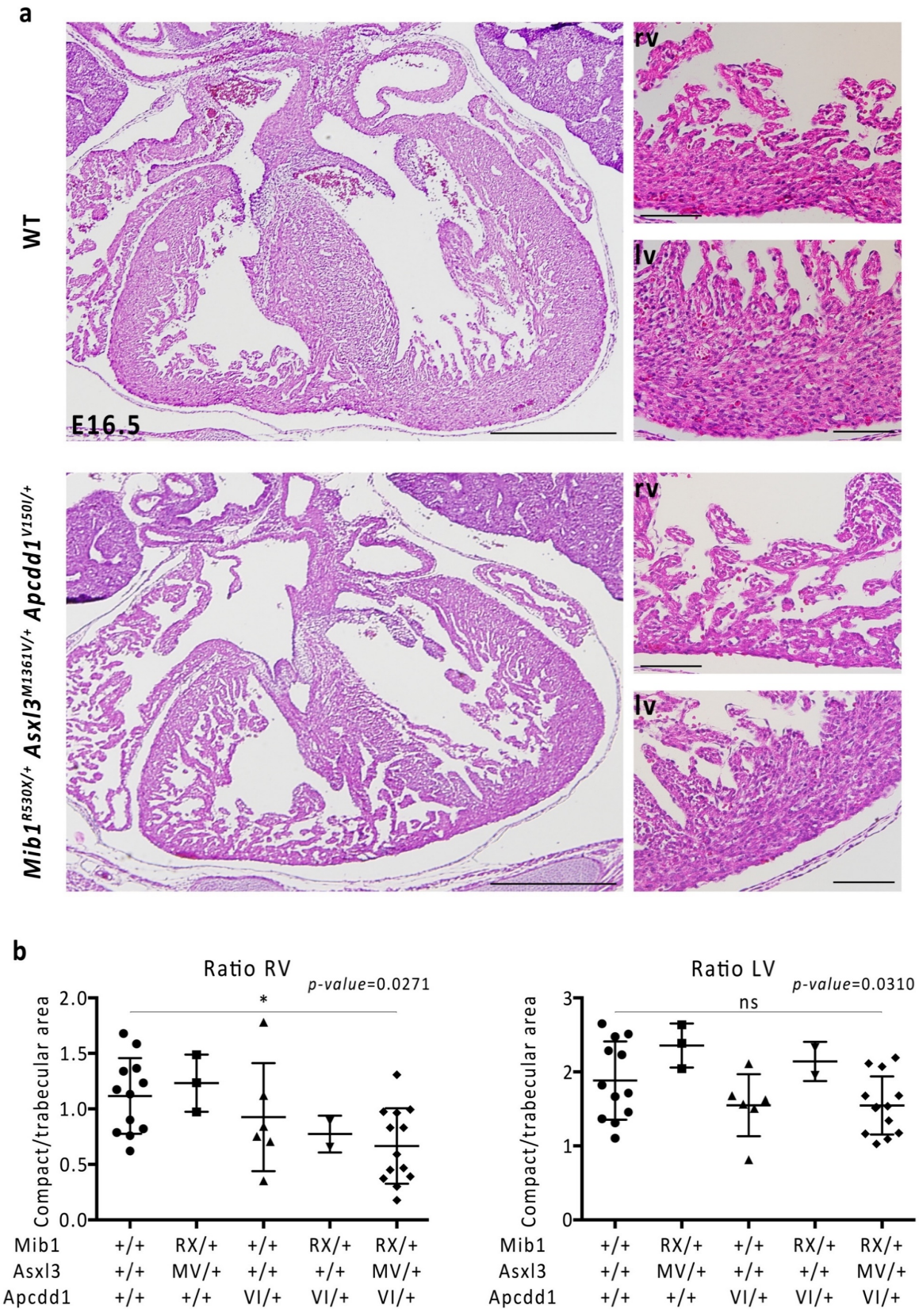

Figure 19: ***Mice carrying the three mutations identified in R530X family show defects in ventricular wall development.*** *a.- H&E staining of E16.5 hearts show thinner compact myocardial walls especially in the right ventricle. b.- Quantification of the ratio of compact and trabecular area for the right ventricle (left panel) and left ventricle (rightmost panel). ANOVA tests showed that genotype is significantly determinant for the ratio (p-values shown in the graphs), but t-tests to determine if triple heterozygotes have diminished ratios compared to the WT mice, were only significant in the right ventricle. *, p-value<0.05. ns, not significant.*

ISH showed that expression of *Hey2*, a compact myocardial marker, is maintained in morphological compact myocardium in the triple mutants. This marker, in contrast to what we observed in *Mib1*$^{R530X/flox}$*; Tnnt2-Cre* mice (Figure 10), was not expanded to the tip of the trabeculae (Figure 20, left panels), which, in turn, still maintained the expression of *Anf* (Figure 20, right panels). This could explain the differences between both models, as trabeculae do not lose their identity and their morphology is thus more conserved, although the compact myocardium is thinner and shows a more trabecular-like structure.

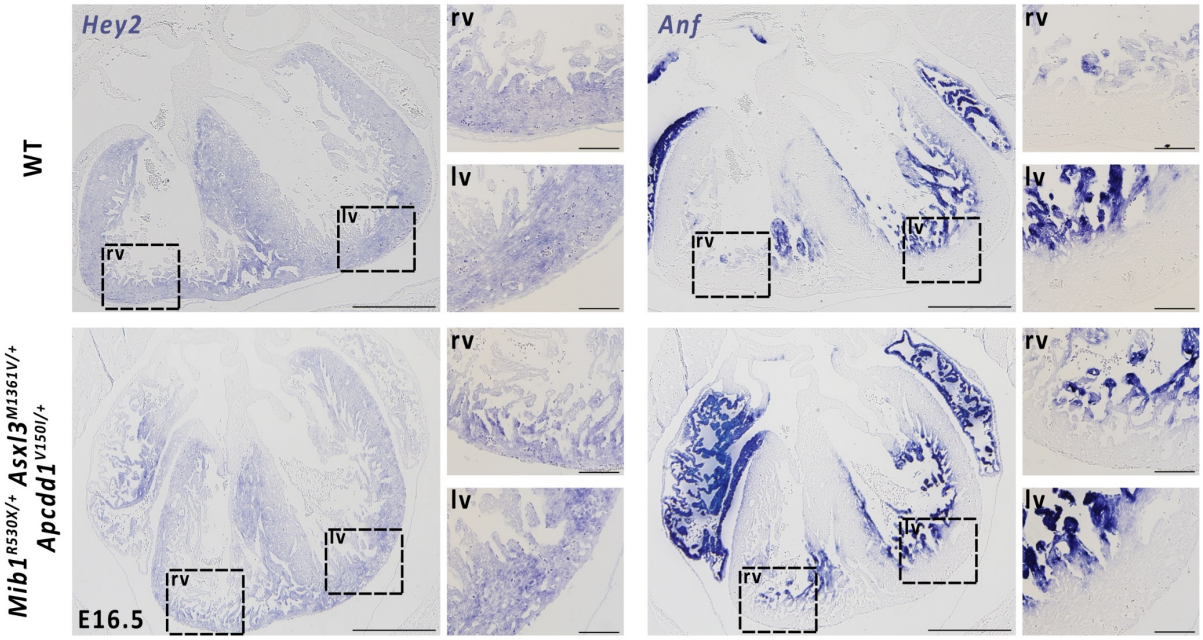

Figure 20: ***Molecular patterning of the compact and trabecular myocardium is not affected in*** **Mib1$^{R530X/+}$ Apcdd1$^{V150I/+}$ Asxl3$^{M1416V/+}$ hearts.** Hey2 ISH *(left panels) shows that the thinned compact myocardium expresses this marker, while the trabecular-like structures found are also composed of cardiomyocytes with compact identity. However, this gene is not expressed in the whole trabeculae, which maintain their molecular identity, expressing* Anf *(right panels). Scale bars: 500 µm in whole heart images, 100 µm in magnifications.*

MIB1$^{R530X/+}$ APCDD1$^{V150I/+}$ ASXL3$^{M1416V/+}$; RBPJ^{KO}/+ MICE SHOW FEATURES OF LVNC

Triple mutants showed a more severe affection of right ventricle without fully altering the identity of myocardial territories (Figure 19). Thus, we decided to cross our mutants with mice heterozygous knock-out for the NOTCH effector Rbpjκ (generated in a CD1 background), to discard the possibility of possible NOTCH pathway compensatory effects and addressing differences of robustness of the pathway in mouse and in human. These quadruple heterozygotes showed no cardiac phenotype at E14.5 (Figure 21a), without any change in compact/trabecular area ratio in both ventricles (Figure 21b). However, at E16.5, when compaction is advanced, we observed a thinner left ventricular compact

myocardium, with trabeculae that resemble those at E14.5 (Figure 21c). Right ventricle was not significantly affected in quadruple mutants, but left ventricular compact to trabecular area ratio was significantly diminished, as is characteristic of LVNC (Figure 21d).

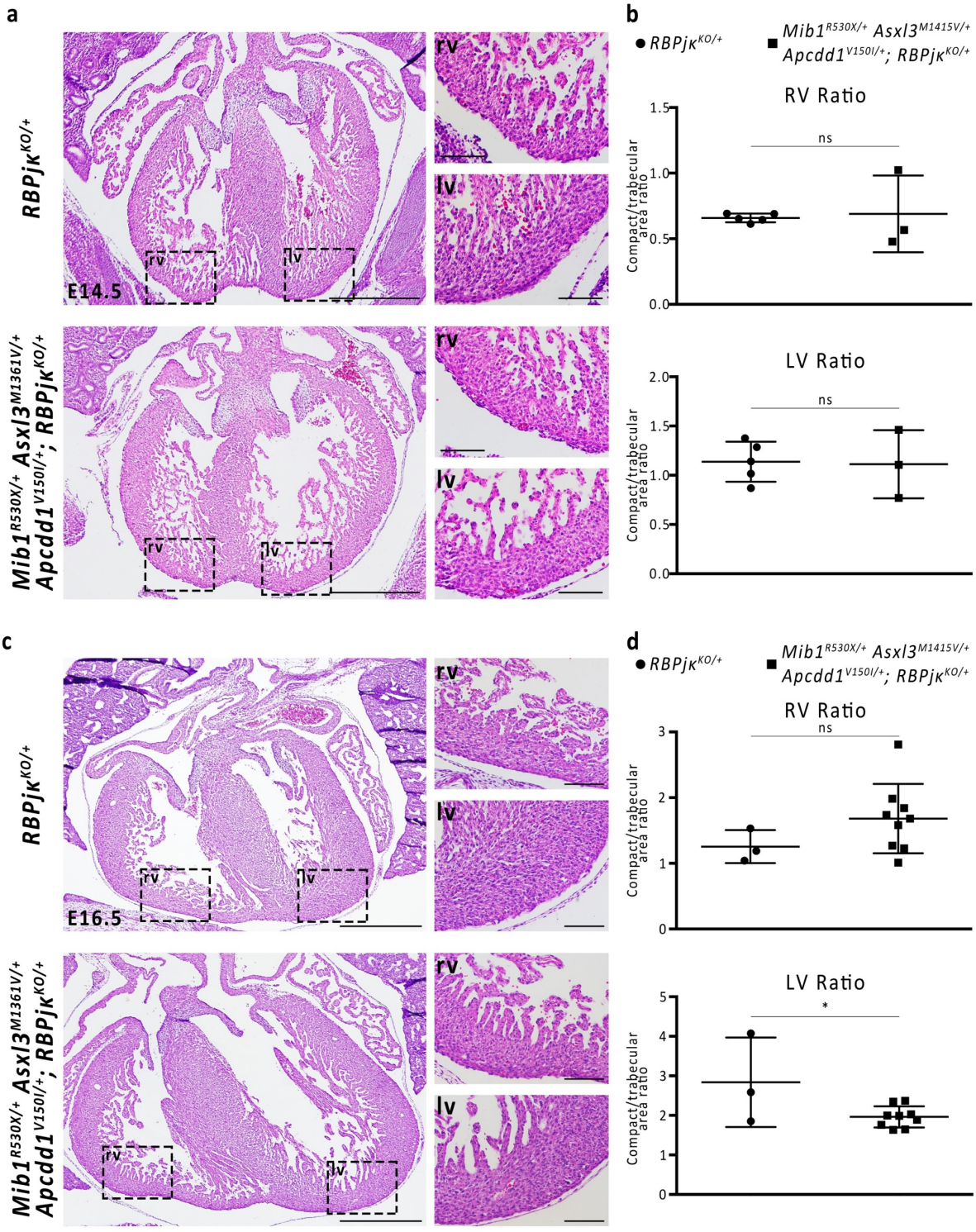

Figure 21: ***NOTCH sensitised*** **Mib1$^{R530X/+}$ Apcdd1$^{V150I/+}$ Asxl3$^{M1416V/+}$** ***hearts show a decreased compact*** **vs.** ***trabecular area ratio at E16.5.*** *a.- H&E stainings reveals that quadruple heterozygote mice show no characteristic of LVNC at initial stages of compaction (E14.5), when compared to* Rbpjk$^{KO/+}$ *littermates in any of the ventricles, as quantified in b. c.- At later stages (E16.5), these mixed background animals show a thinned compact myocardium and d.- a decreased ratio of trabecular* vs. *compact myocardium area in the left ventricle when compared to* Rbpjk$^{KO/+}$. *Scale bars: 500 µm in whole heart images and 100 µm in magnifications. *, p-value<0.05.*

Mib1$^{V943F/+}$ *Cep192*$^{T1522M/+}$ *Tmx3-204*$^{F191X/+}$ MICE DEVELOP BICUSPID AORTIC VALVE AND VENTRICULAR SEPTAL DEFECTS

Unlike the triple mutants carrying the mutations identified in R530X family, mice from this line do not show defects in the myocardium of the free wall of the ventricles, but we observed defects in both the muscular and the membranous ventricular septum. We observed a communication of both ventricles through the medial part of the septum in one *Mib1*$^{V943F/+}$ *Cep192*$^{T1522M/+}$ (Figure 22a, middle panel and magnification, white arrowheads) and lack of septation in the membranous region in another, as was observed in the triple mutant (Figure 22a, lower panels, black arrowhead). In addition, we found BAV in one *Cep192*$^{T1522M/+}$ *Tmx3-204*$^{F191X/+}$ (Figure 17b, middle panel) and two triple mutants (Figure 22b, lower panel). A summary of the different defects in valve and septal development is shown in Table 14. These results point to a role of *Cep192* in valve development and likely genetic interactions with *Mib1* and *Tmx3.*

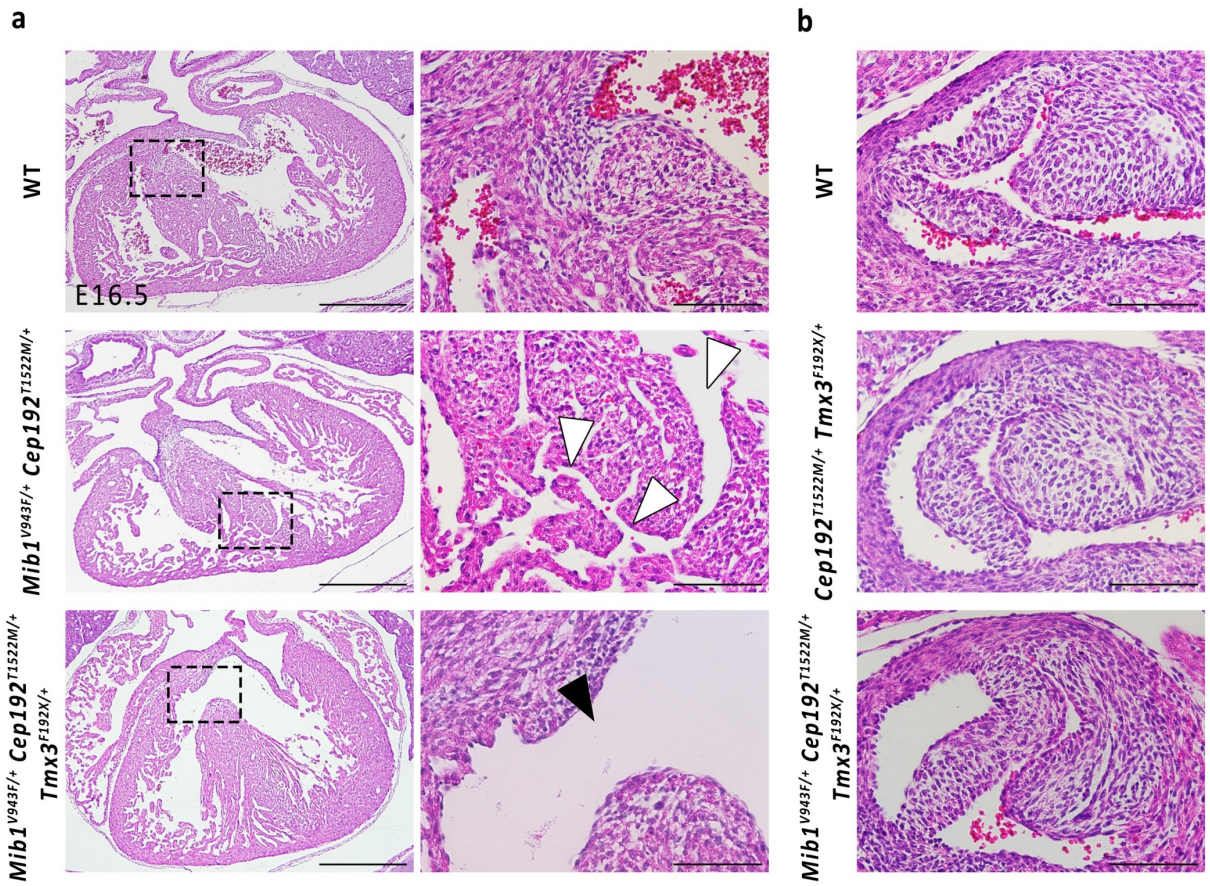

Figure 22: ***Mice carrying the mutations identified in V943F patients show higher penetrance of valve and septal defects.*** *a.- Examples of muscular ventricular septal defect (*Mib1$^{V943F/+}$ Cep192$^{T1522M/+}$ *heart, middle panel) and membranous septal defect (*Mib1$^{V943F/+}$ Cep192$^{T1522M/+}$ Tmx3$^{F191X/+}$ *mouse). b.- We identified one* Cep192$^{T1522M/+}$ Tmx3$^{F191X/+}$ *animal with LCC+NCC bicuspid aortic valve (middle panel) and two* Mib1$^{V943F/+}$ Cep192$^{T1522M/+}$ Tmx3$^{F191X/+}$ *mice showing the same kind of BAV. Scale bars: 500 µm in whole heart images and 100 µm in magnifications and valve images.*

	Mib1$^{V943F/+}$ Cep192$^{T1522M/+}$ Tmx3$^{F191X/+}$	***Mib1$^{+/+}$ Cep192$^{T1522M/+}$ Tmx3$^{F191X/+}$***	***Mib1$^{+/+}$ Cep192$^{+/+}$ Tmx3$^{F191X/+}$***	***Mib1$^{V943F/+}$ Cep192$^{T1522M/+}$ Tmx3$^{+/+}$***	***Mib1$^{V943F/+}$ Cep192$^{+/+}$ Tmx3$^{+/+}$***	***Mib1$^{+/+}$ Cep192$^{+/+}$ Tmx3$^{+/+}$***
Normal	2	6	4	1	5	7
BAV	2	1				
Misaligned PV	2	1	1			
VSD	1			2		1
TOTAL	7	7	5	3	5	8
% with phenotype	71%	14%	20%	66%	0%	13%

Table 14: ***Mice carrying the mutations identified in patients from V943F family show higher penetrance of valve defects.*** *5 out of 7 triple mutants (71%) have valve defects, while only one WT littermate animal (13%) showed VSD. Remarkably, 2 out of three* Mib1$^{V943F/+}$ Cep192$^{T1522M/+}$ Tmx3$^{+/+}$ *mice (66%) developed VSD: one membranous and one muscular.*

DISCUSSION

The generation of animal models is still a fundamental tool to understand the developmental mechanism of a disease, especially in such a complex organ as the heart, subject to mechanical stress, electrical signalling and complex interactions between the different developing tissues and the multiple intervening signalling pathways. This complexity makes it difficult to obtain *in vitro* models that mimic the transcriptional and morphogenetic maturation that cardiomyocytes undergo during trabeculation and compaction (Kodo et al., 2016; Luna-Zurita et al., 2016; Timmerman et al., 2004). However, several experimental approaches are obtaining increasingly mature cardiomyocytes derived from induced pluripotent stem cells by using co-culture with mesenchymal cells or induction with additional signals (Kumar et al., 2019; LaBarge et al., 2019; Ronaldson-Bouchard et al., 2019; Yoshida et al., 2018). *Ex vivo* assays have also been successfully used to model some aspects of early valve development as EMT (Luna-Zurita et al., 2010; MacGrogan et al., 2016), but are not able to recapitulate valve remodelling or septation. Given the importance of the endocardium-myocardium communication and the fundamental role of three-dimensional patterning of the ventricles (trabecular and compact myocardium, coronary vessels development) and the valves (OFT septation, flow mediated remodelling), and the fast and convenient gene edition capacity of CRISPR-Cas9 in fertilised eggs, the animal model was the right tool for us to use.

MIB1 MUTANT MICE

Patients of LVNC identified in Luxán et al., 2013 carried point mutations in heterozygosity, with an autosomal dominant inheritance pattern, and the mouse models in which *Mib1* was completely deleted in the early endocardium or later in the myocardium showed valve defects (Captur et al., 2016; MacGrogan et al., 2016) that were not observed in R530X and V943F familial cases. This led us to generate two mouse lines harbouring the exact mutations found in humans that could be used to better understand pathogenesis of the isolated LVNC. By using CRISPR-Cas9, we were able to edit the genome successfully. We could validate the effect of the nonsense mutation, as homozygous animals died at E10.5 with the previously reported phenotype for $Mib1^{KO}$ mice (Barsi et al., 2005; Koo et al., 2005b), and *Mib1* transcript was almost absent in homozygous hearts. In addition, $Mib1^{R530X/flox}$*; Tnnt2-Cre* mice reproduce the LVNC phenotype found in $Mib1^{flox/flox}$*; Nkx2-5-Cre* hearts (Luxán et al., 2013).

Unexpectedly, both $Mib1^{R530X/+}$ and $Mib1^{V943F/+}$ or $Mib1^{V943F/V943F}$ mice did not show any cardiac phenotype at E16.5. Compensatory function of *Mib2* is not likely to be the cause of this lack of phenotype. Although it has been proposed that mutations in *Mib2* could cause LVNC with Ménétrier-like gastropathy (Piccolo et al., 2017), evidence in mouse models shows that *Mib2* is dispensable in heart development and its expression in embryonic development is almost absent (Koo et al., 2005a) and is not induced in $Mib1^{flox/flox}$*; Tnnt2-Cre* hearts (Luxán et al., 2013). However, we confirmed the deleterious effect of both $Mib1^{R530X}$ and $Mib1^{V943F}$ mutations in heterozygosity at later stages of heart

development by determining the increased prevalence of valve and septal defects when *Mib1* mutations are introduced in a *Notch1* heterozygous knock-out background. Although homozygous *Mib1*$^{V943F/V943F}$*; Notch1*$^{KO/+}$ animals do not show an overall increase in the penetrance of valve defects, they do show more BAV than control mice, but more numbers need to be examined to confirm this increase. The lower penetrance of valve defects in *Mib1*$^{V943F/V943F}$ mice compared to *Mib1*$^{V943F/+}$ in a NOTCH sensitized background could be explained because Mib1 is reported to form dimers (Luxán et al., 2013), and the effect of the mutation could affect more the RING domains when interacting with a WT monomer than when a completely mutant dimer is formed, although the molecular mechanism is somehow difficult to conceive with the limited structural and functional assays available. The results of this sensitisation experiment are compatible with the fundamental role of NOTCH pathway in valve development and homeostasis (reviewed in Lee et al., 2019), and the presence of valve phenotype in sensitised mice with *Mib1*$^{V943F/+}$ mutation is also very interesting as collaborators from Hadassah and George Pompidou hospitals have identified this variant in a family with BAV, and found that several mutations in *MIB1* are present in BAV patients (Durst, Albuisson, Blacklow et al., data not published).
The incomplete penetrance and the variety of phenotypes observed can be explained by different regional thresholds of NOTCH activity for normal development, or by the effect of the mixed genetic background of the mice, as *Mib1*$^{R530X/+}$ and *Mib1*$^{V943F/+}$ parents came from a pure C57Bl/6J strain, and *Notch1*$^{KO/+}$ progenitors were CD1 mice. It has been reported that genetic background in mouse influences cardiac function parameters (Moreth et al., 2014), and some of our WT (C57Bl/6J) controls show septal defects. In addition to this, the activation of the NOTCH pathway at different valve developmental stages is mediated by a temporally defined sequence of ligands (MacGrogan et al., 2016), so it would be interesting to investigate why *Mib1*$^{R530X/+}$ and *Mib1*$^{V943F/+}$ mutations do not impair endocardial cushions formation through the Dll4-Notch1 signalling, but do prevent proper valve remodelling and maturation and septation via Jag1-Notch1.

EXOME SEQUENCING

Our data also suggest that the occurrence of LVNC in the families that we are investigating might be due to additional genes that co-segregate with *MIB1* mutations and the disease, given that the pattern of inheritance was autosomal dominant (Luxán et al., 2013). For this reason, we decided to increase the size of our pedigrees, recruiting more relatives. We obtained data from 11 and 10 relatives more in the R530X and the V943F, and DNA samples from 5 and 4 more, respectively. The information of these additional relatives confirmed the autosomal dominant inheritance pattern, and, in the case of the V943F family, gave us a more interesting scenario of CHDs. One of the members of that family (I.4) suffers HCM, while there is another one (II.8) that was diagnosed with subclinical hypertrabeculation. This is an important observation for our project because, if our hypothesis of oligogenic LVNC is true in

a similar way to the family described by Gifford et al., 2019, we could have a set of mutations causing LVNC of which a subset could be shared with the subclinical hypertrabeculation relative. In a wider perspective, we might discover some common mutations in HCM and LVNC patients supporting the shared genetic basis for these cardiomyopathies. Several sarcomeric genes as MYBPC3 or MYH7 have been implicated in a range of cardiomyopathies including the aforementioned, dilated and restrictive cardiomyopathy (reviewed in Arbustini et al., 2016), so it is interesting to investigate whether this apparent pleiotropy is caused by distinct effects of the mutations in the proteins or it could be due to additional unidentified mutations.

To evaluate if we could find different subsets of mutations cosegregating with *Mib1* variants and with the different observed cardiomyopathies, we sequenced the exome of all the members of the families that we could obtain DNA from. This technique allows the identification of exonic variants, which are, in principle, more directly associated with functional effects, and intronic variants close to splice donor and acceptor sites, somehow more difficult to interpret, but also interesting. This technique also identifies variants directly upstream or downstream of the genes, which we decided to keep out of the scope of this project, as they are less subject to selective pressure and the number of samples we obtained did not allow us to properly analyse them. Due to the genetic heterogeneity of human samples, we obtained around 100,000 valid variants different from reference genome per sample, but thanks to the collaboration of the families and the efficiency of our clinical colleagues recruiting patients and relatives, we could get enough DNA samples to refine the number of cosegregating variants to around 500 unique variants. Pruning the synonymous and upstream and downstream intergenic variants, we reduced the candidates to less than 10 mutations that could have an effect on the gene. Of these, only 2 for the $MIB1^{R530X}$ and 4 for the V943F family survived the filtering regarding the cardiac expression of the gene and the described or presumed function of the encoded protein. The general scheme of the likely interactions between the identified mutated proteins is depicted in Figure 23.

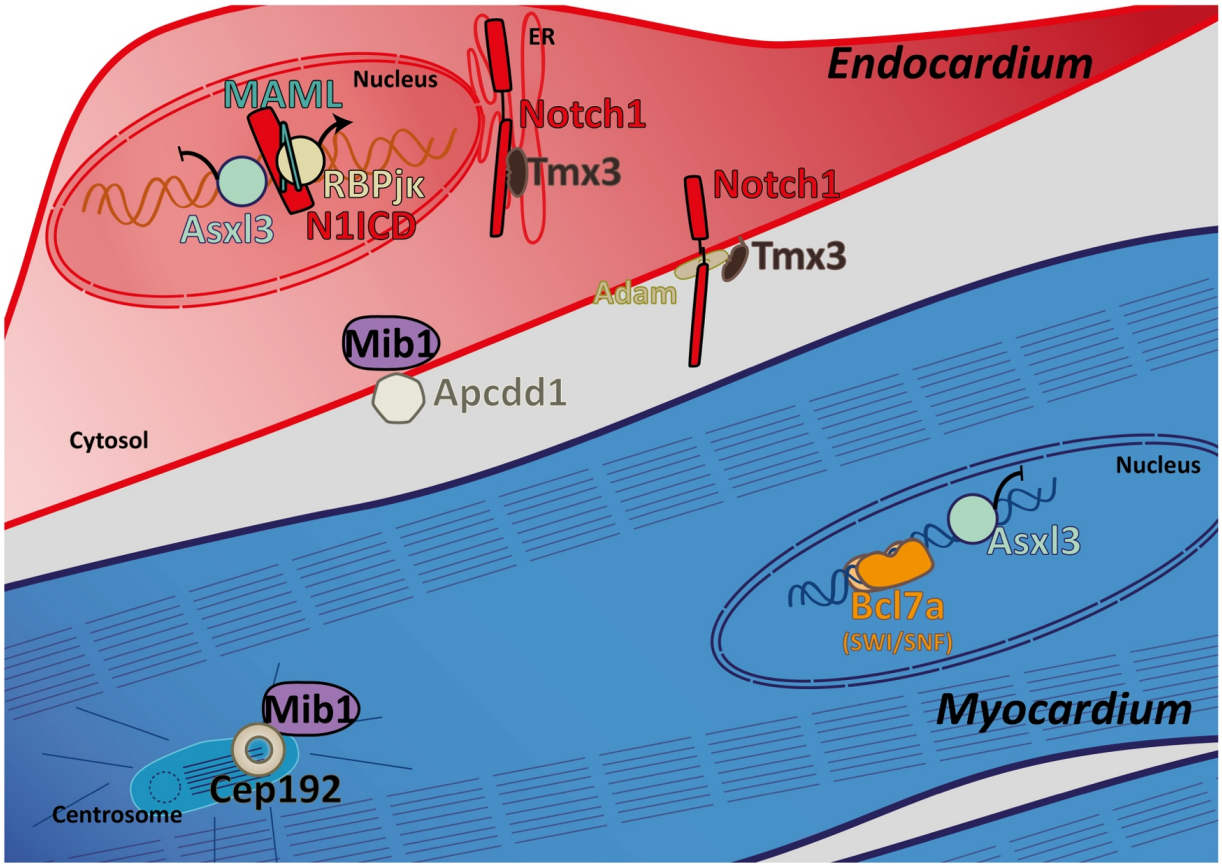

Figure 23: ***General view of the possible interactions and localizations of the proteins found mutated in both families.*** *In the context of endocardial-myocardial signalling, and taking into account the described subcellular localisation of the proteins, we hypothesise that physical interaction between candidates and NOTCH pathway members (directly or indirectly) is more likely to happen in the combinations depicted. In the endocardium: Nucleus: N1ICD transcriptional complex-Bcl7a (SWI/SNF complex); Endoplasmic Reticulum (ER): Notch1-Tmx3; Cytosol or membrane: Mib1-Apcdd1. In the myocardium: Nucleus: Asxl3 and Rbpjκ; Centrosome: Mib1-Cep192.*

MUTATIONS IN R530X FAMILY: LVNC

The mutations identified in R530X family affected APCDD1 and ASXL3. Both are missense mutations and, although they do not affect the polarity of the residue they substitute (V150I for APCDD1 and M1415V for ASXL3), they do change their size, and could alter the three dimensional conformation of the proteins. APCDD1^{V150I} is located in the extracellular part of the protein, between two glycosylation sites. ASXL3^{M1415V} variant affects an amino acid in a string between two disordered fragments of the protein, but the conservation of the amino acid is not high. Predictions of the deleteriousness of the mutations are not conclusive, but suggest to slight alterations of protein function (Figure 15, b and c). However, the most interesting aspect of these mutations are the genes they affect.

ASXL3 is a nuclear protein with LoF mutations highly associated to human Bainbridge-Roper syndrome (Bainbridge et al., 2013; Balasubramanian et al., 2017; Hori et al., 2016). It regulates the ubiquitination of H2aK119 via the interaction with BAP1, and there is increasing evidence showing that it controls the

expression of different sets of genes in several cellular types in a context-dependent manner (Shin et al., 2014; Shukla et al., 2017; Srivastava et al., 2016). As it has been reported to repress the expression of LXRα and thyroid hormone receptor (Shin et al., 2014), and levels of thyroid hormone have been shown to regulate cardiac maturation and regenerative capacity (Hirose et al., 2019), ASXL3 mutations could be implicated in defects in cardiomyocyte proliferation and, subsequently, in compaction. In addition, as a modifier of transcription, it could interact in the endocardium with NICD-RBPjκ-MAML complex to modulate its activity, although no published data to our knowledge regarding this interaction is available. The expression of ASXL3 is slightly increased in heart at E12.5, but decreases afterwards, consistent with the hypothesis that it could inhibit the expression of genes mediating myocardial maturation. It is still to be determined if the mutation found alters the activity of the protein, but a decrease of its function could lead to the premature inhibition of the proliferation and thinned myocardium (Figure 19 and Figure 21).

APCDD1 is a protein of the WNT signalling pathway, which is essential for cardiac specification (Marvin, 2001) and myocardial maturation and compaction (Heallen et al., 2011). *APCDD1* expression is positively regulated by BCAT/TCF4, and high levels of transcript are found in the heart (Takahashi et al., 2002). The encoded protein binds to WNT3A, one of the ligands, and LRP5/6, receptors of the pathway, inhibiting WNT signalling in such different contexts as breast cancer or hair follicle development (Cho, 2017; Shimomura et al., 2010). It has also been reported that during oligodendrocyte differentiation Apcdd1 can bind to βCat, the effector of the pathway, in the cytoplasm, inhibiting its activity in a negative feedback loop (Lee et al., 2015). Intriguingly, *APCDD1* expression is repressed in invasive carcinomas but expressed in non-invasive tumours, differently to other WNT pathway inhibitors as DKK and WIF, pointing to different mechanisms of inactivation of the pathway or different interacting proteins (Cho, 2017). Another interesting aspect of this pathway is that one of the coreceptors, RYK, has been found to interact with MIB1 (Berndt et al., 2011). RYK is highly expressed during heart development, and its absence causes phenotypes as VSD and double outlet right ventricle (Kugathasan et al., 2018). However, RYK intracellular domain is a pseudokinase, and the way this protein activates (or whether it is also able of inactivating) WNT pathway is still unclear (reviewed in Roy et al., 2018).

Considering the literature, we think that it is likely that MIB1 mutations could affect WNT pathway directly through endocytosis of RYK and phospho-LRP6, downregulating the signalling by WNT3A. If APCDD1^{V150I} mutation caused a gain-of-function in the protein, either by stabilization of the structure or by enhancing its binding to WNT pathway members, canonical WNT signalling could be further impaired, affecting cardiomyocyte proliferation and compact wall thickening. And, assuming that APCDD1 interacts with βCAT in the cytoplasm as described in Lee et al., 2015, an additional level of direct interaction between MIB1 and APCDD1 could exist, with lack of a hypothetical MIB1-mediated degradation of APCDD1 further stabilizing the inhibitor. These hypotheses, of course, can be

complicated considering the complexity of non-canonical WNT pathways (involving cell polarity and Ca^{2+}, which are also important for heart morphogenesis) and the different activities of the different ligands.

A depiction of the possible interactions is shown in Figure 24. The combination of the effect of the three mutations in heterozygosity (*MIB1*$^{R530X/+}$ *APCDD1*$^{V150I/+}$ *ASXL3*$^{M1415V/+}$), although none of them led to a mutant phenotype in heterozygosity by itself, could affect compaction through the decrease of proliferative signals, leading to the thinner compact myocardium. It is intriguing why the right ventricle is more clearly affected in the *Mib1*$^{R530X/+}$ *Apcdd1*$^{V150I/+}$ *Asxl3*$^{M1415V/+}$ than in the *Mib1*$^{R530X/+}$ *Apcdd1*$^{V150I/+}$ *Asxl3*$^{M1415V/+}$*; Rbpjκ*$^{KO/+}$ sensitised mice. It may be due to some differences in the genetic background, as triple mutants were generated and maintained within a pure C57Bl/6J line, while the sensitisation experiments were carried out in a mixed CD1B6F1/J background. βCAT has been reported to regulate the transcription of *Hey2* specifically by binding a different enhancer than RBPjκ in the right ventricle at early stages, while losing this specificity between E12.5 and adulthood, even showing a tendency to the left ventricle in adulthood and using another binding site (Li et al., 2018). This makes it possible that subtle differences in expression of members of these pathways or in the sequence of binding sites to these nuclear effectors present in different genetic backgrounds could influence right and left ventricular morphogenesis differentially.

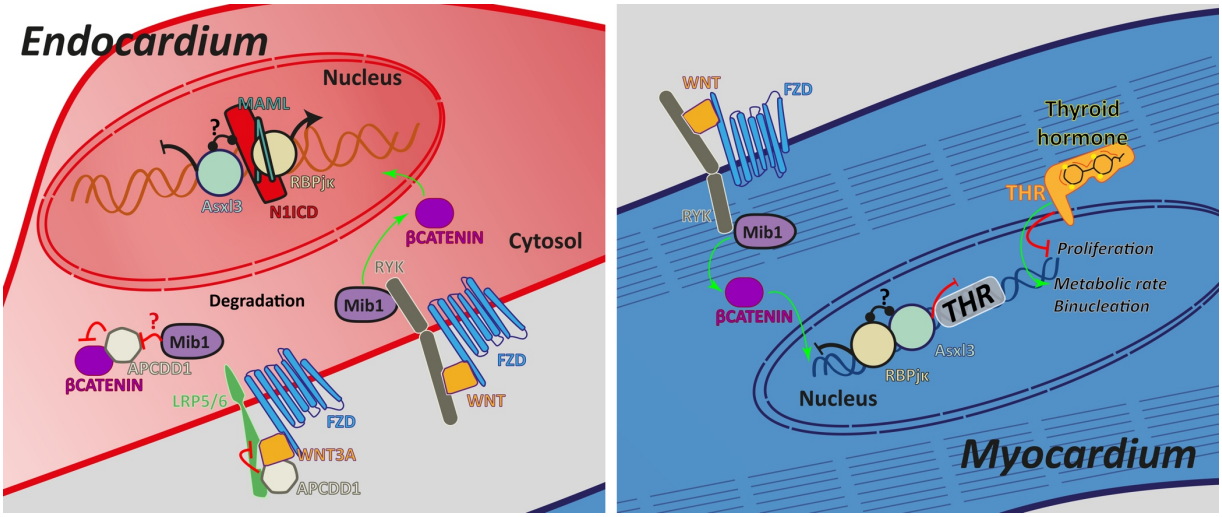

Figure 24: ***Hypothetical interactions among the candidates identified in the R530X family.*** *Briefly, in the endocardium of the ventricles Mib1 could interact with WNT signalling pathway at the level of RYK receptor or with Apcdd1, which could, in turn, modulate βcat activity in this tissue directly or by inhibiting WNT reception. These effects in WNT signaling pathway could also modulate Notch1 activity in this tissue. In addition, Asxl3 could mediate transcriptional activity by itself or in combination with RBPjκ. Asxl3 has been reported to inhibit the expression of THR, which could transduce thyroid hormone activity, fundamental for cardiomyocyte maturation, maybe in combination with RBPjκ.*

VARIANTS IDENTIFIED IN V943F FAMILY: BAV AND LVNC

In the case of the other family, the one carrying *MIB1*^{V943F} mutation, we identified three mutated candidate genes, *CEP192*, *BCL7A* and *TMX3*, whose proposed interactions in valve and ventricular development are summarised in Figure 25.

CEP192 is a centrosome protein that affects cell polarity and migration during interphase and duplication of centrioles during cell division, through the recruitment of Plk4 (O'Rourke et al., 2014; Sonnen et al., 2013). It is also fundamental for the formation of the mitotic spindle via interaction with AurA at the centrosome, and subsequent microtubules assembly (Joukov et al., 2010, 2014). During mouse heart development, this gene is clearly downregulated after the initial steps of compaction, with expression decreasing to less than half from E14.5 to E16.5. The N-terminal half of the protein (1-1000 aa) has been described as necessary for mitotic function of CEP192, but the C-terminal part (1001-2537 aa) might be responsible of the microtubule organisation during interphase, as shown with rescue experiments with isoform 2, which lacks amino acids 1-596 that include the binding region to Plk1 (O'Rourke et al., 2014). The identified mutation, CEP192^{T1547M}, is extremely infrequent in general population (GenomADe MAF=0.00003), indicative of some selective pressure. We propose that this mutation could affect CEP192 function during interphase, misregulating microtubule and cilia organisation. This could affect proper NC cells migration into the mouse valves, affecting the septation and remodelling of the leaflets, thus increasing the prevalence of BAV. It could also disrupt cardiomyocyte polarity and oriented cell division. These effects could be exacerbated by the presence of Mib1^{V943F} mutation, as Mib1 has been described to regulate the availability of Plk4 and PCM1, which are also essential for the formation of microtubular structures. Mib1 inhibits cilia formation by ubiquitinating several pericentriolar proteins as PCM1, whose action sequestering Mib1 in pericentriolar satellites is also fundamental for proper ciliogenesis (Wang et al., 2016). In addition, Mib1 labels Plk4 for degradation, downregulating the number of centrioles (Čajánek et al., 2015).

BCL7A is a subunit of the SWI/SNF complex, responsible of chromatin remodelling. It was described in a lymphoma-linked translocation (Zani et al., 1996), but it is also linked to neurological defects (Wischhof et al., 2017). *Bcl7a* has been found to be downregulated in transverse aortic constriction, a model of pressure-overload hypertrophy, suggesting that it could be implicated in cardiomyocyte homeostasis (Toischer et al., 2010), and *Bcl7-like* has been reported to indirectly regulate NOTCH and WNT signalling pathway in *D. melanogaster* (Haussmann et al., 2008). According to GTEx database (retrieved on October 12th, 2019), both intronic variants identified significantly affect the splicing, diminishing the incorporation of exon 3, and decrease the expression of the gene. This decrease in expression might be due to the potential formation of a possible binding motif of TBX20 (by rs884785) or the disruption of likely HES1/2 and HEY1/2 binding sites (by rs884786), as described in ensembl (data retrieved on October 12th, 2019). Taken together, these data could point to a combination of the *BCL7A*

downregulating intronic mutations in heterozygosity with the cosegregating mutations found in V943F family in the development of LVNC. It is also a possibility that these mutations in homozygosity are involved in the HCM diagnosed in a member of this family.

TMX3, a member of the protein disulphide isomerases family, is located in the deleted region described in the *no turning* mutants, which showed, in addition to defects in left-right asymmetry, defects in somitogenesis and heart development (Melloy et al., 1998) similar to those in *Rbpjκ*$^{-/-}$ mice (Oka et al., 1995). *TMX3* gene has three different protein coding isoforms described in human: *TMX3-201*, the main isoform, is composed of 16 exons that encode 454 amino acids; *TMX3-204*, the second longest isoform, lacks exons 9 to 16, with 18 additional coding nucleotides from canonical intron 8, that extend the protein length up to 195 amino acids; and *TMX3-202*, comprising canonical exon 9 but lacking exon 6, which encodes Arg117, reported to increase active site efficiency (Haugstetter et al., 2007), and resulting in a 197 amino acids long protein. Both short isoforms lack the transmembrane domain, and are likely soluble in the lumen of the endoplasmic reticulum, and might be secreted to the extracellular *milieu* and regulate thrombi formation (Holbrook et al., 2010). The long isoform, in turn, has three thioredoxin-like domains: the N-terminal (25-131), catalytically active; and two inactive domains (from 132 to 225-235 and from 235-235 to 355) that stabilize and aid in the redox activity of the N-terminal domain (Haugstetter et al., 2007). The *TMX3-204* isoform contains 59 amino acids from the first inactive domain, and *TMX3-202* encodes for 82 amino acids out of 93, with a C-terminal modification of 12 aminoacids that is reduced to 5 by the TMX3-202^{F191X} mutation identified. The functional effect of this mutation is yet to be explored, but we think that if this isoform is expressed in the heart, as are *Tmx3* and *Tmx3-204*, it could inactivate Tmx3 or Tmx3-204 proteins, as it would be catalytically inactive by the lack of R117, but the presence of the second domain almost complete could mediate the formation of heterodimers. The other two isoforms could intervene in the formation of the disulphide bridges of several proteins, including ADAM metalloproteinases, described to be regulated by protein disulphide isomerases (Willems et al., 2010), or directly regulating the stability of Notch receptors, rich in EGF-like domains that are highly dependent on disulphide bonds. It is then reasonable to think that TMX3 and TMX3-204 could impair the cleavage of the NOTCH receptor, and that the LoF of their inhibitor (*i.e.*: TMX3-202) would lead to diminished NOTCH signalling. Moreover, if the function of these proteins is the regulation of the folding of EGF-like domains in NOTCH receptor, its dysregulation could affect the functional binding of the ligands. This, in addition to the effect of *MIB1*^{V943F} in NOTCH signalling could be enough to disrupt proper remodelling of the valves, leading to BAV and other valve defects. It also could, in combination with the misregulation of cardiomyocyte homeostasis due to the haploinsufficiency of BCL7A, lead to defective maturation of myocardium and LVNC.

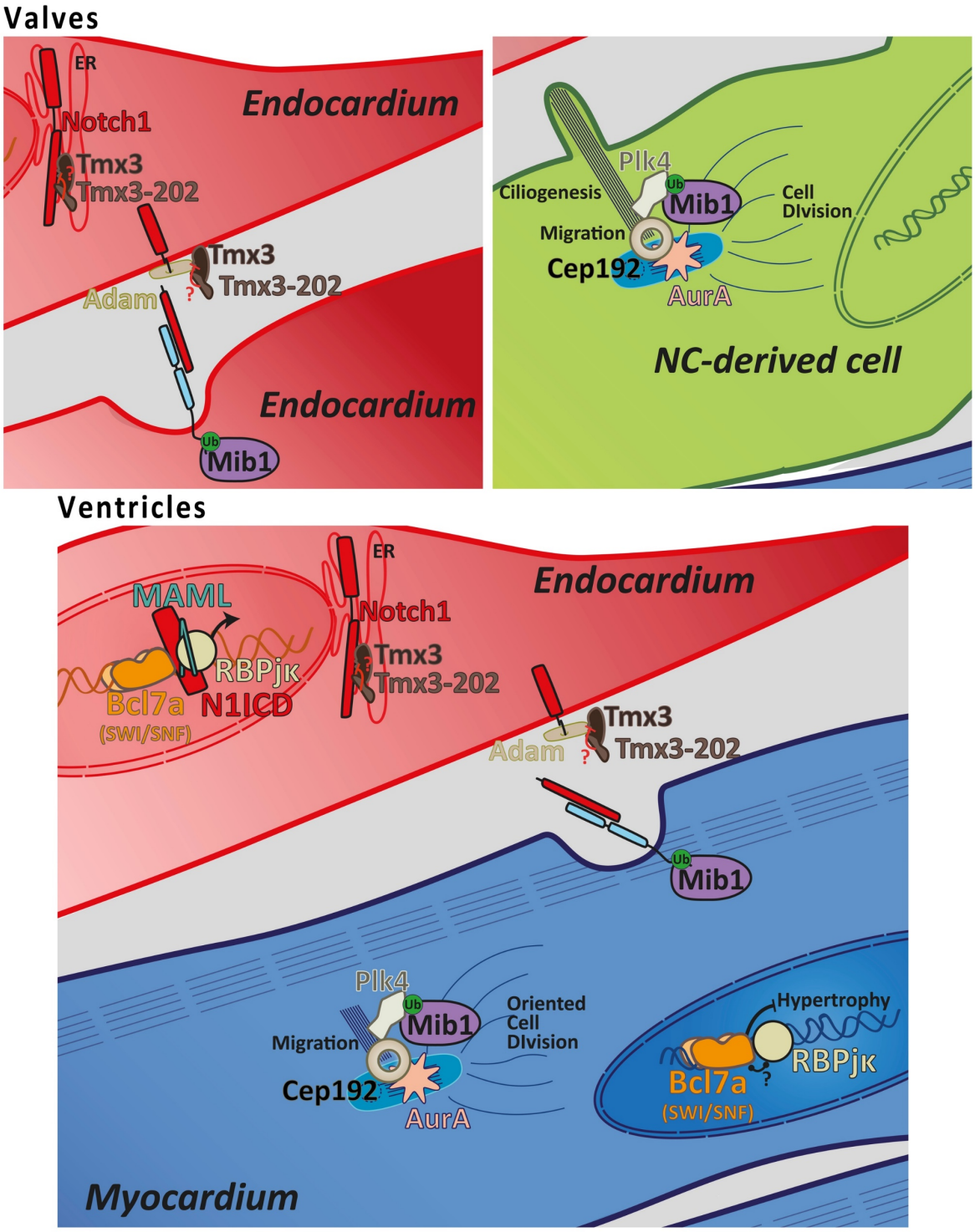

Figure 25: ***Hypothetical interactions between the identified candidate genes in the V943F family.*** *In the valve context (upper panels), Tmx3 could be mediating the proper activation of the NOTCH pathway by modulating Adam metalloproteinases or the stability of EGF like domains in the extracellular domain of the receptor, while Cep192 could regulate the formation of cytoskeletal structures as cilia, migration or cell division. In the ventricles, besides possible Tmx3 regulation of NOTCH signalling pathway from the myocardium to the endocardium, and possible effects of Cep192 in combination with Mib1 in migration or oriented cell division, Bcl7a might mediate the repression of hypertrophic response genes in the myocardium or different transcriptional effects in the endocardium alone or in combination with RBPjκ.*

GENERAL PERSPECTIVE AND FUTURE EXPERIMENTS: MIB1 AND INTERACTING GENES IN LVNC

The lack of LVNC phenotype of the single heterozygous mutants harbouring the described *Mib1* variants, and the confirmation of their impact in NOTCH function, as indicated by N1ICD reduction in *Mib1*$^{R530X/R530X}$ mice and the genetic sensitisation experiments, allowed us to hypothesise that there could be more intervening mutations present in our LVNC families. Using exome sequencing we have identified a number of candidate genes possibly related to LVNC, although their full characterisation has still to be performed. Supporting this idea, during the development of this project LVNC was described as not only a monogenic, but also an oligogenic disease (Gifford et al., 2019), but unlike the genes reported in that paper, that were already known as important for heart development, we have identified novel candidates that could predispose to CHD, explaining the range of severity found in LVNC patients and the incomplete penetrance of valve defects. Advances in gene editing, especially the development of CRISPR-Cas9, enabled us to explore complex diseases caused by mutations present even in the same chromosome that were difficult to investigate with previous techniques. We generated the relevant mouse lines, which showed interaction of the candidate genes in the development of CHD, including LVNC and BAV.

The effect of the promising *Bcl7a* variants still remains to be analysed, both in heterozygosity in combination with the other identified variants in relation to valve development but in LVNC as well, and in homozygosity, regarding hypertrophy. These mouse models will help to describe common pathogenic pathways involved in isolated LVNC, HCM and valve disease, leading to novel diagnostic markers and increasing the knowledge of the interaction of molecular pathways during late embryonic development. In the search for these distinct pathways and markers, our next step is to perform RNA sequencing experiments for the different combinations of candidate genes. In addition, we have generated expression vectors of the candidate genes, to dissect the biochemical interactions between them and Notch1 or Mib1.

To further correlate our results with human cardiac defects, we have generated iPSC-derived cardiomyocytes from skin biopsies of the patients and healthy controls including relatives and non-related donors. This will allow us to explore the contribution of the different identified variants, as we have also generated isogenic controls using CRISPR-Cas9. The analysis of their transcriptome in the course of cardiomyocyte differentiation will help us to understand their role in human myocardial maturation and disease.

CONCLUSIONS
CONCLUSIONES

1. CRISPR-Cas9 is an efficient strategy to generate mouse models harbouring several point mutations in one experiment

2. *Mib1*^{R530X} mutation causes nonsense mediated decay of *Mib1* transcript, causing embryonic lethality at E10.5, reduced N1ICD expression, and LVNC when combined with myocardial heterozygous abrogation of *Mib1*.

3. *Mib1*^{V943F} mutation affects Mib1 function, as it causes BAV in a NOTCH haploinsufficient background.

4. APCDD1^{V150I} and ASXL3^{M1416V} mutations cosegregate perfectly with LVNC and *MIB1*^{R530X} variant.

5. CEP192^{T1547M}, TMX3-202^{F191X} and *BCL7A*^{AG,GA} mutations cosegregate with LVNC and MIB1^{V943F} variant.

6. Mice heterozygous for Mib1^{R530X}, Apcdd1^{V150I} and Asxl3^{M1416V} show LVNC, suggesting that the functional interaction between Mib1, Apcdd1 and Asxl3 regulates compaction.

7. Mice heterozygous for Mib1^{V943F} Cep192^{T1522M} Tmx3-204^{F191X} show BAV and VSD, suggesting that the interaction between Mib1, Cep192 and Tmx3 is required for valvulogenesis.

1. CRISPR-Cas9 es una herramienta eficiente para la generación de mutaciones puntuales simultáneas *in vivo*.

2. La mutación *Mib1*^{R530X} provoca degradación por falta de sentido del tránscrito de *Mib1*, causando letalidad a E10.5, reducción de la actividad de Notch1 y LVNC en combinación con la deleción de *Mib1* en el miocardio.

3. La mutación *Mib1*^{V943F} afecta a la función de Mib1, causando BAV en un fondo haploinsuficiente para NOTCH.

4. Las mutaciones APCDD1^{V150I} y ASXL3^{M1416V} cosegregan perfectamente con la LVNC y la variante *MIB1*^{R530X}.

5. Las mutaciones CEP192^{T1547M}, TMX3-202^{F191X} y *BCL7A*^{AG,GA} cosegregan con la LVNC y la variante MIB1^{V943F}.

6. Los ratones heterocigotos para Mib1^{R530X}, Apcdd1^{V150I} y Asxl3^{M1416V} sufren LVNC, sugiriendo que la interacción entre Mib1, Apcdd1 and Asxl3 regula la compactación.

7. Los ratones heterocigotos para Mib1^{V943F} Cep192^{T1522M} y Tmx3-204^{F191X} muestran BAV y defectos septales, sugiriendo que la interacción entre Mib1, Cep192 y Tmx3 es necesaria durante la valvulogénesis.

BIBLIOGRAPHY

Abdulkareem, N., Smelt, J., and Jahangiri, M. (2013). Bicuspid aortic valve aortopathy: genetics, pathophysiology and medical therapy. Interact. Cardiovasc. Thorac. Surg. *17*, 554–559.

Agarwal, A., Khandheria, B.K., Paterick, T.E., Treiber, S.C., Bush, M., and Tajik, A.J. (2013). Left ventricular noncompaction in patients with bicuspid aortic valve. J. Am. Soc. Echocardiogr. *26*, 1306–1313.

Aleksandrova, A., Czirók, A., Szabó, A., Filla, M.B., Hossain, M.J., Whelan, P.F., Lansford, R., and Rongish, B.J. (2012). Convective tissue movements play a major role in avian endocardial morphogenesis. Dev. Biol. *363*, 348–361.

Alonso-Montes, C., Martín, M., Martínez-Arias, L., Coto, E., Naves-Díaz, M., Morís, C., Cannata-Andía, J.B., and Rodríguez, I. (2018). Variants in cardiac GATA genes associated with bicuspid aortic valve. Eur. J. Clin. Invest. *48*.

Andersen, J.S., Wilkinson, C.J., Mayor, T., Mortensen, P., Nigg, E.A., and Mann, M. (2003). Proteomic characterization of the human centrosome by protein correlation profiling. Nature *426*, 570–574.

Arbustini, E., Favalli, V., Narula, N., Serio, A., and Grasso, M. (2016). Left Ventricular Noncompaction: A Distinct Genetic Cardiomyopathy? J. Am. Coll. Cardiol. *68*, 949–966.

Bainbridge, M.N., Hu, H., Muzny, D.M., Musante, L., Lupski, J.R., Graham, B.H., Chen, W., Gripp, K.W., Jenny, K., Wienker, T.F., et al. (2013). De novo truncating mutations in ASXL3 are associated with a novel clinical phenotype with similarities to Bohring-Opitz syndrome. Genome Med. *5*, 11.

Balasubramanian, M., Willoughby, J., Fry, A.E., Weber, A., Firth, H. V, Deshpande, C., Berg, J.N., Chandler, K., Metcalfe, K.A., Lam, W., et al. (2017). Delineating the phenotypic spectrum of Bainbridge-Ropers syndrome: 12 new patients with de novo, heterozygous, loss-of-function mutations in ASXL3 and review of published literature. J. Med. Genet. *54*, 537–543.

Barsi, J.C., Rajendra, R., Wu, J.I., and Artzt, K. (2005). Mind bomb1 is a ubiquitin ligase essential for mouse embryonic development and Notch signaling. Mech. Dev. *122*, 1106–1117.

Basson, C.T., Bachinsky, D.R., Lin, R.C., Levi, T., Elkins, J.A., Soults, J., Grayzel, D., Kroumpouzou, E., Traill, T.A., Leblanc-Straceski, J., et al. (1997). Mutations in human cause limb and cardiac malformation in Holt-Oram syndrome. Nat. Genet. *15*, 30–35.

Berndt, J.D., Aoyagi, A., Yang, P., Anastas, J.N., Tang, L., and Moon, R.T. (2011). Mindbomb 1, an E3 ubiquitin ligase, forms a complex with RYK to activate Wnt/β-catenin signaling. J. Cell Biol. *194*, 737–750.

de Boer, B.A., van den Berg, G., de Boer, P.A.J., Moorman, A.F.M., and Ruijter, J.M. (2012a). Growth of the developing mouse heart: an interactive qualitative and quantitative 3D atlas. Dev. Biol. *368*, 203–213.

de Boer, B.A., van den Berg, G., Soufan, A.T., de Boer, P.A.J., Hagoort, J., van den Hoff, M.J.B., Moorman, A.F.M., and Ruijter, J.M. (2012b). Measurement and 3D-visualization of cell-cycle length using double labelling with two

thymidine analogues applied in early heart development. PLoS One *7*, e47719.

Bolger, A.M., Lohse, M., and Usadel, B. (2014). Trimmomatic: a flexible trimmer for Illumina sequence data. Bioinformatics *30*, 2114–2120.

Bondue, A., Lapouge, G., Paulissen, C., Semeraro, C., Iacovino, M., Kyba, M., and Blanpain, C. (2008). Mesp1 acts as a master regulator of multipotent cardiovascular progenitor specification. Cell Stem Cell *3*, 69–84.

Borggrefe, T., Lauth, M., Zwijsen, A., Huylebroeck, D., Oswald, F., and Giaimo, B.D. (2016). The Notch intracellular domain integrates signals from Wnt, Hedgehog, TGFβ/BMP and hypoxia pathways. Biochim. Biophys. Acta *1863*, 303–313.

Brida, M., and Gatzoulis, M.A. (2019). Adult congenital heart disease: Past, present and future. Acta Paediatr. *108*, 1757–1764.

Bruneau, B.G., Nemer, G., Schmitt, J.P., Charron, F., Robitaille, L., Caron, S., Conner, D.A., Gessler, M., Nemer, M., Seidman, C.E., et al. (2001). A Murine Model of Holt-Oram Syndrome Defines Roles of the T-Box Transcription Factor Tbx5 in Cardiogenesis and Disease. Cell *106*, 709–721.

Buckingham, M., Meilhac, S., and Zaffran, S. (2005). Building the mammalian heart from two sources of myocardial cells. Nat. Rev. Genet. *6*, 826–835.

Čajánek, L., Glatter, T., and Nigg, E.A. (2015). The E3 ubiquitin ligase Mib1 regulates Plk4 and centriole biogenesis. J. Cell Sci. *128*, 1674–1682.

Campbell, M.J., Czosek, R.J., Hinton, R.B., and Miller, E.M. (2015). Exon 3 deletion of ryanodine receptor causes left ventricular noncompaction, worsening catecholaminergic polymorphic ventricular tachycardia, and sudden cardiac arrest. Am. J. Med. Genet. A *167A*, 2197–2200.

Captur, G., Muthurangu, V., Cook, C., Flett, A.S., Wilson, R., Barison, A., Sado, D.M., Anderson, S., McKenna, W.J., Mohun, T.J., et al. (2013). Quantification of left ventricular trabeculae using fractal analysis. J. Cardiovasc. Magn. Reson. *15*, 36.

Captur, G., Wilson, R., Bennett, M.F., Luxán, G., Nasis, A., de la Pompa, J.L.L., Moon, J.C., and Mohun, T.J. (2016). Morphogenesis of myocardial trabeculae in the mouse embryo. J. Anat. *229*, 314–325.

Chang, B., Gorbea, C., Lezin, G., Li, L., Shan, L., Sakai, N., Kogaki, S., Otomo, T., Okinaga, T., Hamaoka, A., et al. (2013). 14-3-3ε gene variants in a Japanese patient with left ventricular noncompaction and hypoplasia of the corpus callosum. Gene *515*, 173–180.

Chao, R., Nevin, L., Agarwal, P., Riemer, J., Bai, X., Delaney, A., Akana, M., Jimenezlopez, N., Bardakjian, T., Schneider, A., et al. (2010). A male with unilateral microphthalmia reveals a role for TMX3 in eye development. PLoS One *5*.

Chen, C., Copley, J.T., Linse, K., Rogers, A.D., and Sigwart, J.D. (2015). The heart of a dragon: 3D anatomical reconstruction of the "scaly-foot gastropod" (Mollusca: Gastropoda: Neomphalina) reveals its extraordinary circulatory system. Front. Zool. *12*, 1–16.

Chen, H.I., Sharma, B., Akerberg, B.N., Numi, H.J., Kivela, R., Saharinen, P., Aghajanian, H., McKay, A.S., Bogard, P.E., Chang, A.H., et al. (2014a). The sinus venosus contributes to coronary vasculature through VEGFC-stimulated angiogenesis. Development *141*, 4500–4512.

Chen, H.I., Poduri, A., Numi, H., Kivela, R., Saharinen, P., McKay, A.S., Raftrey, B., Churko, J., Tian, X., Zhou, B., et al. (2014b). VEGF-C and aortic cardiomyocytes guide coronary artery stem development. J. Clin. Invest. *124*, 48994914.

Chin, T.K., Perloff, J.K., Williams, R.G., Jue, K., and Mohrmann, R. (1990). Isolated noncompaction of left ventricular myocardium. A study of eight cases. Circulation *82*, 507–513.

Cho, S.G. (2017). APC downregulated 1 inhibits breast cancer cell invasion by inhibiting the canonical WNT signaling pathway. Oncol. Lett. *14*, 4845–4852.

D'Amato, G., Luxán, G., and de la Pompa, J.L.L. (2016a). Notch signalling in ventricular chamber development and cardiomyopathy. FEBS J. *283*, 4223–4237.

D'Amato, G., Luxán, G., Del Monte-Nieto, G., Martínez-Poveda, B., Torroja, C., Walter, W., Bochter, M.S., Benedito, R., Cole, S., Martinez, F., et al. (2016b). Sequential Notch activation regulates ventricular chamber development. Nat. Cell Biol. *18*, 7–20.

DePristo, M.A., Banks, E., Poplin, R., Garimella, K. V, Maguire, J.R., Hartl, C., Philippakis, A.A., del Angel, G., Rivas, M.A., Hanna, M., et al. (2011). A framework for variation discovery and genotyping using next-generation DNA sequencing data. Nat. Genet. *43*, 491–498.

Dho, S.E., Silva-Gagliardi, N., Morgese, F., Coyaud, E., Lamoureux, E., Berry, D.M., Raught, B., and McGlade, C.J. (2019). Proximity interactions of the ubiquitin ligase Mind bomb 1 reveal a role in regulation of epithelial polarity complex proteins. Sci. Rep. *9*, 1–18.

Dolk, H., Loane, M., and Garne, E. (2011). Congenital heart defects in Europe: Prevalence and perinatal mortality, 2000 to 2005. Circulation *123*, 841–849.

EUROCAT Access Prevalence Tables. Available at: http://www.eurocatnetwork.eu/ACCESSPREVALENCEDATA/PrevalenceTables. Accessed: 04/10/2019.

Faber, J.W., Boukens, B.J., Oostra, R.-J.J., Moorman, A.F.M.M., Christoffels, V.M., and Jensen, B. (2019). Sinus venosus incorporation: contentious issues and operational criteria for developmental and evolutionary studies. J. Anat. *234*, 583–591.

Fernández, B., Durán, A.C., Fernández-Gallego, T., Fernández, M.C., Such, M., Arqué, J.M., and Sans-Coma, V. (2009). Bicuspid Aortic Valves With Different Spatial Orientations of the Leaflets Are Distinct Etiological Entities. J. Am. Coll. Cardiol. *54*, 2312–2318.

Fisher, C.L., Randazzo, F., Humphries, R.K., and Brock, H.W. (2006). Characterization of Asxl1, a murine homolog of Additional sex combs, and analysis of the Asx-like gene family. Gene *369*, 109–118.

Garg, V., Kathiriya, I.S., Barnes, R., Schluterman, M.K., King, I.N., Butler, C.A., Rothrock, C.R., Eapen, R.S., Hirayama-Yamada, K., Joo, K., et al. (2003). GATA4 mutations cause human congenital heart defects and reveal an interaction with TBX5. Nature *424*, 443–447.

Garg, V., Muth, A.N., Ransom, J.F., Schluterman, M.K., Barnes, R., King, I.N., Grossfeld, P.D., and Srivastava, D. (2005). Mutations in NOTCH1 cause aortic valve disease. Nature *437*, 270–274.

Le Garrec, J.-F., Domínguez, J.N., Desgrange, A., Ivanovitch, K.D., Raphaël, E., Bangham, J.A., Torres, M., Coen, E., Mohun, T.J., Meilhac, S.M., et al. (2017). A predictive model of asymmetric morphogenesis from 3D reconstructions of mouse heart looping dynamics. Elife *6*.

Gassmann, M., Casagranda, F., Orioli, D., Simon, H., Lai, C., Klein, R., and Lemke, G. (1995). Aberrant neural and cardiac development in mice lacking the ErbB4 neuregulin receptor. Nature *378*, 390–394.

Gerety, S.S., Wang, H.U., Chen, Z.F., and Anderson, D.J. (1999). Symmetrical mutant phenotypes of the receptor EphB4 and its specific transmembrane ligand ephrin-B2 in cardiovascular development. Mol. Cell *4*, 403–414.

Gifford, C.A., Ranade, S.S., Samarakoon, R., Salunga, H.T., de Soysa, T.Y., Huang, Y., Zhou, P., Elfenbein, A., Wyman, S.K., Bui, Y.K., et al. (2019). Oligogenic inheritance of a human heart disease involving a genetic modifier. Science (80-.). *364*, 865–870.

Gomez-Ferreria, M.A., Rath, U., Buster, D.W., Chanda, S.K., Caldwell, J.S., Rines, D.R., and Sharp, D.J. (2007). Human Cep192 Is Required for Mitotic Centrosome and Spindle Assembly. Curr. Biol. *17*, 1960–1966.

Grego-Bessa, J., Luna-Zurita, L., del Monte, G., Bolós, V., Melgar, P., Arandilla, A., Garratt, A.N., Zang, H., Mukouyama, Y.-S. suke, Chen, H., et al. (2007). Notch Signaling Is Essential for Ventricular Chamber Development. Dev. Cell *12*, 415–429.

Haugstetter, J., Blicher, T., and Ellgaard, L. (2005). Identification and characterization of a novel thioredoxin-related transmembrane protein of the endoplasmic reticulum. J. Biol. Chem. *280*, 8371–8380.

Haugstetter, J., Maurer, M.A., Blicher, T., Pagac, M., Wider, G., and Ellgaard, L. (2007). Structure-function analysis of the endoplasmic reticulum oxidoreductase TMX3 reveals interdomain stabilization of the N-terminal redox-active domain. J. Biol. Chem. *282*, 33859–33867.

Haussmann, I.U., White, K., and Soller, M. (2008). Erect wing regulates synaptic growth in Drosophila by

integration of multiple signaling pathways. Genome Biol. *9*.

Heallen, T., Zhang, M., Wang, J., Bonilla-Claudio, M., Klysik, E., Johnson, R.L., and Martin, J.F. (2011). Hippo Pathway Inhibits Wnt Signaling to Restrain Cardiomyocyte Proliferation and Heart Size. Science (80-.). *332*, 458–461.

Hirose, K., Payumo, A.Y., Cutie, S., Hoang, A., Zhang, H., Guyot, R., Lunn, D., Bigley, R.B., Yu, H., Wang, J., et al. (2019). Evidence for hormonal control of heart regenerative capacity during endothermy acquisition. Science (80-.). *364*, 184–188.

Hoffman, J.I.E., and Kaplan, S. (2002). The incidence of congenital heart disease. J. Am. Coll. Cardiol. *39*, 1890–1900.

Hoffmann, A.D., Peterson, M.A., Friedland-Little, J.M., Anderson, S.A., and Moskowitz, I.P. (2009). sonic hedgehog is required in pulmonary endoderm for atrial septation. Development *136*, 1761–1770.

Holbrook, L.M., Watkins, N.A., Simmonds, A.D., Jones, C.I., Ouwehand, W.H., and Gibbins, J.M. (2010). Platelets release novel thiol isomerase enzymes which are recruited to the cell surface following activation. Br. J. Haematol. *148*, 627–637.

Hori, I., Miya, F., Ohashi, K., Negishi, Y., Hattori, A., Ando, N., Okamoto, N., Kato, M., Tsunoda, T., Yamasaki, M., et al. (2016). Novel splicing mutation in the ASXL3 gene causing Bainbridge-Ropers syndrome. Am. J. Med. Genet. A *170*, 1863–1867.

Hori, K., Sen, A., and Artavanis-Tsakonas, S. (2013). Notch signaling at a glance. J. Cell Sci. *126*, 2135–2140.

Ivanovitch, K., Esteban, I., and Torres, M. (2017). Growth and Morphogenesis during Early Heart Development in Amniotes. J. Cardiovasc. Dev. Dis. *4*, 20.

Jacquier, A., Thuny, F., Jop, B., Giorgi, R., Cohen, F., Gaubert, J.-Y.Y., Vidal, V., Bartoli, J.M., Habib, G., and Moulin, G. (2010). Measurement of trabeculated left ventricular mass using cardiac magnetic resonance imaging in the diagnosis of left ventricular non-compaction. Eur. Heart J. *31*, 1098–1104.

Jain, R., Engleka, K.A., Rentschler, S.L., Manderfield, L.J., Li, L., Yuan, L., and Epstein, J.A. (2011). Cardiac neural crest orchestrates remodeling and functional maturation of mouse semilunar valves. J. Clin. Invest. *121*, 422–430.

Jenni, R., Oechslin, E., Schneider, J., Attenhofer Jost, C., and Kaufmann, P.A. (2001). Echocardiographic and pathoanatomical characteristics of isolated left ventricular non-compaction: A step towards classification as a distinct cardiomyopathy. Heart *86*, 666–671.

Jensen, B., Wang, T., Christoffels, V.M., and Moorman, A.F.M. (2013). Evolution and development of the building plan of the vertebrate heart. Biochim. Biophys. Acta - Mol. Cell Res. *1833*, 783–794.

Jensen, B., Agger, P., de Boer, B.A., Oostra, R.-J.J., Pedersen, M., van der Wal, A.C., Nils Planken, R., and Moorman, A.F. (2016). The hypertrabeculated (noncompacted) left ventricle is different from the ventricle of embryos and ectothermic vertebrates. Biochim. Biophys. Acta *1863*, 1696–1706.

Jensen, B., van der Wal, A.C., Moorman, A.F., and Christoffels, V.M. (2017). Excessive trabeculations in noncompaction do not have the embryonic identity. Int. J. Cardiol. *227*, 325–330.

Jostarndt, K., Puntschart, A., Hoppeler, H., and Billeter, R. (1994). The use of 33P-labelled riboprobes for in situ hybridizations: localization of myosin alkali light-chain mRNAs in adult human skeletal muscle. Histochem. J. *26*, 32–40.

Joukov, V., De Nicolo, A., Rodriguez, A., Walter, J.C., and Livingston, D.M. (2010). Centrosomal protein of 192 kDa (Cep192) promotes centrosome-driven spindle assembly by engaging in organelle-specific Aurora A activation. Proc. Natl. Acad. Sci. U. S. A. *107*, 21022–21027.

Joukov, V., Walter, J.C.J., De Nicolo, A., V Joukov, Walter, J.C.J., and Nicolo, A. De (2014). The Cep192-organized Aurora A-Plk1 cascade is essential for centrosome cycle and bipolar spindle assembly. Mol. Cell *10 (2)*, 116–125.

Karczewski, K.J., Francioli, L.C., Tiao, G., Cummings, B.B., Alföldi, J., Wang, Q., Collins, R.L., Laricchia, K.M., Ganna, A., Birnbaum, D.P., et al. (2019). Variation across 141,456 human exomes and genomes reveals the spectrum of loss-of-function intolerance across human protein-coding genes. BioRxiv 531210.

Katoh, M., and Katoh, M. (2003). Identification and characterization of TRIP8 gene in silico. Int. J. Mol. Med. *12*, 817–821.

Kelly, R.G., Brown, N.A., and Buckingham, M.E. (2001). The arterial pole of the mouse heart forms from Fgf10-expressing cells in pharyngeal mesoderm. Dev. Cell *1*, 435–440.

Kirby, M.L., Gale, T.F., and Stewart, D.E. (1983). Neural crest cells contribute to normal aorticopulmonary septation. Science (80-.). *220*, 1059–1061.

Kitajima, S., Takagi, A., Inoue, T., and Saga, Y. (2000). MesP1 and MesP2 are essential for the development of cardiac mesoderm. Development *127*, 3215–3226.

Kodo, K., Ong, S.-G.G., Jahanbani, F., Termglinchan, V., Hirono, K., InanlooRahatloo, K., Ebert, A.D., Shukla, P., Abilez, O.J., Churko, J.M., et al. (2016). iPSC-derived cardiomyocytes reveal abnormal TGF-β signalling in left ventricular non-compaction cardiomyopathy. Nat. Cell Biol. *18*, 1031–1042.

Koo, B.-K.K., Yoon, K.-J.J., Yoo, K.-W.W., Lim, H.-S.S., Song, R., So, J.-H.H., Kim, C.-H.H., and Kong, Y.-Y.Y. (2005a). Mind bomb-2 is an E3 ligase for Notch ligand. J. Biol. Chem. *280*, 22335–22342.

Koo, B.-K.K., Lim, H.-S.S., Song, R., Yoon, M.-J.J., Yoon, K.-J.J., Moon, J.-S.S., Kim, Y.-W.W., Kwon, M.-C.C., Yoo, K.-W.W., Kong, M.-P.P., et al. (2005b). Mind bomb 1 is essential for generating functional Notch ligands to activate

Notch. Development *132*, 3459–3470.

Koo, B.-K.K., Yoon, M.-J.J., Yoon, K.-J.J., Im, S.-K.K., Kim, Y.-Y.Y., Kim, C.-H.H., Suh, P.-G.G., Jan, Y.N., and Kong, Y.-Y.Y. (2007). An obligatory role of mind bomb-1 in notch signaling of mammalian development. PLoS One *2*.

Kopan, R., and Ilagan, M.X.G. (2009). The Canonical Notch Signaling Pathway: Unfolding the Activation Mechanism. Cell *137*, 216–233.

Kosaka, Y., Cieslik, K.A., Li, L., Lezin, G., Maguire, C.T., Saijoh, Y., Toyo-oka, K., Gambello, M.J., Vatta, M., Wynshaw-Boris, A., et al. (2012). 14-3-3ε plays a role in cardiac ventricular compaction by regulating the cardiomyocyte cell cycle. Mol. Cell. Biol. *32*, 5089–5102.

Koshiba-Takeuchi, K., Mori, A.D., Kaynak, B.L., Cebra-Thomas, J., Sukonnik, T., Georges, R.O., Latham, S., Beck, L., Henkelman, R.M., Black, B.L., et al. (2009). Reptilian heart development and the molecular basis of cardiac chamber evolution. Nature *461*, 95–98.

Kovall, R.A., Gebelein, B., Sprinzak, D., and Kopan, R. (2017). The Canonical Notch Signaling Pathway: Structural and Biochemical Insights into Shape, Sugar, and Force. Dev. Cell *41*, 228–241.

Kugathasan, K., Halford, M.M., Farlie, P.G., Bates, D., Smith, D.P., Zhang, Y.F., Roy, J.P., Macheda, M.L., Zhang, D., Wilkinson, J.L., et al. (2018). Deficiency of the Wnt receptor Ryk causes multiple cardiac and outflow tract defects. Growth Factors *36*, 58–68.

Kumar, N., Dougherty, J.A., Manring, H.R., Elmadbouh, I., Mergaye, M., Czirok, A., Greta Isai, D., Belevych, A.E., Yu, L., Janssen, P.M.L., et al. (2019). Assessment of temporal functional changes and miRNA profiling of human iPSC-derived cardiomyocytes. Sci. Rep. *9*, 13188.

de la Pompa, J.L.L., and Epstein, J.A. (2012). Coordinating tissue interactions: Notch signaling in cardiac development and disease. Dev. Cell *22*, 244–254.

LaBarge, W., Mattappally, S., Kannappan, R., Fast, V.G., Pretorius, D., Berry, J.L., and Zhang, J. (2019). Maturation of three-dimensional, hiPSC-derived cardiomyocyte spheroids utilizing cyclic, uniaxial stretch and electrical stimulation. PLoS One *14*, e0219442.

de Lange, F.J., Moorman, A.F.M., Anderson, R.H., Männer, J., Soufan, A.T., Vries, C. de G., Schneider, M.D., Webb, S., van den Hoff, M.J.B., and Christoffels, V.M. (2004). Lineage and Morphogenetic Analysis of the Cardiac Valves. Circ. Res. *95*, 645–654.

Lee, A., Wei, S., and Schwertani, A. (2019). A Notch more: Molecular players in bicuspid aortic valve disease. J. Mol. Cell. Cardiol. *134*, 62–68.

Lee, H.K., Laug, D., Zhu, W., Patel, J.M., Ung, K., Arenkiel, B.R., Fancy, S.P.J., Mohila, C., and Deneen, B. (2015). Apcdd1 stimulates oligodendrocyte differentiation after white matter injury. Glia *63*, 1840–1849.

Lee, K.-F., Simon, H., Chen, H., Bates, B., Hung, M.-C., and Hauser, C. (1995). Requirement for neuregulin receptor erbB2 in neural and cardiac development. Nature *378*, 394–398.

Lee, T.C., Zhao, Y.D., Courtman, D.W., and Stewart, D.J. (2000). Abnormal aortic valve development in mice lacking endothelial nitric oxide synthase. Circulation *101*, 2345–2348.

Li, H., and Durbin, R. (2009). Fast and accurate short read alignment with Burrows-Wheeler transform. Bioinformatics *25*, 1754–1760.

Li, B., Jia, Z., Wang, T., Wang, W., Zhang, C., Chen, P., Ma, K., and Zhou, C. (2012). Interaction of Wnt/β-catenin and notch signaling in the early stage of cardiac differentiation of P19CL6 cells. J. Cell. Biochem. *113*, 629–639.

Li, D., Hallett, M.A., Zhu, W., Rubart, M., Liu, Y., Yang, Z., Chen, H., Haneline, L.S., Chan, R.J., Schwartz, R.J., et al. (2011). Dishevelled-associated activator of morphogenesis 1 (Daam1) is required for heart morphogenesis. Development *138*, 303–315.

Li, G., Khandekar, A., Yin, T., Hicks, S.C., Guo, Q., Takahashi, K., Lipovsky, C.E., Brumback, B.D., Rao, P.K., Weinheimer, C.J., et al. (2018). Differential Wnt-mediated programming and arrhythmogenesis in right versus left ventricles. J. Mol. Cell. Cardiol. *123*, 92–107.

Li, J.J., Miao, L., Shieh, D., Spiotto, E., Li, J.J., Zhou, B., Paul, A., Schwartz, R.J., Firulli, A.B., Singer, H.A., et al. (2016). Single-Cell Lineage Tracing Reveals that Oriented Cell Division Contributes to Trabecular Morphogenesis and Regional Specification. Cell Rep. *15*, 158–170.

Liu, X., Yagi, H., Saeed, S., Bais, A.S., Gabriel, G.C., Chen, Z., Peterson, K.A., Li, Y., Schwartz, M.C., Reynolds, W.T., et al. (2017). The complex genetics of hypoplastic left heart syndrome. Nat. Genet. *49*, 1152–1159.

Los, J.A., and Eijndthoven, E. (1973). The fusion of the endocardial cushions in the heart of the chick embryo. Z. Anat. Entwicklungsgesch. *141*, 55–75.

Luna-Zurita, L., Prados, B., Grego-Bessa, J., Luxán, G., del Monte, G., Benguría, A., Adams, R.H., Pérez-Pomares, J.M.M., and de la Pompa, J.L.L. (2010). Integration of a Notch-dependent mesenchymal gene program and Bmp2-driven cell invasiveness regulates murine cardiac valve formation. J. Clin. Invest. *120*, 3493–3507.

Luna-Zurita, L., Stirnimann, C.U., Glatt, S., Kaynak, B.L., Thomas, S., Baudin, F., Samee, M.A.H., He, D., Small, E.M., Mileikovsky, M., et al. (2016). Complex Interdependence Regulates Heterotypic Transcription Factor Distribution and Coordinates Cardiogenesis. Cell *164*, 999–1014.

Luxán, G., Casanova, J.C.C., Martínez-Poveda, B., Prados, B., D'Amato, G., MacGrogan, D., Gonzalez-Rajal, A., Dobarro, D., Torroja, C., Martinez, F., et al. (2013). Mutations in the NOTCH pathway regulator MIB1 cause left ventricular noncompaction cardiomyopathy. Nat. Med. *19*, 193–201.

Ma, L., Lu, M.-F., Schwartz, R.J., and Martin, J.F. (2005). Bmp2 is essential for cardiac cushion epithelial-

mesenchymal transition and myocardial patterning. Development *132*, 5601–5611.

MacGrogan, D., D'Amato, G., Travisano, S., Martinez-Poveda, B., Luxán, G., Del Monte-Nieto, G., Papoutsi, T., Sbroggio, M., Bou, V., Gomez-Del Arco, P., et al. (2016). Sequential Ligand-Dependent Notch Signaling Activation Regulates Valve Primordium Formation and Morphogenesis. Circ. Res. *118*, 1480–1497.

MacGrogan, D., Münch, J., and de la Pompa, J.L. (2018). Notch and interacting signalling pathways in cardiac development, disease, and regeneration. Nat. Rev. Cardiol. *15*, 685–704.

Männer, J. (1992). The development of pericardial villi in the chick embryo. Anat. Embryol. (Berl). *186*, 379–385.

Markwald, R.R., Fitzharris, T.P., and Manasek, F.J. (1977). Structural development of endocardial cushions. Am. J. Anat. *148*, 85–119.

Marvin, M.J. (2001). Inhibition of Wnt activity induces heart formation from posterior mesoderm. Genes Dev. *15*, 316–327.

McBride, K.L., Riley, M.F., Zender, G.A., Fitzgerald-Butt, S.M., Towbin, J.A., Belmont, J.W., and Cole, S.E. (2008). NOTCH1 mutations in individuals with left ventricular outflow tract malformations reduce ligand-induced signaling. Hum. Mol. Genet. *17*, 2886–2893.

McKellar, S.H., Tester, D.J., Yagubyan, M., Majumdar, R., Ackerman, M.J., and Sundt, T.M. (2007). Novel NOTCH1 mutations in patients with bicuspid aortic valve disease and thoracic aortic aneurysms. J. Thorac. Cardiovasc. Surg. *134*, 290–296.

McKenna, A., Hanna, M., Banks, E., Sivachenko, A., Cibulskis, K., Kernytsky, A., Garimella, K., Altshuler, D., Gabriel, S., Daly, M., et al. (2010). The Genome Analysis Toolkit: A MapReduce framework for analyzing next-generation DNA sequencing data. Genome Res. *20*, 1297–1303.

McLaren, W., Gil, L., Hunt, S.E., Riat, H.S., Ritchie, G.R.S., Thormann, A., Flicek, P., and Cunningham, F. (2016). The Ensembl Variant Effect Predictor. Genome Biol. *17*, 122.

McMillan, B.J., Schnute, B., Ohlenhard, N., Zimmerman, B., Miles, L., Beglova, N., Klein, T., and Blacklow, S.C. (2015). A Tail of Two Sites: A Bipartite Mechanism for Recognition of Notch Ligands by Mind Bomb E3 Ligases. Mol. Cell *57*, 912–924.

Melloy, P.., Ewart, J.., Cohen, M.., Desmond, M.., Kuehn, M.., and Lo, C.. (1998). No turning,a Mouse Mutation Causing Left–Right and Axial Patterning Defects. Dev. Biol. *193*, 77–89.

Meyer, D., and Birchmeier, C. (1995). Multiple essential functions of neuregulin in development. Nature *378*, 386–390.

Miquerol, L., Beyer, S., and Kelly, R.G. (2011). Establishment of the mouse ventricular conduction system.

Cardiovasc. Res. *91*, 232–242.

del Monte-Nieto, G., Ramialison, M., Adam, A.A.S., Wu, B., Aharonov, A., D'Uva, G., Bourke, L.M., Pitulescu, M.E., Chen, H., de la Pompa, J.L., et al. (2018). Control of cardiac jelly dynamics by NOTCH1 and NRG1 defines the building plan for trabeculation. Nature *557*, 439–445.

Del Monte, G., Grego-Bessa, J., González-Rajal, A., Bolós, V., and De La Pompa, J.L.L. (2007). Monitoring Notch1 activity in development: Evidence for a feedback regulatory loop. Dev. Dyn. *236*, 2594–2614.

Moreth, K., Fischer, R., Fuchs, H., Gailus-Durner, V., Wurst, W., Katus, H.A., Bekeredjian, R., and Hrabě de Angelis, M. (2014). High-throughput phenotypic assessment of cardiac physiology in four commonly used inbred mouse strains. J. Comp. Physiol. B *184*, 763–775.

Morray, B.H. (2019). Ventricular Septal Defect Closure Devices, Techniques, and Outcomes. Interv. Cardiol. Clin. *8*, 1–10.

Niessen, K., Fu, Y., Chang, L., Hoodless, P.A., McFadden, D., and Karsan, A. (2008). Slug is a direct Notch target required for initiation of cardiac cushion cellularization. J. Cell Biol. *182*, 315–325.

O'Rourke, B.P., Gomez-Ferreria, M.A., Berk, R.H., Hackl, A.M., Nicholas, M.P., O'Rourke, S.C., Pelletier, L., and Sharp, D.J. (2014). Cep192 controls the balance of centrosome and non-centrosomal microtubules during interphase. PLoS One *9*.

Oka, C., Nakano, T., Wakeham, A., De la Pompa, J.L., Mori, C., Sakai, T., Okazaki, S., Kawaichi, M., Shiota, K., Mak, T.W., et al. (1995). Disruption of the mouse RBP-Jκ gene results in early embryonic death. Development *121*, 3291–3301.

Olson, E.N. (2006). Gene regulatory networks in the evolution and development of the heart. Science (80-.). *313*, 1922–1927.

Otto, C.M. (2002). Calcification of bicuspid aortic valves. Heart *88*, 321–322.

Page, D.J., Miossec, M.J., Williams, S.G., Monaghan, R.M., Fotiou, E., Cordell, H.J., Sutcliffe, L., Topf, A., Bourgey, M., Bourque, G., et al. (2019). Whole Exome Sequencing Reveals the Major Genetic Contributors to Nonsyndromic Tetralogy of Fallot. Circ. Res. *124*, 553–563.

Papoutsi, T., Luna-Zurita, L., Prados, B., Zaffran, S., and de la Pompa, J.L.L. (2018). Bmp2 and Notch cooperate to pattern the embryonic endocardium. Development *145*.

Patten, B.M. (1922). The formation of the cardiac loop in the chick. Am. J. Anat. *30*, 373–397.

Peralta, M., Steed, E., Harlepp, S., González-Rosa, J.M., Monduc, F., Ariza-Cosano, A., Cortés, A., Rayón, T., Gómez-Skarmeta, J.L., Zapata, A., et al. (2013). Heartbeat-driven pericardiac fluid forces contribute to epicardium

morphogenesis. Curr. Biol. *23*, 1726–1735.

Pérez-Lescure Picarzo, J., Mosquera González, M., Latasa Zamalloa, P., and Crespo Marcos, D. (2018). Incidencia y evolución de las cardiopatías congénitas en España durante 10 años (2003-2012). An. Pediatría *89*, 294–301.

Perez-Pomares, J.M.M., and De La Pompa, J.L. (2011). Signaling during epicardium and coronary vessel development. Circ. Res. *109*, 1429–1442.

Perez-Pomares, J.M., Carmona, R., González-Iriarte, M., Atencia, G., Wessels, A., and Muñoz-Chapuli, R. (2002). Origin of coronary endothelial cells from epicardial mesothelium in avian embryos. Int. J. Dev. Biol. *46*, 1005–1013.

Petersen, S.E., Selvanayagam, J.B., Wiesmann, F., Robson, M.D., Francis, J.M., Anderson, R.H., Watkins, H., and Neubauer, S. (2005). Left ventricular non-compaction: insights from cardiovascular magnetic resonance imaging. J. Am. Coll. Cardiol. *46*, 101–105.

Piccolo, P., Attanasio, S., Secco, I., Sangermano, R., Strisciuglio, C., Limongelli, G., Miele, E., Mutarelli, M., Banfi, S., Nigro, V., et al. (2017). MIB2 variants altering NOTCH signalling result in left ventricle hypertrabeculation/non-compaction and are associated with Ménétrier-like gastropathy. Hum. Mol. Genet. *26 VN-r*, 33–43.

Pitsouli, C., and Delidakis, C. (2005). The interplay between DSL proteins and ubiquitin ligases in Notch signaling. Development *132*, 4041–4050.

de Pompa, L.J.L., Timmerman, L.A., Takimoto, H., de la Pompa, J.L., Timmerman, L.A., Takimoto, H., Yoshida, H., Elia, A.J., Samper, E., Potter, J., et al. (1998). Role of the NF-ATc transcription factor in morphogenesis of cardiac valves and septum. Nature *392*, 182–186.

Pucéat, M. (2013). Embryological origin of the endocardium and derived valve progenitor cells: From developmental biology to stem cell-based valve repair. Biochim. Biophys. Acta - Mol. Cell Res. *1833*, 917–922.

Raissadati, A., Nieminen, H., Jokinen, E., and Sairanen, H. (2015). Progress in Late Results Among Pediatric Cardiac Surgery Patients. Circulation *131*, 347–353.

Ranger, A.M., Grusby, M.J., Hodge, M.R., Gravallese, E.M., de la Brousse, F.C., Hoey, T., Mickanin, C., Baldwin, H.S., and Glimcher, L.H. (1998). The transcription factor NF-ATc is essential for cardiac valve formation. Nature *392*, 186–190.

Rawles, M.E. (1936). A study in the localization of organ-forming areas in the chick blastoderm of the head-process stage. J. Exp. Zool. *72*, 271–315.

Risebro, C.A., Vieira, J.M., Klotz, L., and Riley, P.R. (2015). Characterisation of the human embryonic and foetal epicardium during heart development. Dev. *142*, 3630–3636.

Ritter, M., Oechslin, E., Sütsch, G., Attenhofer, C., Schneider, J., and Jenni, R. (1997). Isolated Noncompaction of the Myocardium in Adults. Mayo Clin. Proc. *72*, 26–31.

Rivera-Feliciano, J., and Tabin, C.J. (2006). Bmp2 instructs cardiac progenitors to form the heart-valve-inducing field. Dev. Biol. *295*, 580–588.

Ronaldson-Bouchard, K., Yeager, K., Teles, D., Chen, T., Ma, S., Song, L., Morikawa, K., Wobma, H.M., Vasciaveo, A., Ruiz, E.C., et al. (2019). Engineering of human cardiac muscle electromechanically matured to an adult-like phenotype. Nat. Protoc. *14*, 2781–2817.

Ross, S.B., Jones, K., Blanch, B., Puranik, R., McGeechan, K., Barratt, A., and Semsarian, C. (2019). A systematic review and meta-analysis of the prevalence of left ventricular non-compaction in adults. Eur. Heart J.

Roy, J.P., Halford, M.M., and Stacker, S.A. (2018). The biochemistry, signalling and disease relevance of RYK and other WNT-binding receptor tyrosine kinases. Growth Factors *36*, 15–40.

Schneider, V.A., and Mercola, M. (2001). Wnt antagonism initiates cardiogenesis in Xenopus laevis. Genes Dev. *15*, 304–315.

Sedaghat-Hamedani, F., Haas, J., Zhu, F., Geier, C., Kayvanpour, E., Liss, M., Lai, A., Frese, K., Pribe-Wolferts, R., Amr, A., et al. (2017). Clinical genetics and outcome of left ventricular non-compaction cardiomyopathy. Eur. Heart J. *38*, 3449–3460.

Sedmera, D., Pexieder, T., Vuillemin, M., Thompson, R.P., and Anderson, R.H. (2000). Developmental patterning of the myocardium. Anat. Rec. *258*, 319–337.

Shimomura, Y., Agalliu, D., Vonica, A., Luria, V., Wajid, M., Baumer, A., Belli, S., Petukhova, L., Schinzel, A., Brivanlou, A.H., et al. (2010). APCDD1 is a novel Wnt inhibitor mutated in hereditary hypotrichosis simplex. Nature *464*, 1043–1047.

Shin, N., Lee, Y.-K.K., Park, U.-H.H., Jeong, J.-C.C., and Um, S.-J.J. (2014). Repression of LXRα by a novel member of additional sex comb-like family, ASXL3. Biochem. Biophys. Res. Commun. *454*, 479–485.

Shukla, V., Rao, M., Zhang, H., Beers, J., Wangsa, D.D., Wangsa, D.D., Buishand, F.O., Wang, Y., Yu, Z., Stevenson, H.S., et al. (2017). ASXL3 is a novel pluripotency factor in human respiratory epithelial cells and a potential therapeutic target in small cell lung cancer. Cancer Res. *77*, 6267–6281.

Sonnen, K.F., Gabryjonczyk, A.-M., Anselm, E., Stierhof, Y.-D., and Nigg, E.A. (2013). Human Cep192 and Cep152 cooperate in Plk4 recruitment and centriole duplication. J. Cell Sci. *126*, 3223–3233.

Srivastava, A., Ritesh, K.C., Tsan, Y.C., Liao, R., Su, F., Cao, X., Hannibal, M.C., Keegan, C.E., Chinnaiyan, A.M., Martin, D.M., et al. (2016). De novo dominant ASXL3 mutations alter H2A deubiquitination and transcription in Bainbridge-Ropers syndrome. Hum. Mol. Genet. *25*, 597–608.

Srivastava, D., Thomas, T., Lin, Q., Kirby, M.L., Brown, D., and Olson, E.N. (1997). Regulation of cardiac mesodermal and neural crest development by the bHLH transcription factor, dHAND. Nat. Genet. *16*, 154–160.

Staudt, D.W., Liu, J., Thorn, K.S., Stuurman, N., Liebling, M., and Stainier, D.Y. (2014). High-resolution imaging of cardiomyocyte behavior reveals two distinct steps in ventricular trabeculation. Development *141*, 585–593.

Stöllberger, C., Finsterer, J., and Blazek, G. (2002). Left ventricular hypertrabeculation/noncompaction and association with additional cardiac abnormalities and neuromuscular disorders. Am. J. Cardiol. *90*, 899–902.

Suzuki, H.R., Solursh, M., and Baldwin, H.S. (1995). Relationship between fibronectin expression during gastrulation and heart formation in the rat embryo. Dev. Dyn. *204*, 259–277.

Takahashi, M., Fujita, M., Furukawa, Y., Hamamoto, R., Shimokawa, T., Miwa, N., Ogawa, M., and Nakamura, Y. (2002). Isolation of a novel human gene, APCDD1, as a direct target of the β-catenin/T-cell factor 4 complex with probable involvement in colorectal carcinogenesis. Cancer Res. *62*, 5651–5656.

Theis, J.L., Hrstka, S.C., Evans, J.M., O'Byrne, M.M., de Andrade, M., O'Leary, P.W., Nelson, T.J., and Olson, T.M. (2015). Compound heterozygous NOTCH1 mutations underlie impaired cardiogenesis in a patient with hypoplastic left heart syndrome. Hum. Genet. *134*, 1003–1011.

Tian, X., Li, Y.Y., He, L., Zhang, H., Huang, X., Liu, Q., Pu, W.W.T., Zhang, L., Li, Y.Y., Zhao, H., et al. (2017). Identification of a hybrid myocardial zone in the mammalian heart after birth. Nat. Commun. *8*, 87.

Timmerman, L.A., Grego-Bessa, J., Raya, Á., Bertrán, E., Pérez-Pomares, J.M., Díez, J., Aranda, S., Palomo, S., McCormick, F., Izpisúa-Belmonte, J.C., et al. (2004). Notch promotes epithelial-mesenchymal transition during cardiac development and oncogenic transformation. Genes Dev. *18*, 99–115.

Toischer, K., Rokita, A.G., Unsöld, B., Zhu, W., Kararigas, G., Sossalla, S., Reuter, S.P., Becker, A., Teucher, N., Seidler, T., et al. (2010). Differential cardiac remodeling in preload versus afterload. Circulation *122*, 993–1003.

Tomanek, R.J., Hu, N., Phan, B., and Clark, E.B. (1999a). Rate of coronary vascularization during embryonic chicken development is influenced by the rate of myocardial growth. Cardiovasc. Res. *41*, 663–671.

Tomanek, R.J., Ratajska, A., Kitten, G.T., Yue, X., and Sandra, A. (1999b). Vascular endothelial growth factor expression coincides with coronary vasculogenesis and angiogenesis. Dev. Dyn. *215*, 54–61.

Towbin, J.A., and Jefferies, J.L. (2017). Cardiomyopathies due to left ventricular noncompaction, mitochondrial and storage diseases, and inborn errors of metabolism. Circ. Res. *121*, 838–854.

Towbin, J.A., Lorts, A., and Jefferies, J.L. (2015). Left ventricular non-compaction cardiomyopathy. Lancet (London, England) *386*, 813–825.

Villumsen, B.H., Danielsen, J.R., Povlsen, L., Sylvestersen, K.B., Merdes, A., Beli, P., Yang, Y.G., Choudhary, C.,

Nielsen, M.L., Mailand, N., et al. (2013). A new cellular stress response that triggers centriolar satellite reorganization and ciliogenesis. EMBO J. *32*, 3029–3040.

Viragh, S., and Challice, C.E. (1981). The origin of the epicardium and the embryonic myocardial circulation in the mouse. Anat. Rec. *201*, 157–168.

Wang, L., Lee, K., Malonis, R., Sanchez, I., and Dynlacht, B.D. (2016). Tethering of an E3 ligase by PCM1 regulates the abundance of centrosomal KIAA0586/Talpid3 and promotes ciliogenesis. Elife *5*.

Wang, X., Xin, Q., Li, L., Li, J., Zhang, C., Qiu, R., Qian, C., Zhao, H., Liu, Y., Shan, S., et al. (2014). Exome sequencing reveals a heterozygous DLX5 mutation in a Chinese family with autosomal-dominant split-hand/foot malformation. Eur. J. Hum. Genet. *22*, 1105–1110.

van Weerd, J.H., and Christoffels, V.M. (2016). The formation and function of the cardiac conduction system. Development *143*, 197–210.

Weir-McCall, J.R., Yeap, P.M., Papagiorcopulo, C., Fitzgerald, K., Gandy, S.J., Lambert, M., Belch, J.J.F.F., Cavin, I., Littleford, R., Macfarlane, J.A., et al. (2016). Left Ventricular Noncompaction: Anatomical Phenotype or Distinct Cardiomyopathy? J. Am. Coll. Cardiol. *68*, 2157–2165.

Wessels, A., Markman, M.W.M., Vermeulen, J.L.M., Anderson, R.H., Moorman, A.F.M., and Lamers, W.H. (1996). The Development of the Atrioventricular Junction in the Human Heart. Circ. Res. *78*, 110–117.

Willems, S.H., Tape, C.J., Stanley, P.L., Taylor, N.A., Mills, I.G., Neal, D.E., McCafferty, J., and Murphy, G. (2010). Thiol isomerases negatively regulate the cellular shedding activity of ADAM17. Biochem. J. *428*, 439–450.

Wirkner, C.S. (2009). The circulatory system in Malacostraca - Evaluating character evolution on the basis of differing phylogenetic hypotheses. Arthropod Syst. Phylogeny *67*, 57–70.

Wischhof, L., Maida, S., Piazzesi, A., Gioran, A., Barragan Sanz, K., Irsen, S., Beyer, M., Schultze, J.L., Dyer, M.J., Salomoni, P., et al. (2017). The SWI/SNF subunit Bcl7a contributes to motor coordination and Purkinje cell function. Sci. Rep. *7*, 17055.

Wu, B., Zhang, Z., Lui, W., Chen, X., Wang, Y., Chamberlain, A.A., Moreno-Rodriguez, R.A., Markwald, R.R., O'Rourke, B.P., Sharp, D.J., et al. (2012). Endocardial cells form the coronary arteries by angiogenesis through myocardial-endocardial VEGF signaling. Cell *151*, 1083–1096.

Xie, L., Hoffmann, A.D., Burnicka-Turek, O., Friedland-Little, J.M., Zhang, K., and Moskowitz, I.P. (2012). Tbx5-Hedgehog Molecular Networks Are Essential in the Second Heart Field for Atrial Septation. Dev. Cell *23*, 280–291.

Xu, H. (2004). Tbx1 has a dual role in the morphogenesis of the cardiac outflow tract. Development *131*, 3217–3227.

Yi Li, Q., Newbury-Ecob, R.A., Terrett, J.A., Wilson, D.I., Curtis, A.R.J., Ho Yi, C., Gebuhr, T., Bullen, P.J., Robson, S.C., Strachan, T., et al. (1997). Holt-Oram syndrome is caused by mutations in TBX5, a member of the Brachyury (T) gene family. Nat. Genet. *15*, 21–29.

Yoshida, S., Miyagawa, S., Fukushima, S., Kawamura, T., Kashiyama, N., Ohashi, F., Toyofuku, T., Toda, K., and Sawa, Y. (2018). Maturation of Human Induced Pluripotent Stem Cell-Derived Cardiomyocytes by Soluble Factors from Human Mesenchymal Stem Cells. Mol. Ther. *26*, 2681–2695.

Zaffran, S., and Frasch, M. (2002). Early signals in cardiac development. Circ. Res. *91*, 457–469.

Zani, V.J., Asou, N., Jadayel, D., Heward, J.M., Shipley, J., Nacheva, E., Takasuki, K., Catovsky, D., and Dyer, M.J. (1996). Molecular cloning of complex chromosomal translocation t(8;14;12)(q24.1;q32.3;q24.1) in a Burkitt lymphoma cell line defines a new gene (BCL7A) with homology to caldesmon. Blood *87*, 3124–3134.

Zhang, H., Pu, W., Li, G., Huang, X., He, L., Tian, X., Liu, Q., Zhang, L., Wu, S.M., Sucov, H.M., et al. (2016). Endocardium Minimally Contributes to Coronary Endothelium in the Embryonic Ventricular Free Walls. Circ. Res. *118*, 1880–1893.

Zhang, J., Ko, J.M., Guileyardo, J.M., and Roberts, W.C. (2015). A review of spontaneous closure of ventricular septal defect. Proc. (Bayl. Univ. Med. Cent). *28*, 516–520.

So you were born, and that was a good day.
Someday you'll die, and that is a shame.
But somewhere in the between was a life of which we all dream,
and nothing and no one will ever take that away.
Somewhere in the between, Streetlight manifesto

ANNEXES

Ventricular parameters quantification script (ImageJ)

```
title = getTitle();
Directorio = "/Volumes/RATONES/Mib1-STOP-Apcdd1-Asxl3/HE-MAAR/Cuantificaciones-MAAR/";
run("8-bit");
run("Auto Threshold", "method=Intermodes");
run("Set Scale...", "distance=1 known=1.09 pixel=1 unit=micron global");
run("Set Measurements...", "area limit redirect=None decimal=2");
setThreshold(100, 255);
setOption("BlackBackground", false);
setTool("polygon");
waitForUser("Selecciona el compacto");
run("Measure");
run("Copy");
run("Internal Clipboard");
selectWindow(title);
setBackgroundColor(0, 0, 0);
run("Clear", "slice");
waitForUser("Selecciona las trabéculas");
setTool("freehand");
run("Measure");
run("Copy");
run("Internal Clipboard");
selectWindow("Clipboard");
rename(title+"Compacto.png");
run("Save");
selectWindow("Clipboard-1");
rename(title+"Trabecula.png");
run("Save");
areaC = Table.get("Area",0);
areaT = Table.get("Area",1);
String.copy(areaC + "\t" + areaT);
waitForUser("Copia los datos", "Áreas");
String.resetBuffer;
run("Clear Results");
run("Gaussian Blur...", "sigma=1 scaled");
run("Find Edges");
setOption("BlackBackground", false);
run("Make Binary");
run("Set Measurements...", "area limit redirect=None decimal=3");
run("Fractal Box Count...", "box=1,2,3,4,6,8,12,16,32,64,128,256");
close();
FD=Table.get("D");
String.copy(FD);
```

```
waitForUser("Copia los datos", "FD");
run("Clear Results");

run("Close");
run("Set Measurements...", "area limit redirect=None decimal=2");
setTool("polyline");
waitForUser("Endereza el compacto", "Traza la línea paralela al epicardio");
run("Straighten...", "title line=1040");
setOption("BlackBackground", true);
run("Convert to Mask");
width=getWidth();
for(i=0; i<width;  i+=3) {
        makeLine(i , 0 , i , getHeight());
        run("Measure");
}
close();
close();
close();
run("Summarize");
Table.deleteRows(0, nResults - 5);
Table.deleteRows(1, nResults);
String.resetBuffer;
v=Table.get("Area");
x=v / 1.08667;
String.copy(x)
run("Clear Results");
String.resetBuffer;
```

Endocardial N1ICD positive nuclei quantification macro (ImageJ)

```
//Macro based upon Vera Lúcia Ferreira Oliveira's scripts
run("Duplicate...", "title=Foto duplicate");
if (nSlices() > 4) {
	run("Z Project...", "projection=[Max Intensity]");
} else {
	rename("MAX_Foto");
}
run("Make Composite");
run("Split Channels");
selectWindow("C2-MAX_Foto");
run("Gaussian Blur...", "sigma=1 scaled stack");
setTool("polygon");
waitForUser("Bordea el endocardio");
run("Auto Threshold", "method=Huang2 white");
run("Clear Outside");
run("Create Selection");
run("Make Inverse");
roiManager("add");
selectWindow("C1-MAX_Foto");
roiManager("Select", 0);
run("Clear Outside");
run("8-bit");
run("Auto Threshold", "method=Default white");
run("Convert to Mask");
run("Watershed");
run("Analyze Particles...", "size=3-infinity circularity=0.00-0.90 show=Outlines display
		summarize");
selectWindow("C4-MAX_Foto");
roiManager("select",0);
run("Clear Outside");
run("8-bit");
run("Auto Threshold", "method=MaxEntropy white");
run("Convert to Mask");
run("Analyze Particles...", "size=3-Infinity circularity=0.05-0.90 show=Outlines display
		summarize add");
selectWindow("Summary");
waitForUser("Revisa las cuantificaciones", "copia los datos");
run("Close");
selectWindow("Results");
run("Close");
roiManager("deselect");
roiManager("delete");
close("*Foto*");
```